



Durham E-Theses

Hydrocarbon prospectivity to the north-west of the assumood field, Sirt Basin, Libya

Salem, Amjed Ahmed Ben

How to cite:

Salem, Amjed Ahmed Ben (2000) *Hydrocarbon prospectivity to the north-west of the assumood field, Sirt Basin, Libya*, Durham theses, Durham University. Available at Durham E-Theses Online: <http://etheses.dur.ac.uk/4379/>

Use policy

The full-text may be used and/or reproduced, and given to third parties in any format or medium, without prior permission or charge, for personal research or study, educational, or not-for-profit purposes provided that:

- a full bibliographic reference is made to the original source
- a [link](#) is made to the metadata record in Durham E-Theses
- the full-text is not changed in any way

The full-text must not be sold in any format or medium without the formal permission of the copyright holders.

Please consult the [full Durham E-Theses policy](#) for further details.

**Hydrocarbon Prospectivity
to the North-West of the Assumood Field,
Sirt Basin, Libya**

by

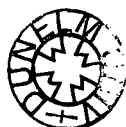
Amjed Ahmed Ben Salem

Department of Geological Sciences

University of Durham

The copyright of this thesis rests with the author. No quotation from it should be published in any form, including Electronic and the Internet, without the author's prior written consent. All information derived from this thesis must be acknowledged appropriately.

**A thesis submitted in partial fulfilment of the requirements for
the degree of Master of Science**



17 JAN 2001

August 2000

ABSTRACT

The area of study covers parts of the Assumood Ridge and the Wadayat Trough in the Sirt Basin, onshore Libya. The area is surrounded on three sides by gas fields producing from the Lower Oligocene Arida Formation, the Middle Eocene Gialo Formation and the Bahi /Gargaf Formation. The DDD1-6 well was drilled in the study area in 1965 and tested gas at low rates from carbonates of the Upper Palaeocene Harash Formation. Re-evaluation of data from this well in 1996 confirmed the presence of untested gas intervals in the Upper Cretaceous Kalash Formation and in the Gialo Formation. The re-evaluation encouraged Sirte Oil Company to acquire more seismic data in 1998 and to interpret all available seismic data in the area.

The study area is about 380 km² and contains 1196 km of 2-D seismic data comprising 48 seismic lines. The data consist of eight vintages of seismic data from 1971 to 1998. Borehole data from 10 wells were utilised. Three time structure maps were generated in this study for the tops of the following carbonate formations: the Kalash Formation, the Upper Palaeocene-Lower Eocene Kheir Formation and the Gialo Formation. The Kheir Formation was mapped because direct mapping of the Harash carbonate is not possible as its contact with the overlying Harash/Kheir limestone beds is usually not seismically resolvable.

Two structural closures were identified as prospective locations for the Kalash Formation, the first located south of the DDD1-6 well and the second located southwest of the ZZ1-6 well. One structural closure for the Gialo Formation was identified, approximately at the same location as the first closure at the Top Kalash horizon. No prospective locations were identified for the Kheir Formation. The new prospective location located south of DDD1-6 well is particularly recommended for exploration drilling since the same well could test structural closures in both the Kalash and Gialo formations.

C O N T E N T S

Abstract	ii
Contents	iii
List of Figures	vii
List of Tables	ix
Acknowledgements	x
Chapter 1. Introduction	1
1.1. Project background	1
1.2. Project aims.....	4
1.3. Data sources and techniques.....	4
1.4. Outline of the thesis.....	6
Chapter 2. Structure and stratigraphy of the Sirt Basin	7
2.1. Introduction.....	7
2.2. Tectonic framework of the Sirt Basin.....	7
2.3. Stratigraphic framework of the Sirt Basin.....	14
2.4. Hydrocarbon potential in the Sirt Basin.....	18
2.5. Reservoirs, source and seal rocks in the Sirt Basin.....	19
2.5.1. Reservoirs.....	19
2.5.2. Source rocks.....	20
2.5.3. Seals.....	21

Chapter 3. Geology of the study area.....	22
3.1. Stratigraphy in the study area.....	22
3.1.1. Precambrian basement.....	22
3.1.2. Cambro-Ordovician Gargaf Formation.....	22
3.1.3. Lower Cretaceous Nubian Formation.....	24
3.1.4. Upper Cretaceous Bahi Formation.....	24
3.1.5. Upper Cretaceous Lidam/Etel Formation.....	25
3.1.6. Upper Cretaceous Rachmat Formation.....	25
3.1.7. Upper Cretaceous Sirte Shale Formation.....	26
3.1.8. Upper Cretaceous Waha Formation.....	26
3.1.9. Upper Cretaceous Kalash Formation.....	27
3.1.10. Lower Palaeocene Hagfa Formation.....	28
3.1.11. Middle Palaeocene Beda Formation.....	28
3.1.12. Upper Palaeocene Khalifa Formation.....	29
3.1.13. Upper Palaeocene Zelten Formation.....	29
3.1.14. Upper Palaeocene Harash Formation.....	30
3.1.15. Upper Palaeocene-Lower Eocene Kheir Formation...	30
3.1.16. Lower Eocene Gir Formation.....	31
3.1.17. Middle Eocene Gialo Formation.....	32
3.1.18. Upper Eocene Augila Formation.....	32
3.1.19. Lower Oligocene Arida Formation.....	33
3.1.20. Upper Oligocene Diba Formation.....	33
3.2. Hydrocarbon potential in North Concession 6.....	34
3.2.1. Assumood Gas Field.....	35
3.2.2. Sahl Gas Field.....	35
3.2.3. Hateiba Gas Field.....	35

3.2.4. Attahaddy Gas Field.....	35
3.3. Reservoir, source and seal rocks in the study area.....	36
3.3.1. Reservoirs.....	36
3.3.2. Source rocks.....	36
3.3.3. Seals.....	36
3.4. Lithological description of the well data.....	37
3.4.1. DDD1-6 well description.....	37
3.4.2. ZZ1-6 well description.....	37
3.4.3. S12-6 well description, Hateiba Field.....	40
3.4.4. H12-6 well description, Assumood Field.....	42
Chapter 4. Data acquisition and processing.....	45
4.1. Introduction.....	45
4.2. Seismic data acquisition.....	49
4.2.1. History and data quality.....	49
4.2.2. Receiver arrays.....	60
4.2.3. Source arrays.....	62
4.2.4. Static corrections.....	63
4.3. Seismic data processing.....	64
Chapter 5. Interpretation.....	66
5.1. Introduction.....	66
5.2. Synthetic seismograms.....	67
5.3. Mis-tie corrections.....	75
5.4. Calculation of dip angles and expected mis-tie values.....	78
5.5. Middle Eocene Gialo Formation.....	81
5.6. Lower Eocene-Upper Palaeocene Kheir Formation.....	84

5.7. Upper Cretaceous Kalash Formation.....	86
5.8. General structure of the area.....	89
5.9. Velocity investigations.....	90
5.10. Reserves.....	94
5.11. Carbonate buildups in the Palaeocene.....	96
Chapter 6 Conclusions and Recommendations.....	99
6.1. Conclusion.....	99
6.2. Recommendations.....	100
References	101
Appendix1. Well data available.....	107
Appendix2. The 1998 processing sequence.....	112

LIST OF FIGURES

Figure 1.1. Study area, location map

Figure 1.2. The tectonic framework of Concession 6

Figure 1.3. Location of oil and gas fields in the Sirt Basin

Figure 2.1. Geographical location map of Sirt Basin

Figure 2.2. Cross-section across the Sirt Basin shows the main troughs and platforms

Figure 2.3. Series of cross-sections showing the structural evolution of the Sirt Basin

Figure 2.4. Model showing the possible extension of opening of the South Atlantic during the Early Cretaceous.

Figure 2.5. Tectonic elements of Sirt Basin.

Figure 3.1. Schematic lithostratigraphy of North Concession 6.

Figure 3.2. Lithologic log of Well DDD1-6.

Figure 3.3. Lithologic log of Well ZZ1-6.

Figure 3.4. Lithologic log of Well S12-6.

Figure 3.5. Lithologic log of Well H12-6.

Figure 4.1. Seismic base map.

Figure 4.2. Line F53-71.

Figure 4.3. Line 6V38-84.

Figure 4.4. Line 6V307-85.

Figure 4.5. Line 6V455-87.

Figure 4.6. Line 6V826-92.

Figure 4.7. Line 6V854-93.

Figure 4.8. Line 6V858-96.

Figure 4.9. Line 6V943-98.

Figure 4.10. The 1998 data source and receiver arrays.

Figure 5.1. DDD1-6 synthetic seismogram.

Figure 5.2. ZZ1-6 synthetic seismogram.

Figure 5.3. S12-6 synthetic seismogram.

Figure 5.4. H12-6 synthetic seismogram.

Figure 5.5. The correlation between DDD1-6 synthetic seismogram and seismic data.

Figure 5.6. The correlation between H121-6 synthetic seismogram and seismic data.

Figure 5.7. Four-node example illustrating translational and rotational adjustments.

Figure 5.8. Diagram to illustrate how the mis-tie between migrated strike and dip lines occurs.

Figure 5.9. The Middle Eocene channel on line 6V927-93.

Figure 5.10. The Middle Eocene channel on line 6V943-98.

Figure 5.11. Middle Eocene Gialo Formation time structure map.

Figure 5.12. Upper Cretaceous Kalash Formation time structure map.

Figure 5.13. Types of carbonate buildups most easily recognised from seismic interpretation.

Figure 5.14. Direct and indirect criteria for recognising carbonate buildups.

Enclosure 1. Two-way time map of the Top Gialo horizon.

Enclosure 2. Two-way time map of the Top Kheir horizon.

Enclosure 3. Two-way time map of the Top Kalash horizon.

LIST OF TABLES

- 4.1. The North Assumood area line numbers, shot point numbers and line lengths in kilometers.
- 4.2. The geophysical companies which acquired the data.
- 4.3. Data acquisition parameters in the area of study.
- 4.4. Geophone array parameters used for each data vintage.
- 4.5. The vibrator array parameters used in each data vintage.
- 5.1. Dip angle and mis-ties expected error at the intersection between dip and strike lines.
- 5.2. Depth conversion calculations for the Gialo Formation.
- 5.3. Depth conversion calculations for the Kheir Formation.
- 5.4. Depth conversion calculations for the Kalash Formation.
- 5.5. The average velocity calculations for the Gialo Formation.
- 5.6. The average velocity calculations for the Kheir Formation.
- 5.7. The average velocity calculations for the Kalash Formation.
- 5.8. Reservoir parameters used to calculate reserves.

ACKNOWLEDGEMENTS

I am most grateful to my supervisor Dr. Neil Goulty who gave his time and effort generously with ideas, discussions and editing this thesis. Also for his endless patience and continuous care.

I would like to thank my family, particularly my mother “Salha” for her prayers to God and continuous encouragement during my study.

Many thanks are due to the academic and technical staff of the Geological Sciences at Durham University, especially Mr. D. Asbery, Mrs. K. Atkinson, Mrs. C. Blair and Mrs. C. Whitehill for their kindness and help which provided a conducive academic atmosphere.

Many thanks to all my colleagues at the Geological department, particularly Mr. Carl Fredrik Gyllenhammar for his help and constructive discussions and N. Fello for his encouragement.

My Arab friends in Durham are thanked for making my study years enjoyable and to make me overcome the homesickness.

Last, but by no means least, this research would not have been possible without the generous funding of the Sirte Oil Company and for providing the data.

INTRODUCTION

1.1 Project background

This project concerns the hydrocarbon prospectivity of an area located in the central part of North Concession 6, Sirt Basin (Figure.1.1). The area of study covers part of the Assumood Ridge and part of the Wadayat Trough (Fig.1.2). Geographically, the area is located between latitudes $29^{\circ} 30' 00''$ and $29^{\circ} 40' 00''$ and longitudes $19^{\circ} 52' 00''$ and $20^{\circ} 02' 00''$, and covers an area of 380 km².

Exploration activity in Concession 6 in the onshore part of the Sirt Basin started in late 1950s. Following gravity and magnetic surveys over the whole concession, the C1-6 discovery well was drilled. This well is considered to be the first commercial well in Libya. The field was developed to form the giant Nasser (Zelten) oil field (Fig. 1.2) (El-Ghoul, 1996). Since this discovery, the whole concession was regarded as prospective, so more geophysical surveys were acquired to cover the whole concession.

Exploration work in North Concession 6 started in 1960 with the discovery of the Assumood Field (Fig. 1.2). In 1963 the Hateiba Field was discovered, followed by Attahaddy Field in 1964 and the Sahl Field in 1962. In the area of study, exploration started in May 1965 by drilling the ZZ1-6 well, which reached Cambro-Ordovician



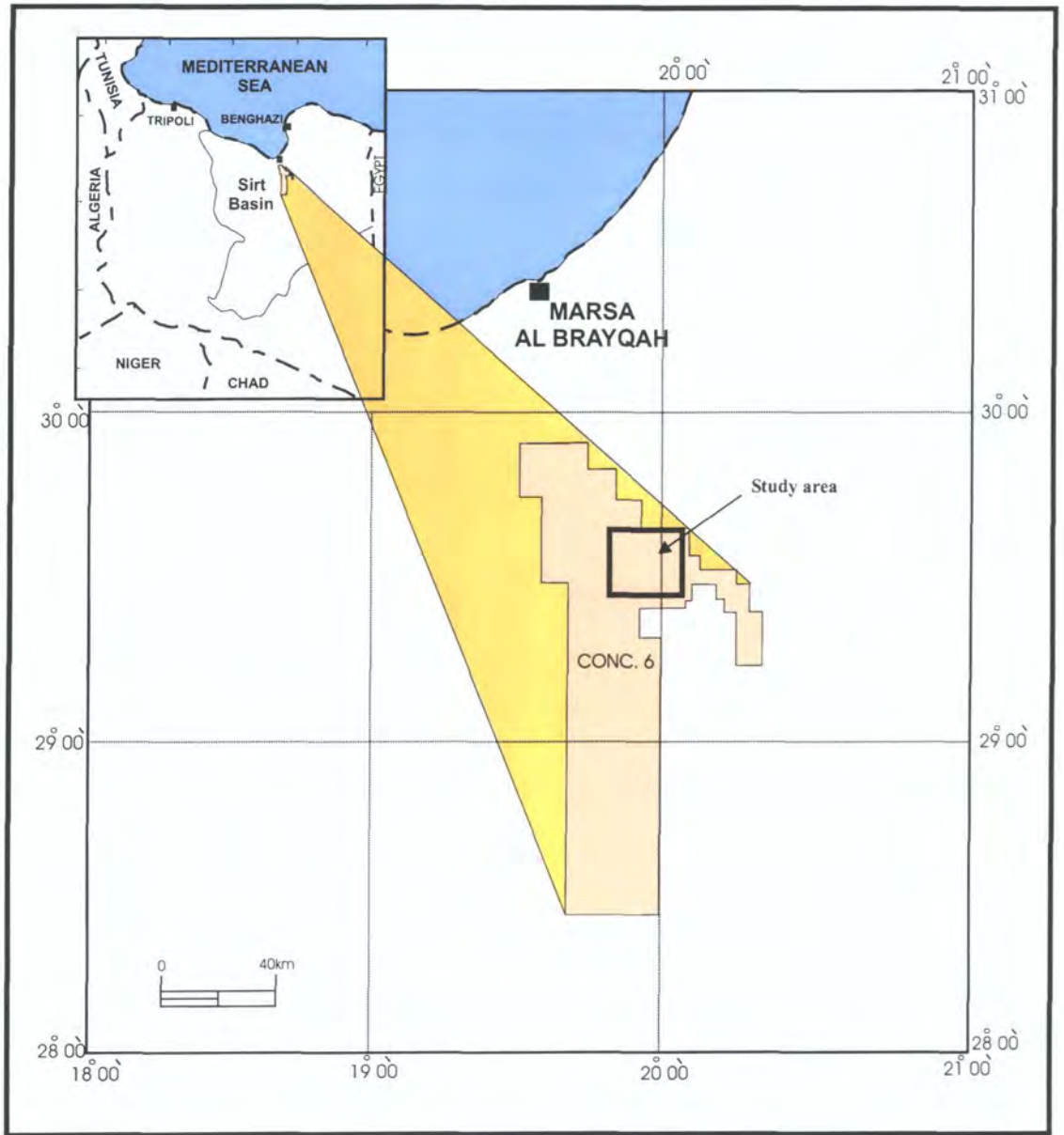


Fig. 1.1. Study area, location map.

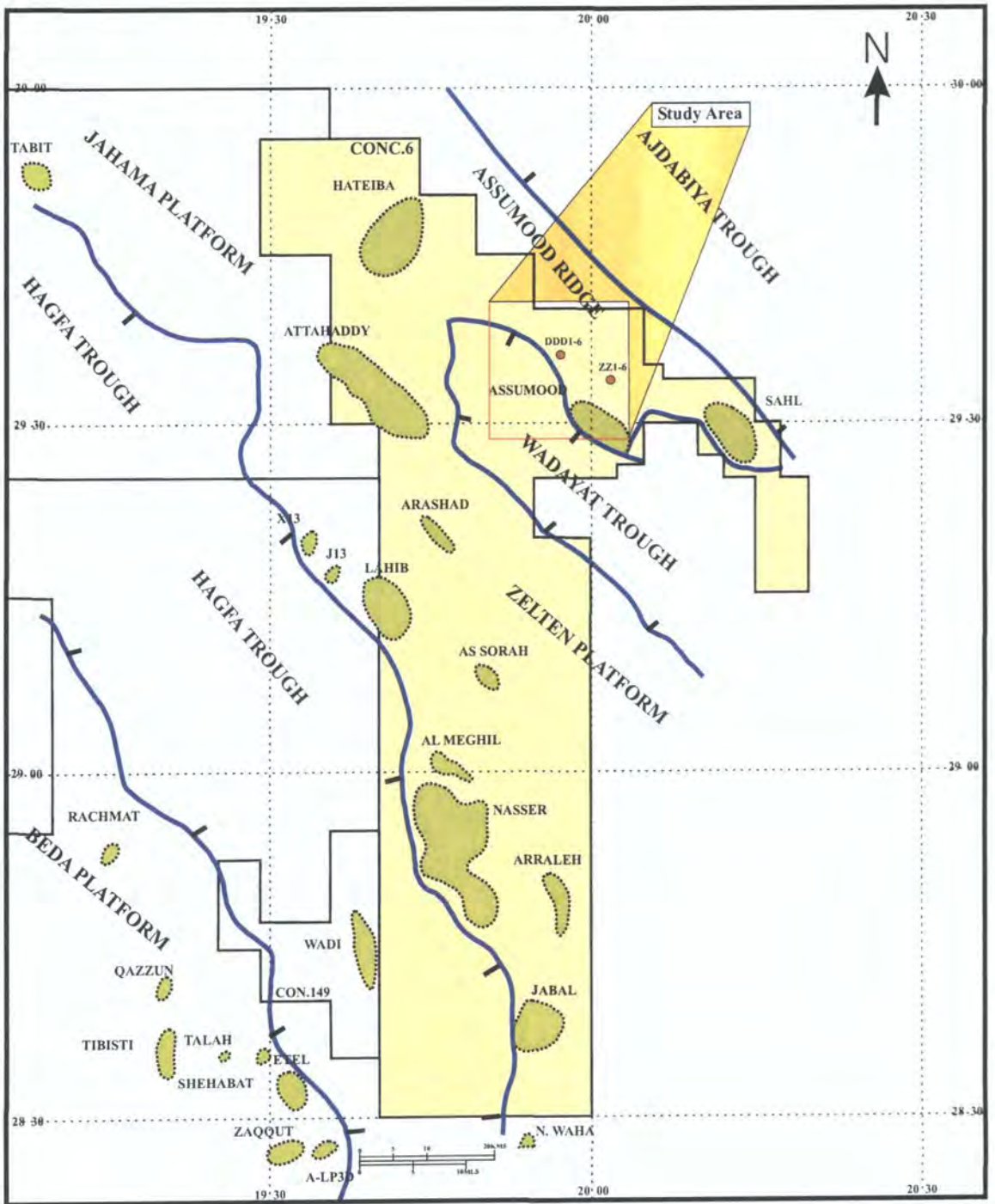


Fig. 1.2. The tectonic framework of Concession 6 showing the main subsurface features that developed during Late Cretaceous rifting. Producing oil and gas fields are marked in green. (After Perrella, 1990).

strata at a total depth of 10319 feet sub-sea. The well was dry. In September 1965 the DDD1-6 well was drilled to a total depth of 9716 feet and also tested dry.

The northern part of Concession 6 is thought to have potential only for new discoveries of gas, since all four discovered hydrocarbon fields in the area contain only gas (Fig. 1.3). The surrounding gas fields are the Assumood and Sahl fields to the southeast, the Hateiba Field to the north-west and the Attahaddy Field to the west.

1.2 Project aims

The original main objectives of this study were: 1) to map the top of the Middle Eocene Gialo Formation, which is the main reservoir in the nearby Assumood and Sahl gas fields; and 2) to map the Upper Cretaceous Kalash Formation and the Cambro-Ordovician quartzite (Gargaf Formation).

Two subsidiary objectives for the study were to evaluate the structure around the DDD1-6 well, which tested gas in the Upper Palaeocene Harash Formation and in the Gargaf Formation; and to investigate whether the area contains carbonate mounds and buildups in the Palaeocene. The Top of the Harash Formation is not seismically resolvable, so the overlying Kheir Formation was mapped.

1.3 Data sources and techniques

A total of 1196 km of 2-D seismic data have been interpreted. These data are comprised of 48 seismic lines which were available on paper sections. The only well in the study area is the DDD1-6 well, but another nine wells from the Assumood, Hateiba and Attahaddy fields have been utilised. Well logs from all ten wells were available. Well data and formation tops are listed in the Appendix (1).

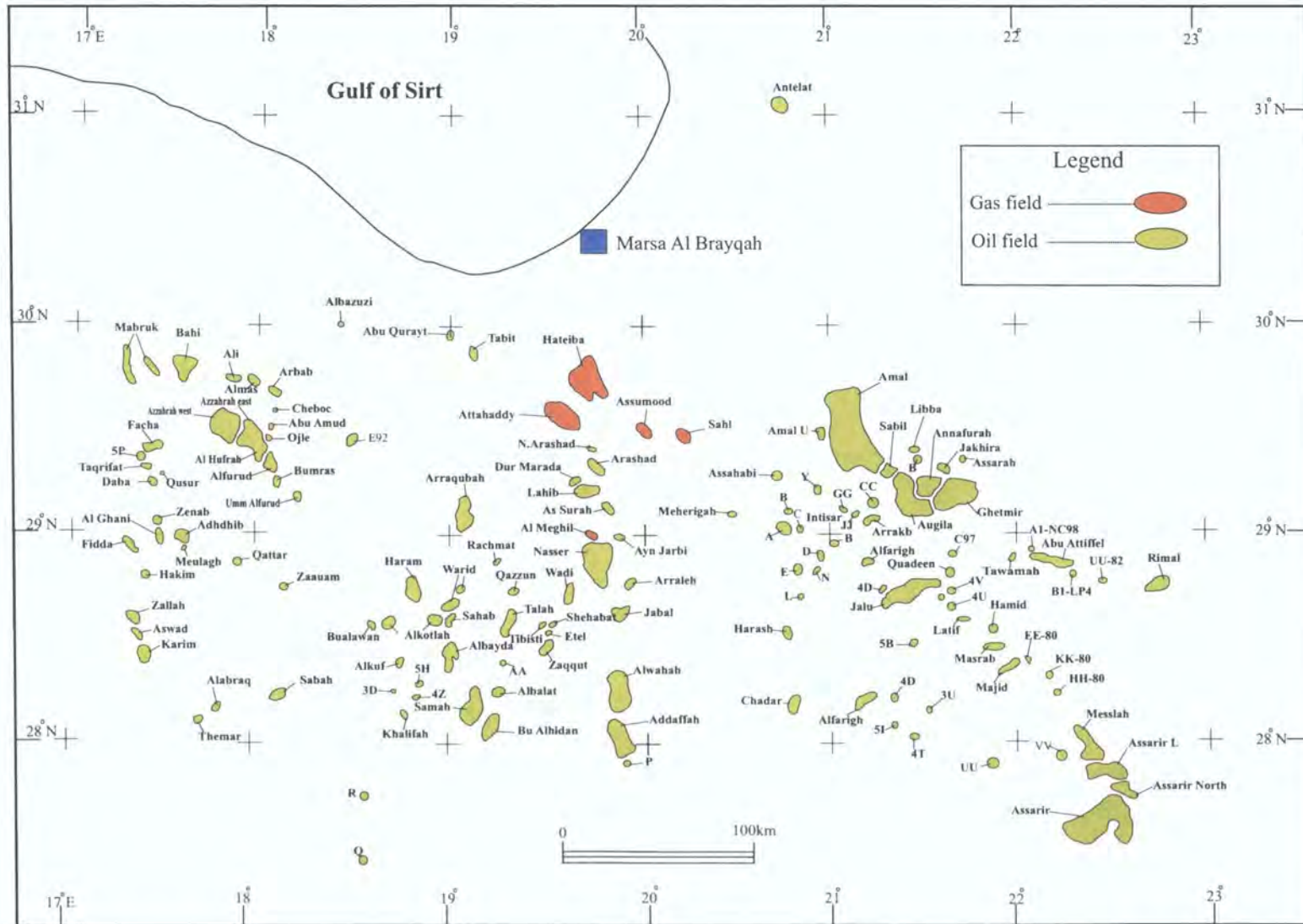


Fig. 1.3 Location of oil and gas fields in the Sirt Basin (after Wennekens et al., 1996).

1.4 Outline of the thesis

Chapter 2 summarises the structural evolution, stratigraphy and hydrocarbon potential of the Sirt Basin. A more detailed description of the geology in the study area is given in Chapter 3. It includes discussion of the stratigraphy, hydrocarbon potential, reservoir character and the geology proved in some wells. Chapter 4 describes the acquisition parameters used to collect the data and briefly outlines the data processing procedures. The original part of this project is the interpretation of the seismic data presented in Chapter 5. Two-way time maps for three horizons have been produced: the Upper Cretaceous Kalash horizon, the Upper Palaeocene-Lower Eocene Kheir horizon and the Middle Eocene Gialo horizon. Depth conversion has not been done due to the limited velocity information available, but an analysis of the effects of depth conversion has been carried out. This analysis suggests that structural features would not be greatly altered by depth conversion.

Two prospective leads have been identified for the Kalash Formation and one prospective lead for the Gialo Formation. The study showed that both wells DDD1-6 and ZZ1-6 were drilled on locations where there was no structural closure. The main conclusions of this study and the recommendations resulting from it are summarised in Chapter 6.

STRUCTURE AND STRATIGRAPHY OF THE SIRT BASIN

2.1 Introduction

The Sirt Basin is located in north central Libya (Fig. 2.1). It is bordered in the east by the Cyrenaica Platform, in the west by the Ghadames Basin, in the south-east by the Al Kufrah Basin, in the south-west by the Murzuq Basin and in the north by the Mediterranean Sea. It covers an area of approximately 400 000 km² onshore (Bender et al., 1996) and extends offshore into the Gulf of Sirt.

The importance of the Sirt Basin for hydrocarbon production has encouraged many researchers to study the basin in order to understand the history behind its evolution. The stratigraphic information included in this chapter has been taken principally from Wennekers et al. (1996).

2.2 Tectonic framework of the Sirt Basin

The general process leading to the structure of sedimentary basins is horizontal extension of the crust and lithosphere. This idea evolved from two basic observations. The first is that sea-floor depth increases away from mid-ocean ridges due to thermal contraction as newly formed oceanic crust cools with time. The other observation is that much of the subsidence of a sedimentary basin is due to the loading effect of the sediments (Bender et al., 1996).

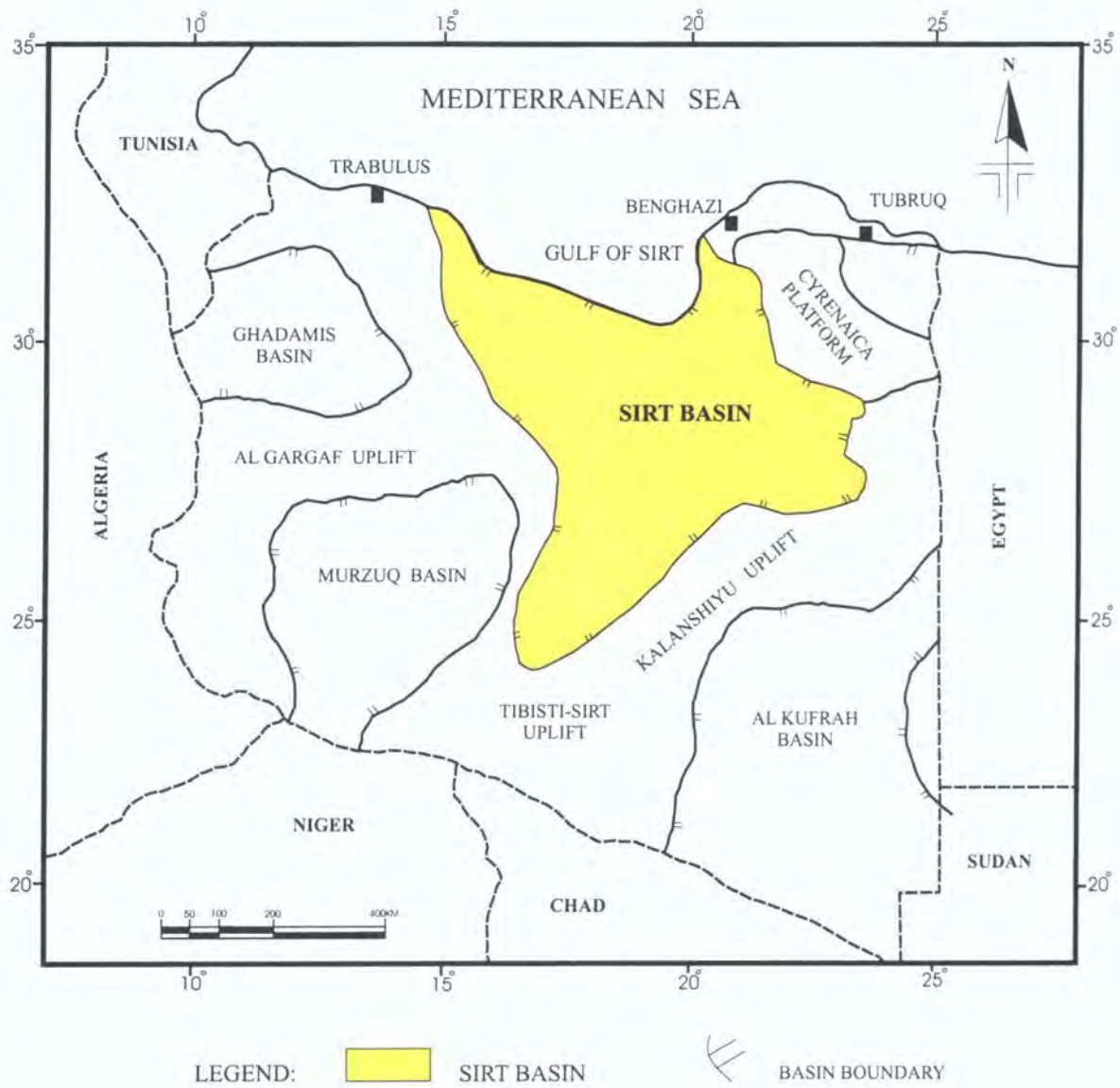


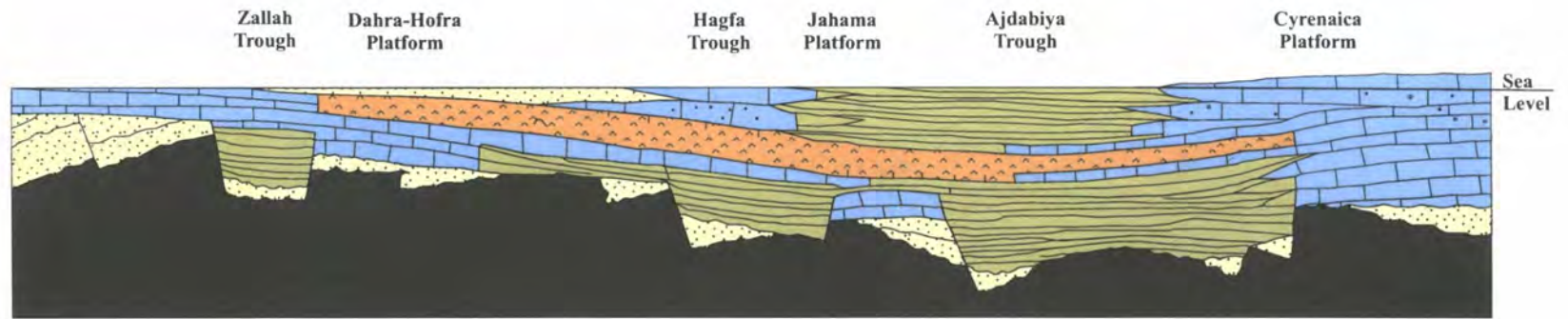
Fig. 2.1 Geographical location map of Sirt Basin.

Structurally, the Sirt Basin consists of a series of depositional troughs separated by platform areas (Bu-Argoub, 1996). The main troughs are, from west to east, the Hun, Zallah (Tagrifet), Hagfa (Marada) and Ajdabiya (Marsa Al Brayqah) (Fig. 2.2). The Ajdabiya (Marsa Al Brayqah) Trough is the deepest, longest and widest trough in the basin, and contains more than 6 km of Upper Cretaceous and Tertiary sediments. To date, no well has yet penetrated the complete sedimentary sequence within the trough (Skuce, 1996). These troughs were the “kitchens” in which the oil in the basin was generated. The oil then migrated upwards along the faults to be trapped in the high areas of the platforms. The graben areas were predominantly filled with thick sequences of shales and marls, while the highest parts of the horst blocks commonly have only thin sediment cover, partly consisting of carbonate buildups.

The Sirt Basin is the youngest sedimentary basin in Libya, as it was formed by large-scale subsidence and block faulting which only started in Late Cretaceous times (Conant and Goudarzi, 1967). In another early paper, Klitzsch (1968) described the Sirt Basin as having been formed in a tensional tectonic regime with large-scale areas of uplift and subsidence and associated normal faulting, but a noticeable absence of compressional folds.

Selley (1997) explained the evolution of the Sirt Basin as follows. The Tibisti-Sirt arch uplifted and domed as a result of the uplifting events of the Caledonian and Hercynian orogenies. The uplifted arch was subjected to the erosion of the pre-rift Palaeozoic sediments covering the arch. This arch, which was oriented north-south, separated the Murzuq and Kufrah basins. The progressive opening up of the Atlantic Ocean was associated with an extensive rift systems across much of Africa. This rift system led to the collapse of the northern part of the Tibisti-Sirt arch, which consequently formed the Sirt Basin. The cross-sections in Fig. 2.3 show the stages in the Sirt Basin's evolution.

South West ————— 575 km ————— North-west



Key

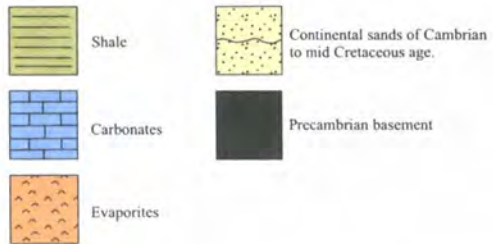


Fig. 2.2. Cross-section across the Sirt Basin showing the main troughs and platforms (after Selley, 1997).

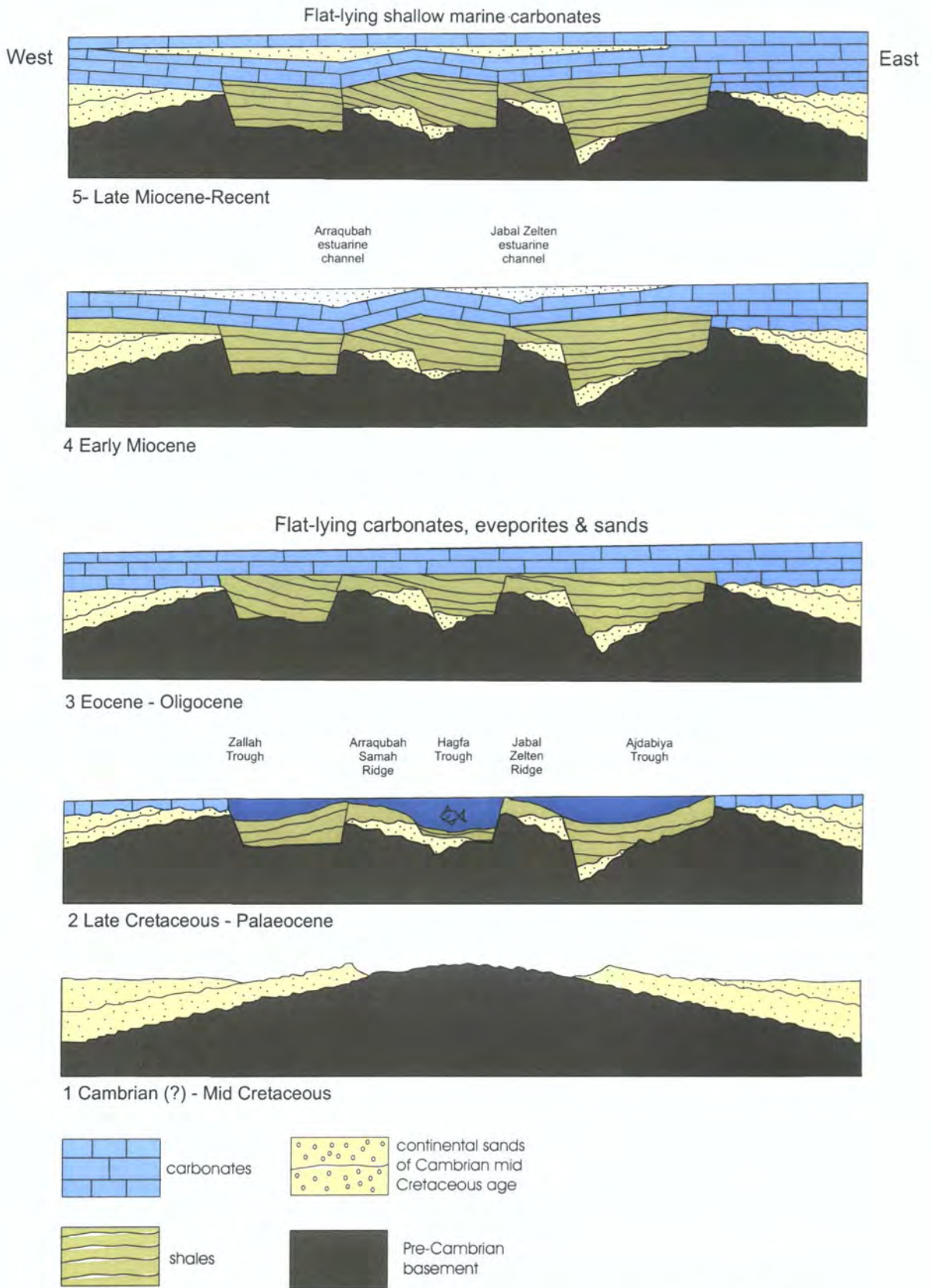


Fig. 2.3. Series of cross-sections showing the structural evolution of the Sirt Basin (after Selley, 1997).

The hot-spot hypothesis was first proposed by Wilson (1963) and then reviewed for Libya by many authors including Burke and Dewey (1974), Van Houten (1983) and Fouad (1991).

Burke and Dewey (1974) proposed that Africa during the Cretaceous was divided into two major subplates, the Saharan plate to the north-west and the East African plate. These two plates were separated by a major belt extending south from the Sirt Basin to the Tibisti mountains and south-westwards through the Chad Basin to the Benue Trough and the Gulf of Guinea (Fig. 2.4). Rifting in the Sirt Basin may have resulted from extensional strains generated in a wide zone between the two subplates when the Africa continent was slowly moving over a fixed Cameroon hot-spot during the past 200 Myr (Burke and Dewey, 1974; Van Houten, 1983).

Fouad (1991) argued that one hot-spot doming event is not sufficient to explain the complex history of the Sirt Basin. He suggested the existence of two hot-spots, one tracking NW-SE and the other NE-SW.

While Burke and Dewey (1974) proposed that the African plate was comprised of two subplates, other researchers referenced by El-Makhrouf (1996) suggested that the African continent during the rifting events was divided into three blocks moving relative to each other (Fig. 2.4). El-Makhrouf (1996) explained that Africa has been affected by three major rift systems as a result of the progressive breakup of Gondwana since early Mesozoic times. The first rifting phase was in the early Mesozoic and was associated with the breakup of Madagascar and Antarctica from east and southeast Africa. The second rifting phase was in the Cretaceous and was associated with the breakup of South America from west and southwest Africa and the opening of the central and south Atlantic Ocean. During this phase of rifting the three blocks of Africa moved relative to each other (Fig. 2.4).

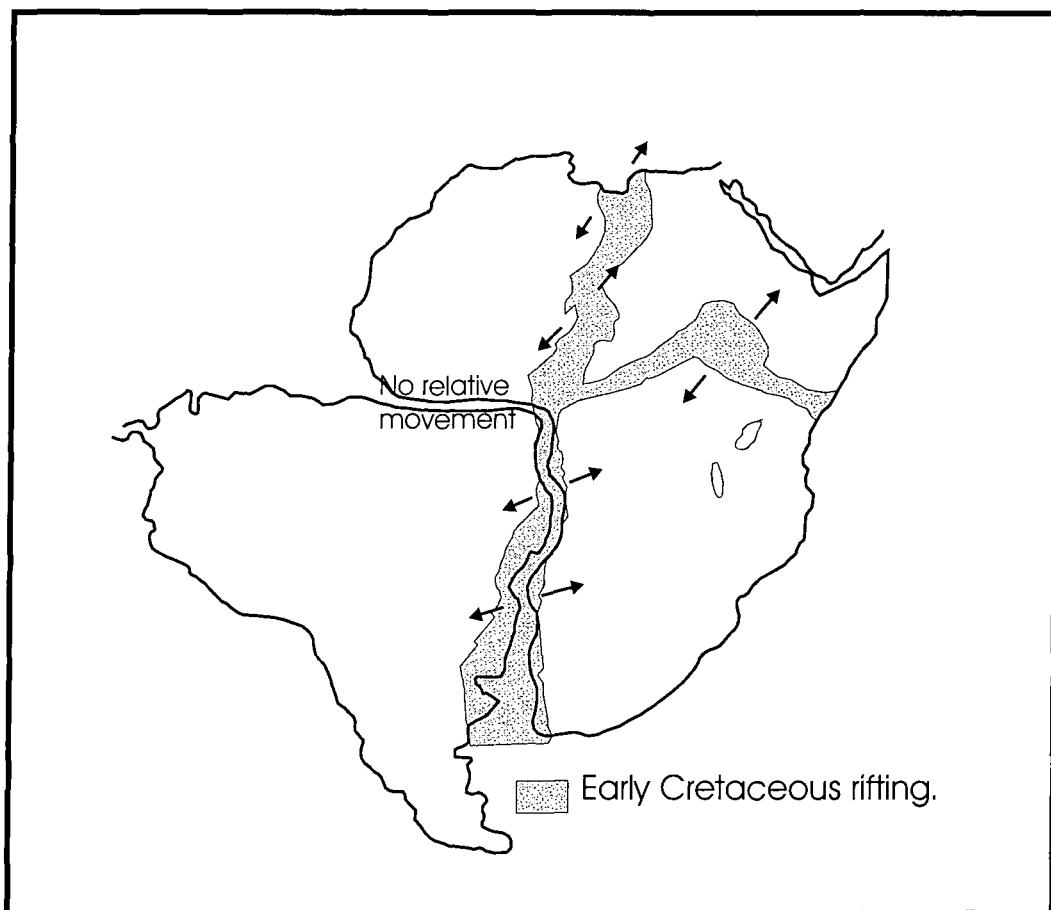


Fig. 2.4. Model showing the possible extension of the opening of the South Atlantic during the Early Cretaceous through Nigeria and eastern Niger and possibly into the Tibisti, Al Kufrah and Sirt basins of Libya (after Fairhead and Green, 1989 as reproduced in El-Makhrouf, 1996).

The third major rifting phase, which started in the Tertiary and continues to the present, was associated with the breakup of Arabia from North Africa and the opening of the Red Sea.

Subsidence in the Sirt Basin started in Cenomanian time, reached its highest rate in the Palaeocene and Eocene, and has subsequently slowed down gradually. This indicates that the major tectonic development of the basin was during the Early Tertiary and not the early Late Cretaceous (Gumati and Kanes, 1985; Gumati and Nairn, 1991).

Faulting in the Sirt Basin has resulted in many structural trends, but the most distinctive structural feature which distinguishes it from the neighbouring basins is the predominant NW-SE fault trend (Fig. 2.5) (Wennekers et al., 1996). The individual troughs are generally asymmetric with north-east dipping western flanks and fault-bounded eastern sides.

2.3 Stratigraphic framework of the Sirt Basin

The sedimentary sequence in the Sirt Basin unconformably overlies the igneous and metamorphic rocks of the Precambrian basement. It consists of Cambro-Ordovician clastic sediments and Early Cretaceous sandstones (pre-rift sequence) which are unconformably overlain by Late Cretaceous-Early Tertiary marine sediments (syn-rift sequence). This sequence is overlain by an Eocene-Early Miocene (post-rift) sequence (Van der Meer and Cloetingh, 1993).

The Precambrian basement is comprised of a wide range of igneous and metamorphic rocks, including granites and volcanics. These rocks serve as petroleum reservoirs where they have been uplifted, weathered and fractured, which is usually the case on horsts, as in the Augila Field (Fig. 1.3) (e.g. Selley, 1997).

The Gargaf Formation (or Hofra as previously named) is a quartzitic sandstone; the bulk of this formation is believed to be of Cambro-Ordovician age. The Ordovician

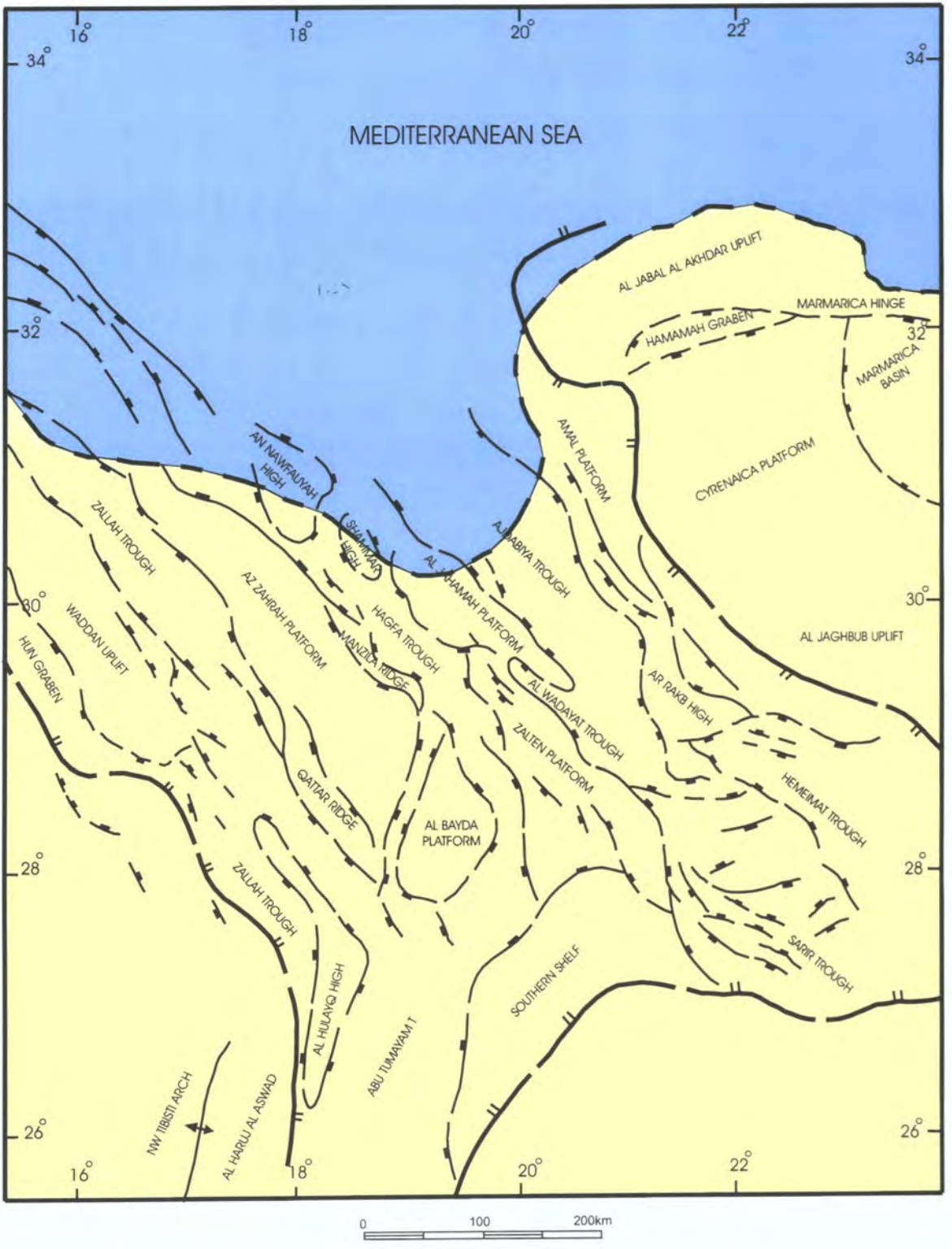


Fig. 2.5. Tectonic elements of Sirt Basin (after Bender et al., 1996).

rocks include sedimentary strata, volcanic, plutonic and metamorphic rocks. Upper and Lower Ordovician strata are present over most of the subsurface of the Sirt Basin. Silurian rocks are predominantly sedimentary in origin with rare volcanics. These rocks have been proved at many localities in the Sirt Basin.

No rocks of Devonian age have yet been found. Carboniferous rocks have recently been documented for the first time in the Sirt Basin. They are represented by sedimentary rocks, depositional environments were mainly continental which changed to marine at the end of the Middle Carboniferous.

Permian, Triassic and Jurassic rocks have been found in the subsurface of the Sirt Basin. Permian rocks are predominantly of non-marine origin, but volcanic rocks have been reported in the central Sirt Basin. They were documented in the Amal Field (Fig. 1.3) according to Wennekers et al. (1996) who referred to Van Eeve (pers. comm., 1993). Triassic rocks are mainly of sedimentary origin, but some volcanic and plutonic rocks are known from boreholes in the central and eastern Sirt Basin. They are producing in the Jakhira Field (Fig. 1.3). Jurassic rocks are predominantly sedimentary in origin, but volcanic and plutonic rocks are known from several boreholes in the Sirt Basin. These rocks have recently been recognized in the Nasser (Zelten) Field according to Wennekers et al. (1996), who referred to Abdullah (pers. comm., 1993).

Rocks of Cretaceous age form important reservoirs in the Sirt Basin. Quartzitic sandstones of Early Cretaceous age form the main oil reservoirs in the eastern Sirt Basin. Clastic and carbonate rocks of the Upper Cretaceous form reservoirs and source rocks. The Upper Cretaceous Sirte Shale is considered to be the principal source rock of hydrocarbons in the Sirt Basin (Selley, 1997).

The Palaeocene sequence in Sirt Basin consists of open marine calcareous shales, shelf carbonates (Bezan, 1996) and evaporites (Abushagur, 1988). Rapid changes in the lateral facies occurred between the platform areas and the deeper parts of

the basin which has resulted in the Palaeocene sequence being the most complex sedimentological sequence in the Sirt Basin (Wennekers et al., 1996). Several unconformities are present in this sequence which make it difficult to map. These unconformities played a major role in the trapping of oil and gas in the Palaeocene sequence.

Unlike the Palaeocene, the Eocene sediments are marked by a greater lateral continuity of stratigraphy, which indicates that the faulting regime slowed down dramatically (Selley, 1997). Several unconformities within these rocks have been recognized in western and eastern exposures and in the subsurface of the Sirt Basin. These rocks consist of a thick variable sequence of carbonates, evaporites and clastics. The Eocene rocks consist of the Gir, Gialo and Augila formations. The Middle and Upper Eocene rocks form an important reservoir in the Sirt Basin, where they are estimated to contribute 15% of the total basin reserves.

The Oligocene strata are bounded by unconformities (Bezan, 1996). Three major types of depositional environments are recognized in the Oligocene sediments: these are represented by continental sandstone in the south, marine shale or carbonates in the north, and a complex pattern of lithological alternations in the marine/continental interface zone (Bezan and Malak, 1996). This sequence is represented in the Sirt Basin by the Arida and Diba Formations (Barr and Weegar, 1972). The sand member of the Arida Formation forms an oil reservoir in some fields (Bezan, 1996). The Diba Formation is producing from only one well located south-west of the Ar Rakb Field (Fig. 1.3).

The Miocene rocks are represented by the Marada Formation. This formation consists of a large number of lithofacies including shales, sandstones, sandy limestones and calcarenites (Barr and Weegar, 1972). In the western part of the basin, the Lower Miocene is represented by the Fortino Formation (Barr and Weegar, 1972). There is an unconformity which separates the Middle and Upper Miocene strata, although the Marada

Formation conformably overlies shales and sands of the Oligocene Diba Formation. The Miocene strata do not form reservoirs in the Sirt Basin (Wennekers et al., 1996).

2.4 Hydrocarbon potential in the Sirt Basin

Oil production in the Sirt Basin started in the late 1950s. The discovery wells were drilled following gravity and magnetic surveys (Selley, 1997). According to Gras and Thusu (1998), over 1600 exploration wells have been drilled in the basin leading to the discovery of 340 oil and gas fields within 18 reservoirs. The basin is the most productive in North Africa, producing 1.4 MMBL of oil per day, with estimated original oil in place of 100 BBBL (Gras and Thusu, 1998). It contains about 70% of the proven hydrocarbons in the region within the Mesozoic section (excluding the Triassic reserves of Algeria) (Macgregor and Moody, 1998). The Sirt Basin contains about 96% of Libya's oil reserves (35.2 BBBL) and 93% of the total oil-in-place (Gumati et al., 1996).

The Sirt Basin has a distinctive property in that its reservoir rocks have been faulted against the source rocks. Consequently, there are good connections between oil kitchens and reservoirs (Harding, 1984). Macgregor and Moody (1996) suggested several factors which lead to the high petroleum productivity of the basin:

- 1- Multiple source rocks.
- 2- Ease of communication between source and reservoirs rocks.
- 3- Traps developed close to kitchens.
- 4- High state of preservation.
- 5- Well-developed regional seals.

It is widely believed that the hydrocarbons in the Sirt Basin were generated from mature intervals which are restricted to the deep parts of the major troughs, from which hydrocarbons have migrated to traps on the structural highs (Fig. 2.5) (Futyan and Jawzi, 1996). Roohi (1996) suggested that the deep Ajdabiya Trough could have generated the hydrocarbon accumulations found on the Zelten Platform, and that the

Al Hagfa (Marada) Trough is the source area for the Az Zahrah-Al Hufrah and Al Bayda platforms (Fig. 2.5).

Most of the discoveries are restricted to the platforms, whereas the troughs remain largely undrilled. Hallett and El Ghoul (1996) suggested that more exploration activity should be undertaken in the troughs. Only 100 wells have been drilled in the troughs which is less than 10% of the total.

2.5 Reservoir, source and seal rocks in the Sirt Basin

2.5.1 Reservoirs

Hydrocarbons in the Sirt Basin have been found in multiple clastic and carbonate reservoirs from Precambrian to Oligocene age (Futyan and Jawzi, 1996; Gumati et al., 1996; Macgregor and Moody, 1996). These hydrocarbons were found within 18 reservoirs (Gras and Thusu, 1998) ranging in depth from 800 m to 4100 m (Macgregor and Moody, 1996).

Three different traps have been identified to accommodate the hydrocarbon reserves in the Sirt Basin. These are structural traps containing about 68%, stratigraphic traps containing about 24%, and the combination of structural-stratigraphic traps containing about 8%. Most of the structural traps occur on highs and tend to be normal-faulted closed anticline type, but the sealed-nose type also exists. Reef carbonates tend to form the most important stratigraphic traps and are mostly Palaeocene in age. Other stratigraphic traps include algal banks, facies changes and shale-out of calcarenites (Futyan and Jawzi, 1996).

Major reservoirs are located in the fractured basement (Precambrian) and in Cambro-Ordovician sandstones of the Gargaf Formation in the Augila, An Nafurah and Amal fields (Fig. 1.3). The Lower Cretaceous Sandstones (Nubian/Sarir) are considered to be the main reservoir for oil accumulations in the eastern Sirt Basin (Gras and Thusu, 1996). They are producing at the Assarir, Amal and Augila fields (Fig. 1.3). Upper

Cretaceous, Palaeocene, Eocene and Oligocene carbonates constitute the main reservoirs at the Bahi, Az Zahrah, Gialo, Al Hufrah, Nasser (Zelten), Al Bayda, Ad Daffah and Ar Raqubah fields (Fig. 1.3) (Gumati et al., 1996).

Over a third of the total oil in place in the Sirt Basin occurs in sandstones. Also of great importance are the uppermost Palaeocene carbonates. The reserves in this pay zone are largely in the Nasser (Zelten) Field (Fig. 1.3) and the Intisar group of reef fields. The third most outstanding interval is the Lower Palaeocene Danian interval which contains large carbonate reservoirs at the Bahi Az Zahrah and Ad Daffah fields (Fig. 1.3). Fourthly, the Senonian interval contains sandstone and carbonate reservoirs.

2.5.2 Source rocks

It is widely known that the main source rocks for hydrocarbons in Sirt Basin are the Lower Cretaceous Nubian variegated shale (Ibrahim, 1991; Gumati et al., 1996), the Upper Cretaceous Sirte and Rachmat shales (Bezan and Malak, 1996) and Danian Hagfa shales (Gumati et al., 1996; Futyan and Jawzi, 1996; Gumati, 1985). Of these, the most productive are the Sirte and Rachmat shales. Silurian and Upper Devonian strata are also expected to contain mature source rocks (Futyan and Jawzi, 1996).

Futyan and Jawzi (1996) stated that the source rocks for the Abu Attiffel and Assarir/Messlah oil fields (Fig. 1.3) have not been identified for certain, although El-Alami (1996) has suggested that the shale intervals within the Rachmat Formation are the principal source rock for the hydrocarbons accumulated in the Hameimat Trough (Fig. 1.3), in which the Abu Attiffel and Assarir/Messlah oil fields are located. Analysis of thermal maturation by Gumati and Schamel (1988) indicated that the Sirt Shales are well matured in terms of oil generation, while the Hagfa Shales have reached the middle stage of maturity.

Bezan and Malak (1996) suggested that the widespread hydrocarbon shows in the Eocene and younger sediments indicate that these hydrocarbons were possibly

generated from Eocene-Miocene shales. Bezan (1996) suggested that the widespread oil shows in the Oligocene and the comparatively high degree of carbonisation of the organic matter of the Upper Eocene and younger shales provide circumstantial evidence of their maturity.

Within the Upper Palaeocene to Lower Eocene, few shale and marl intervals contain oil-prone source rocks. The only area where Eocene source rocks may reach maturity is the northern part of the Ajdabiya Trough (Futyan and Jawzi, 1996).

2.5.3 Seals

Seals in the Sirt Basin are formed by anhydrites, evaporites and shales of Late Cretaceous and Tertiary ages (Gumati et al., 1996). Anhydrites and shales are the principal seals for the Cretaceous reservoirs. Shales and evaporites form the seals for the carbonate reservoirs of the Palaeocene. Lower Eocene carbonate reservoirs are sealed by the shales of the Kheir Formation (Macgregor and Moody, 1996).

GEOLOGY OF THE STUDY AREA

3.1 Stratigraphy in the study area

A generalised stratigraphic section for North Concession 6 is displayed in Fig. 3.1. The sequence contains Cambro-Ordovician, Cretaceous and Tertiary strata. The sedimentary strata in the area of study are over 10500 ft (3.2 km) thick and were deposited on Precambrian basement.

3.1.1 Precambrian Basement

The basement crops out in the south Libyan Mountains (e. g. Jabal Tibisti) and has been reached in some deep wells. It is overlain by the Cambro-Ordovician Gargaf Formation with a regional unconformity. Wells in the study area did not reach the Precambrian basement.

3.1.2 Cambro-Ordovician Gargaf Formation

Rocks of the Gargaf Formation are of Cambro-Ordovician age, and mainly consist of a thick sandstone sequence. This sequence is present throughout most of the subsurface of the Sirt Basin (Barr and Weegar, 1972).

The Gargaf Formation was deposited over the whole of North Concession 6. It unconformably overlies the Precambrian basement and is overlain by the Nubian and Bahi formations. In the study area, the Gargaf Formation is represented by very hard quartzite with some white weathered feldspar grains, and the lithology is very similar to

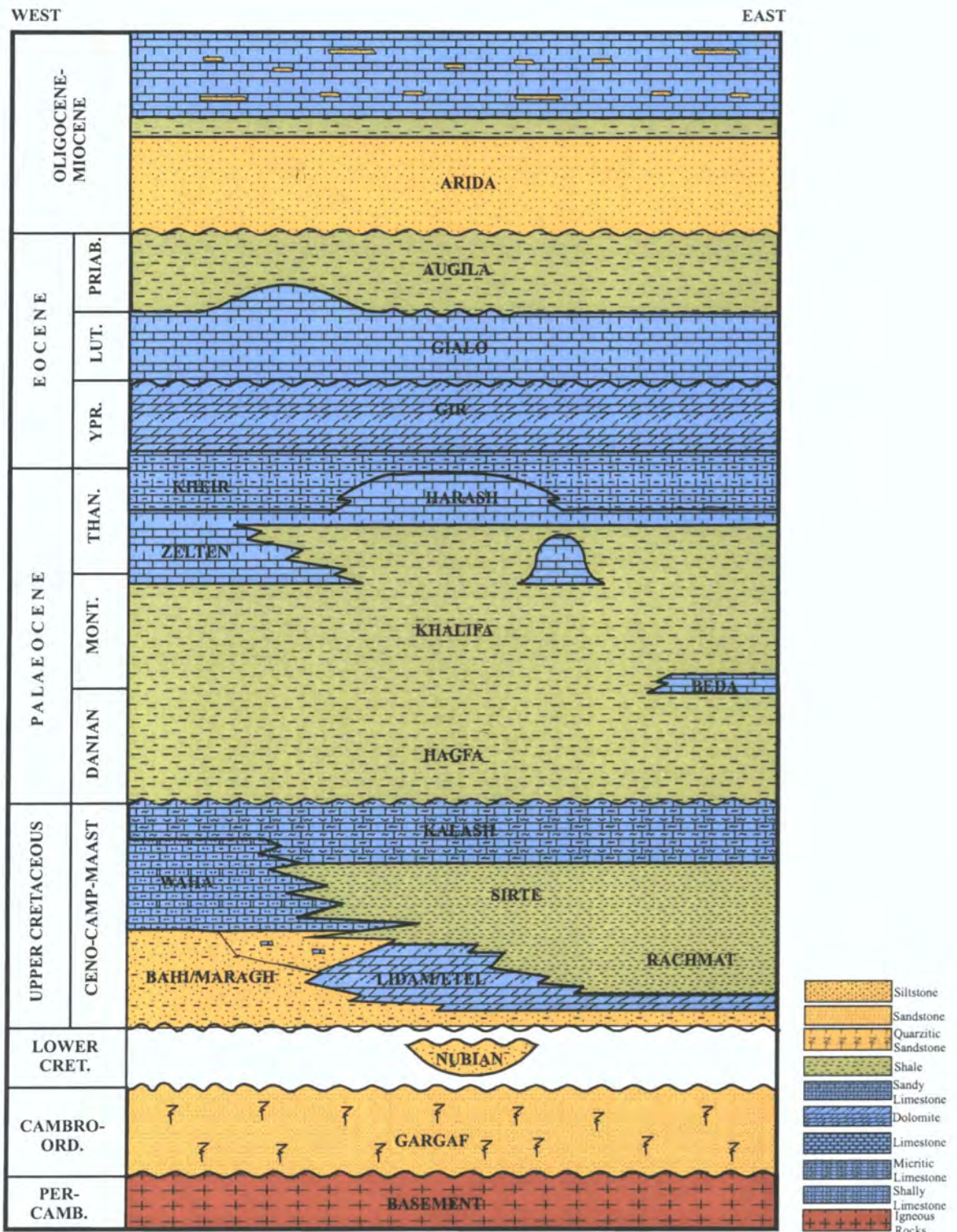


Fig. 3.1 Schematic lithostratigraphy of North Concession 6 (after Weimer, 1998).

the Gargaf Formation in the Assumood Field. The top of the Gargaf Formation is at a depth of 9658 ft sub-sea in well DDD1-6, 10319 ft in well ZZ1-6, 10627 ft in well H12-6 in the Assumood Field southeast the study area, and at 9403 ft in well S12-6 in the Hateiba Field northwest of the study area (Fig. 1.3).

3.1.3 Lower Cretaceous Nubian Formation

The Nubian Formation consists of a variety of interbedded non-marine lithofacies including sandstones, siltstones, shales and conglomerates (Barr and Weegar, 1972). The Nubian Formation has only been reported in the central part of North Concession 6, where it is not productive. The only production to date in Nubian equivalent rock in the western part of the basin is from the Wadi Field (Fig. 1.3), which is located on a fault block in the southern Al Hagfa-Marada Trough (Fig. 2.5). In the study area, the Nubian Formation has not been encountered, but most wells have not reached this level.

3.1.4 Upper Cretaceous Bahi Formation

The Bahi Formation is a sandstone unit interbedded with siltstone, conglomerate and shale. It is present mostly in the subsurface of the western Sirt Basin. It has been formally divided into two members, lower and upper (Sghair, 1996). This formation is known by three names: Bahi, Maragh and Basal Sandstone (Barr and Weegar, 1972). It unconformably overlies the Cambro-Ordovician Gargaf Formation and is commonly overlain by the Etel/Lidam Formation, but in some places is overlain by other Upper Cretaceous formations, such as the Argub, Rachmat, Sirte, Kalash and Waha formations, ranging in age from Cenomanian to Maastrichtian (Sghair, 1996). This formation is considered to represent the first product of the major Upper Cretaceous marine transgression in the Sirt Basin (Gras and Thusu, 1998). It forms the main reservoir at such fields as Haram, Bahi and Attahaddy (Fig. 1.3). Also it is a major reservoir for the Nafurah-Augila, Waha, Ar Raqubah and Hateiba fields (Fig. 1.3)

(Macgregor and Moody, 1996). The boundaries of this formation are poor seismic reflectors, especially the lower boundary, so it cannot be differentiated from the Gargaf on seismic sections. Therefore they map as one formation called Bahi/Gargaf (Wennekers et al., 1996).

The Bahi-Gargaf Formation is one of the reservoirs in the Assumood Gas Field (Perrella, 1990). This formation was found in the H8-6 and H12-6 wells in the Assumood Field. It was not present in the H1-6 well and was not reached in the rest of the Assumood Field wells (Broughton and Buthfer, 2000). This formation was not present in O2-6 well in the Sahl Field (Fig. 1.3) and was not reached by drilling in the other Sahl Field wells (Broughton and Buthfer, 2000).

3.1.5 Upper Cretaceous Lidam/Etel Formation

This formation is a carbonate sandstone formation that provides reservoirs at several fields, such as the Khalifa, Dur Mansur, Masrab, Mabruk and Bualawan fields (Fig. 1.3). The equivalent formation to the Lidam/Etel formation in the western Sirt Basin is the Nalut Formation.

In North Concession 6, the Lidam/Etel Formation is present in the eastern and central parts of the area, while it is absent in the western part. It overlies the Bahi/Maragh Formation and is overlain by the Rachmat Formation in the eastern part and by Sirte Formation in the central part. The Lidam/Etel Formation has not been recognised in the available well data in the study area.

3.1.6 Upper Cretaceous Rachmat Formation

According to Barbieri (1996), this formation was first informally proposed by Williams (1968) as the Rachmat Shale. Subsequently it was formally described by Barr and Weegar (1972). It consists mainly of a shale section with minor limestone, sandstone and occasional dolomite interbeds (Barr and Weegar, 1972). The carbonate beds within

the upper portion of this formation form reservoirs at several places, mainly in the eastern Sirt Basin. The Rachmat Formation has been found in the eastern and central parts of North Concession 6, but has not been reported in the western part of the area. It overlies the Etel/Lidam Formation and is overlain by the Sirte Formation. In the study area, the Rachmat Formation has not been reported in the wells which were drilled to this level.

3.1.7 Upper Cretaceous Sirte Shale Formation

The Sirte Shale Formation in the Sirt Basin consists mainly of a shale sequence with thin limestone interbeds. This formation unconformably overlies the Rachmat Formation and is conformably overlain by limestones of the Upper Cretaceous Kalash Formation. It is considered to be the principal source rock of hydrocarbons in the Sirt Basin (Selley, 1997) and also serves as a caprock for Tagrifet Limestone reservoirs in the eastern Sirt Basin. At certain localities in the Sirt Basin it sources reservoirs in the Kalash Limestone. The Sirte Shale is absent at several places in the Sirt Basin.

In the area of study, the Sirte Shale Formation has been reported only in wells H2-6 and H12-6 of the Assumood Gas Field and is absent in well H1-6. It was not reached in the other Assumood Field wells. It consists of three units, shale, dolomite and sand. This formation is not present at the DDD1-6 and ZZ1-6 wells. It was found at a depth of 10541ft in well H2-6 and at 10172 ft in well H12-6 (Broughton and Buthfer, 2000). In the Sahl Field, the Sirte Shale Formation has been found in three wells at depths around 11000ft.

3.1.8 Upper Cretaceous Waha Formation

The Waha Formation has long been recognised as a hydrocarbon reservoir in the Sirt Basin. It consists of skeletal calcarenites with subordinate lime muds in the type section (Barr and Weegar, 1972). It is the principal reservoir in the giant Al Waha Field (Fig. 1.3) in the central Sirt Basin. This formation also produces oil in several fields in Concession

6, notably the Lahib, Jabal and South East Nasser (Zelten) fields, all located on the Zelten Platform (El-Ghoul, 1996), amongst others. In North Concession 6, a thick section of Waha Formation is present in the west, while it is absent in the east part and very thin in the centre. It overlies the Sirte, Bahi and Gargaf formations (Fig 3.1). The Waha Formation has not been reported from the wells in the area of study and the surrounding gas fields, although drilling has not reached the level of the Waha Formation in many wells in the Assumood and Sahl fields.

3.1.9 Upper Cretaceous Kalash Formation

This formation was identified and named by Barr and Weegar (1972) who determined that it is of Maastrichtian age. It consists mainly of limestone with interbeds of shale and was deposited throughout most of the Sirt Basin. It generally ranges in thickness from 100 to 300 feet and conformably overlies the Sirte Shale, but in some places it conformably overlies other Upper Cretaceous formations such as the Samah Dolomite and the Waha Limestone, or unconformably overlies older rocks such as the Early Cretaceous rocks, the Gargaf/Hofra Formation or the Precambrian igneous basement. The Kalash is commonly conformably overlain by the Palaeocene Hagfa Shale or Lower Sabil Carbonate. The lateral equivalents of the Kalash Limestone are the Waha Limestone and Lower Satal Formation. It produces gas in some of the Assumood Field wells (Perrella, 1990).

In North Concession 6, the Kalash Formation believed to be deposited over all the area. It overlies the Sirte Formation in the eastern and central parts of North Concession 6 while it overlies the Waha Formation in the western part. The Kalash Formation is unconformably overlain by the Hagfa Formation. In the area of study, the Kalash Formation ranges in depth from 9298 feet in the Hateiba Field to 10364 ft at well H2-6 in the Assumood Field. It was found at a depth of 10301 ft in the DDD1-6 well.

3.1.10 Lower Palaeocene Hagfa Formation

The Hagfa Formation is the oldest unit of the Palaeocene sequence and was developed throughout the whole of the Sirt Basin except on the west of the Al Bayda Platform and the crestal parts of Ad Daffah High (Fig. 2.5) (Sinha and Mriheel, 1996). This formation mainly consists of a shale sequence with interbeds of limestone (Barr and Weegar, 1972). It conformably overlies the Maastrichtian Kalash Limestone or the Lower Satal Formation, and is conformably overlain by the Lower Beda or Khalifa Formation (Sinha and Mriheel, 1996). There is a difficulty in mapping the top of Hagfa Formation in areas where the Beda Formation is absent because there is no distinctive lithological boundary between the top of the Hagfa and the Khalifa Shale (Wennekers et al., 1996).

In terms of oil maturity, the Hagfa Formation is less mature than the Sirte Shale Formation (Sinha and Mriheel, 1996). Nevertheless, it is considered to be the second major source rock in the Sirt Basin, as it supplies the Palaeocene reservoirs (Selley, 1997; Sinha and Mriheel, 1996).

This formation has been reported in all wells in the area that have reached this level. It serves as a seal for Kalash Limestone reservoirs in the area of study. Its depth ranges from 7876 ft at the S12-6 well in the Hateiba Field to 8586 ft at the H2-6 well in the Assumood Field, and it is at a depth of 8141 ft in well DDD1-6. In the Sahl Field to the south-east of the study area it is at a depth of 9195 ft (Broughton and Buthfer, 2000).

3.1.11 Middle Palaeocene Beda Formation

The Beda Formation consists of various interbedded limestone lithofacies with subordinate dolomite and calcareous shale. It forms reservoirs in some fields in the Sirt Basin (Barr and Weegar, 1972). It is thought to be the major producing interval in the Lower Palaeocene.

In North Concession 6 (Fig. 3.1), the Beda Formation has been found in the western part where it is represented by a thin limestone bed. It overlies the Hagfa

Formation and is overlain by the Khalifa Formation. In the study area, the Beda Formation has not been recognized.

3.1.12 Upper Palaeocene Khalifa Formation

This formation is found in the subsurface of the western and central Sirt Basin. It is divided into two members, an upper limestone unit and lower shale unit. Its age was suggested by Barr and Weegar (1972) to be Early Landenian.

The lateral equivalent of the lower shale unit of this formation is the Dahra Limestone Formation (Barr and Weegar, 1972), so in areas where the Dahra is present, the Khalifa Formation is represented only by its upper limestone unit. The Khalifa Shale unit was deposited as a result of a rise in sea level that occurred by the close of Early Landanian time. This sea level rise covered most of the Sirt Basin (Bezan, 1996). The limestone unit of this formation was deposited in a shallow marine environment (Barr and Weegar, 1972) and forms a mappable unit over most of the central and western Sirt Basin.

In the area of study, the Khalifa Formation is represented by both shale and limestone units. Its two units were recognized clearly in the H12-6 well, where the shale unit is much thicker than the limestone unit. This formation is present throughout the Assumood and Sahl fields and in both wells DDD1-6 and ZZ1-6. The Khalifa Formation ranges in depth from 7916 ft at the H1-6 well to 8325 ft at the ZZ1-6 well. Its depth is 8975 ft in the O1-6 well at the Sahl Field (Broughton and Buthfer, 2000).

3.1.13 Upper Palaeocene Zelten Formation

The Zelten Group is divided into two formations, Zelten and Harash. The Zelten Group normally overlies the Khalifa Formation and is conformably overlain by the Kheir Formation or, rarely, by the Lower Eocene Gir Formation (Barr and Weegar, 1972). The Zelten Formation consists of a limestone sequence with very subordinate amounts of

shale (Barr and Weegar, 1972). It forms reservoirs at such fields as Intesar, Nasser (Zelten) and Az Zahrah.

In North Concession 6 (Fig. 3.1), the Zelten Formation has been found in the western part, while it is replaced by the Harash Formation in the eastern and central part. It overlies the Khalifa Formation and overlain by the Kheir Formation. In the area of study and surrounding fields; the Zelten Formation has not been recognised.

3.1.14 Upper Palaeocene Harash Formation

The Harash Formation consists mainly of soft, chalky argillaceous calcilutite and muddy calcarenite with thin interbeds of calcareous, fossiliferous shale (Barr and Weegar, 1972). It conformably overlies the Upper Palaeocene Zelten Limestone or Upper Sabil Carbonate. It is conformably overlain by the Kheir Formation or more rarely the Lower Eocene Gir Formation (Barr and Weegar, 1972).

In the study area the Zelten Group is represented only by the Harash Formation. This formation consists mainly of calcilutites and shales. The Harash Formation was found in all wells drilled in the area. Other wells in the Assumood and Sahl fields were not drilled deep enough to reach this formation. It ranges in depth from 7622 ft in well H1-6 in the Assumood Field to 8847 ft in well O1-6 at the Sahl Field, while it is at a depth of 7721 ft in well DDD1-6 and at a depth of 8103 ft in well ZZ1-6 (Broughton and Buthfer, 2000).

3.1.15 Upper Palaeocene-Lower Eocene Kheir Formation

The Kheir Formation has lithologies ranging from shale through marl to limestone. It is conformably overlain by the Lower Eocene Gir Formation and conformably overlies the Palaeocene Upper Sabil Carbonate (Barr and Weegar, 1972). It was deposited over a large portion of the Sirt Basin. There is some evidence that this formation straddles the Eocene-Palaeocene boundary (Ypresian–Landenian) with a thin shale unit marking the

close of Palaeocene time (Bezan, 1996). The Kheir Formation was deposited as a result of a major transgression of the Late Palaeocene sea which brought deeper water conditions over the whole area of the Sirt Basin. In general, the thickness of the Kheir Formation extends to more than 400 ft. Thicker sections usually developed in the troughs while those over the platforms are much thinner (Sinha and Mriheel, 1996). This formation marks the end of the Palaeocene as the succeeding upper part of the Kheir Shale is of Early Eocene age.

In the area of study the Kheir Formation has been found in most of the wells. Some wells in the Assumood and Sahl fields were not drilled deep enough to reach this formation. The Kheir Formation ranges in depth from 7057 ft in well S12-6 to 7935 ft in well O1-6, while it is at a depth of 7411 ft in well DDD1-6, and at a depth of 7678 ft in well ZZ1-6. Its thickness ranges from 310 ft at well DDD1-6 to 920 ft at well O4-6 in the Sahl Field.

3.1.16 Lower Eocene Gir Formation

The Gir Formation consists of a sequence of interbedded dolomites and anhydrites with subordinate amounts of limestone and shale (Barr and Weegar, 1972). This formation is conformably overlain by the Gialo formation in most of the Sirt Basin, but in the north-west it is unconformably overlain by the Gedari Formation (Barr and Weegar, 1972). The Gir Formation usually overlies either the Upper Palaeocene Harash Formation or the Kheir Formation. Palaeontological evidence indicates that the Gir Formation is Lower Eocene in age. This formation forms an oil reservoir in some areas in the Sirt Basin such as the Daba and Facha fields (Fig. 1.3).

In the study area, the Gir Formation is present in all wells. Some wells in the Assumood and Sahl fields were not drilled deep enough to reach the Gir Formation. It is represented in the study area by limestone which makes it difficult to differentiate between this formation and the overlying Middle Eocene Gialo Formation. It ranges in

depth from 6132 ft in well O15-6 to 6809 ft in well O8-6, both in the Sahl Field, while it is at a depth of 6331 ft in well DDD1-6 and at 6648 ft in well ZZ1-6.

3.1.17 Middle Eocene Gialo formation

This formation consists of a thick shallow marine limestone sequence. The existence of abundant nummulites in this formation indicates that most of the formation is Middle Eocene in age (Barr and Berggren, 1980), but there is some evidence indicating that the upper few feet of this formation may be Upper Eocene (Barr and Weegar, 1972). The Gialo Formation forms a hydrocarbon reservoir in some areas in the Sirt Basin.

In the area of study, the Middle Eocene Gialo Formation has been found in all wells drilled in the area. It is represented by a thick limestone section and ranges in depth from 4703 ft in well H7-6 at the Assumood Field to 6641 ft in well S12-6 at the Hateiba Field, while it is at 5159 ft depth in well DDD1-6 and at 5209 ft depth in well ZZ1-6.

3.1.18 Upper Eocene Augila Formation

This formation is divided into three units: the lowest unit is shale, the middle unit is quartz sandstone and the upper unit is sandy limestone. It is Upper Eocene in age (Barr and Weegar, 1972). The shale unit was deposited under inner to middle neritic open sea conditions, while the sandstone and limestone units were deposited in a shallower water, more restricted environment. This formation marks the close of the Eocene epoch (Barr and Berggren, 1980).

In the area of study, this formation has been found in all wells. It ranges in depth from 4231 ft in well H6-6 at the Assumood Field to 4903 ft in well ZZ1-6. The top of this formation was not differentiated at the S12-6 well.

3.1.19 Lower Oligocene Arida Formation

The Arida Formation is divided into two members, a lower sandstone unit and an overlying shale unit. It is confirmed to be of Early Oligocene age by biostratigraphic data. It unconformably overlies Eocene strata and is conformably overlain by the Upper Oligocene Diba Formation (Barr and Weegar, 1972). The sandstone member of this formation is widely known as the Chadra Sandstone member (Bezan and Malak, 1996), which forms the main oil reservoir in the Jalu Field (Fig. 1.3), amongst others (Bezan, 1996). Late movement of faults may have allowed oil to move from deep source beds into the Arida reservoir and/or to remigrate from already entrapped oil. The cap-rock for the Arida Sandstone is the thin shale within the formation itself (Wennekers et al., 1996).

In the Assumood Field this formation was penetrated in all wells and consists of sandstones interbedded with subordinate shales. It ranges in depth from 2570 ft in well H8-6 at the Assumood Field to 3066 ft in the well ZZ1-6, while it is at a depth of 2976 ft in well DDD1-6. The thickness of Arida Formation in the study area ranges from 1665 ft in well H1-6 at the Assumood Field to 1837 ft in well ZZ1-6, while it was at 1740 ft in well DDD1-6. The gas reservoir in this formation occurs in the upper part of two sandstone units separated by approximately 150 ft of shale and thin beds of sandstone. The seal for this gas unit is formed by the overlying alternating shale, shaley sandstone and siltstone beds (Sirte Oil Company, 1999. OOOO1-6 Prospect Description. Unpublished internal report).

3.1.20 Upper Oligocene Diba Formation

This formation consists of an alternating sequence of thick sandstone units and thin shales. It conformably overlies the shale member of the Arida Formation and is overlain by the Lower Miocene Marada Formation (Barr and Weegar, 1972). Where the shale

bed which separates the two formations is absent, the distinction between the Arida and Diba formations becomes difficult (Barr and Weegar, 1972; Bezan and Malak, 1996).

The Diba Formation is believed to exist throughout the area of study, but as this formation has no hydrocarbon prospectivity in the area, it was not logged in all the wells.

3.2 Hydrocarbon potential in North Concession 6

The hydrocarbons discovered in North Concession 6 to date are gas and are producing from four gas fields. Walston (1970) gave a possible explanation for the absence of oil in North Concession 6. Early migration of hydrocarbons occurred shortly after deposition, filling the structures present. Continued generation and migration of hydrocarbons through Tertiary time could have resulted in gas displacing oil downwards in these structures. Intermittent tilting of the basin northwards eventually may have raised the spill point to above the level of the oil column trapped within these closures. This in turn allowed secondary migration of fluids up the regional dip of the Zelten Platform towards the south.

The area of study is surrounded by the above-mentioned gas fields which suggests that any prospective location found in this area is more likely to contain gas. The origin of the gas accumulations in North Concession 6 has not been proved. Hallett and El Ghoul (1996) suggested that the Sirte Shale in the Wadayat Trough is gas-prone and probably sourced the gas fields of Sahl, Assumood and perhaps Attahaddy. Meanwhile Roohi (1996) argued that the asymmetrical shapes of the troughs in the western Sirt Basin and the regional structural downward slopes of both platforms and troughs towards the axis of the Ajdabiya Trough suggest that hydrocarbon migration trends had to be mainly WSW. Therefore, the hydrocarbons generated in the Ajdabiya Trough could have been trapped in the Zelten Platform and high areas, while hydrocarbons generated in the Al Hagfa Trough could have been trapped in the Az

Zahrah-Al Hufrah Platform (Futyan and Jawzi, 1996 and Roohi, 1996). In conclusion, either or both the Ajdabiya and Wadayat troughs may have contributed to the hydrocarbon accumulations in the Zelten Platform.

3.2.1 Assumood Gas Field

Located in North Concession 6 (Fig. 1.2), in the south-east of the area of study, this field is bounded to the north by the Ajdabiya Trough and to the south by the Wadayat Trough. The discovery well H1-6 was drilled in 1960. Geologically it is located on a structural high. This field is producing mainly from the Middle Eocene carbonates of the Gialo Formation. Also commercial quantities of gas were found in the Oligocene Arida Formation, the Upper Cretaceous Kalash Formation and the Cambro-Ordovician Bahi Formation (Perrella, 1990).

3.2.2 Sahl Gas Field

This field is located south-east of the area of study (Fig. 1.2). It was discovered in 1962 and is producing gas from Middle Eocene carbonates of the Gialo Formation, which is considered to be the main reservoir in this field.

3.2.3 Hateiba Gas Field

This field is located in North Concession 6 (Fig. 1.2), north-west of the area of study. The S1-6 discovery well was drilled in 1963. It is producing gas from the Early Upper Cretaceous sandstones of the Bahi Formation.

3.2.4 Attahaddy Gas Field

This field is located in the north-west of Concession 6 (Fig. 1.2), west of the area of study on the far side of the Wadayat Trough. The FF1-6 discovery well was drilled in 1964. It is producing gas from the fractured Cambro-Ordovician Bahi-Gargaf Formation.

3.3 Reservoir, source and seal rocks in study area

3.3.1 Reservoirs

The reservoirs which have been found in the surrounding fields and are expected to exist in the area of study are: Cambro-Ordovician Bahi/Gargaf Formation, Upper Cretaceous Kalash Formation, Middle Eocene Gialo Formation and Lower Oligocene Arida Formation.

3.3.2 Source rocks

In the area of study, the main source rocks are the Sirte and Hagfa shales. The source of the gas in the study area is likely to be the same as in the Assumood and Sahl fields. They were sourced from the Sirte and Hagfa shale formations in the Wadayat Trough and Ajdabiya Trough. In the Wadayat Trough, gas appears to have migrated up through the faults from the south-east side of the structure. The source of gas in the Arida Formation and in the Gialo Formation is likely to be the Sirte Shale with migration upwards through the faults.

3.3.3 Seals

In the area of study, there are two possible ways of sealing for the Gargaf Formation, by either Hagfa or Sirte shales, dependent on the presence of the pre-Kalash section (Sirte Shale). If the Sirte Shale is present, it serves as a thin seal for the Gargaf Formation; if the Sirte Shale is absent, the Gargaf Formation will be sealed by Hagfa Shale. The Gialo Formation is sealed by the thick calcareous shale of the Augila Formation, and the Arida Formation is sealed by interbedded shales within the Arida Formation.

3.4 Lithological description of the well data

3.4.1 DDD1-6 well description

The sedimentary sequence in well DDD1-6 is illustrated in Fig. 3.2. The well was drilled to a total depth of 9805 ft sub-sea and reached the Cambro-Ordovician Gargaf Formation at a depth of 9658 ft. The Gargaf Formation is overlain by the Upper Cretaceous Kalash Formation, represented by 37 ft of micritic limestone. The Upper Cretaceous Sirte, Waha, and Bahi formations are absent at the well location.

The Lower Palaeocene Hagfa Formation overlies the Kalash Formation and it consists mainly of shale with a thickness of about 1480 ft. The Khalifa Formation overlies the Hagfa Formation and is represented by its limestone member. It is about 180 ft thick. It is overlain by the Zelten Group which is represented by the Harash Formation and consists of limestone divided into two units, a lower porous limestone unit overlain by an upper tight limestone unit. The Zelten Group is overlain by the Kheir Formation which consists of two units at this location, a calcareous shale and limestone unit overlain by a marl unit. The Gir Formation overlying the Kheir Formation is a clean limestone section, which makes it difficult to differentiate it from the overlying Middle Eocene Gialo Formation of similar lithology.

The Augila Formation overlying the Gialo Formation is about 450 ft thick and consists of calcareous shale. It is overlain by the Oligocene Arida Formation which consists of interbedded sand and shale beds. The shale units are thicker in the upper part while the sand units are thicker in the lower part. The Arida Formation is overlain by an undifferentiated Oligocene and Miocene sequence consisting mainly of sand and shale units.

3.4.2 ZZ1-6 well description

The sedimentary sequence in well ZZ1-6 is illustrated in Fig. 3.3. The well was drilled to total depth of 10515 ft sub-sea and reached the Cambro-Ordovician Gargaf Formation at



Figure 3.2. Lithologic log of Well DDD1-6. Depths were measured in feet from sea level. Not to scale.

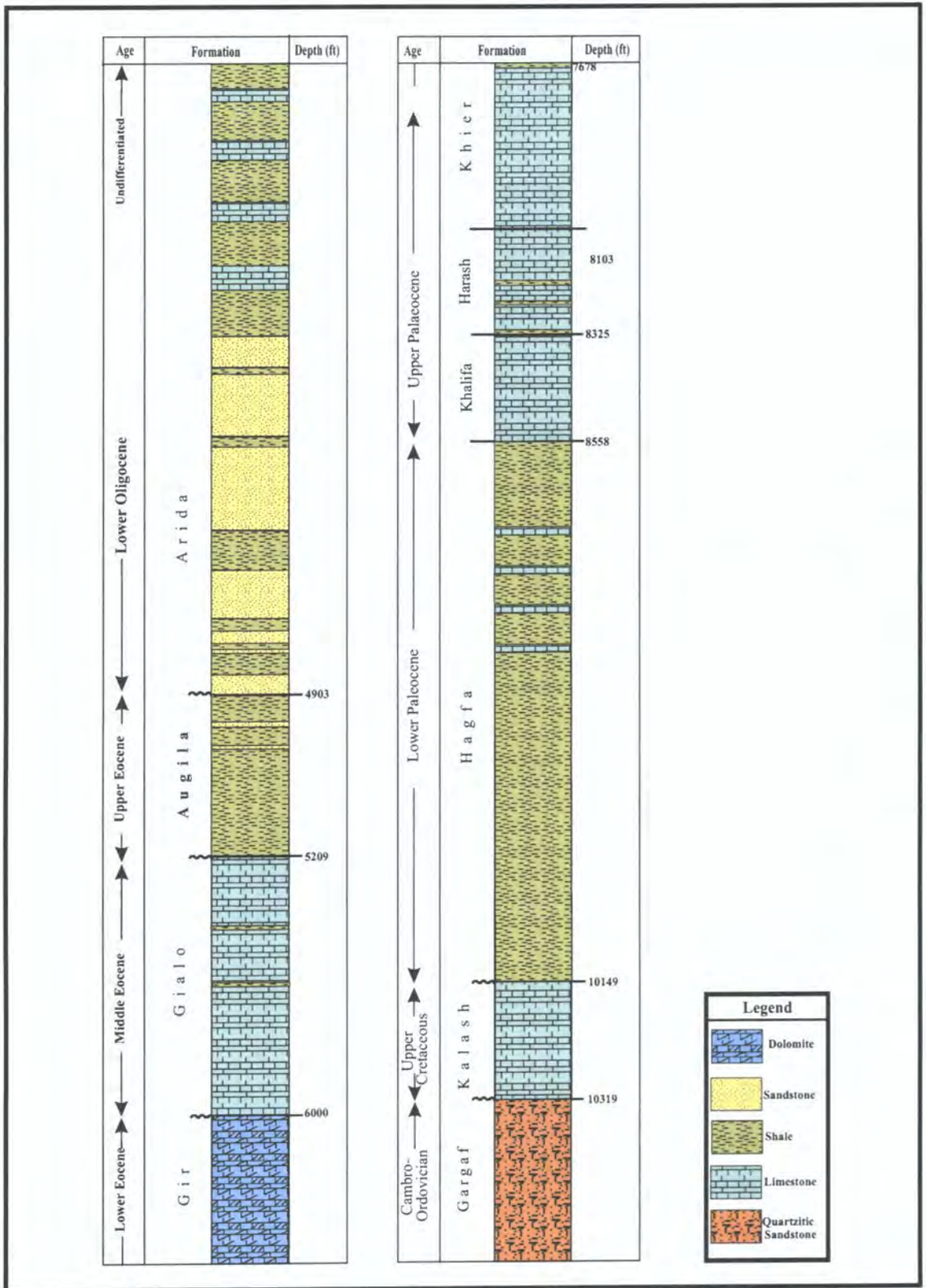


Figure 3.3 Lithologic log of Well ZZ1-6. Depths were measured in feet from sea level. Not to scale.

a depth of 10319 ft. The Gargaf Formation is overlain by 170 ft of limestones of the Upper Cretaceous Kalash Formation. The Bahi, Waha and Sirte formations are absent in this well.

The Hagfa Formation overlies the Kalash Formation and consists of a thick shale section with micritic and argillaceous limestone interbeds. The Khalifa Formation is represented by its shale unit in this area. It is overlain by the Harash Formation which consists of a limestone section divided into two units, porous and tight. The Kheir Formation is divided into two units, a limestone unit and a marl unit. The Gir Formation is represented by a limestone section overlain by limestones of the Gialo Formation with a combined thickness of 2464 ft.

The Augila Formation unconformably overlies the Gialo Formation and consists mainly of a shale section. It is separated by another unconformity from the overlying Arida Formation which consists of a sand section. From the Arida Formation to the surface, there are limestone interbeds with shales, sand and dolomite. The Oligocene and Miocene rocks are not differentiated.

3.4.3 S12-6 well description, Hateiba Field

The sedimentary sequence in well S12-6 is illustrated in Fig 3.4. The total depth was 9493 ft. The lithology of well S12-6 starts with the Cambro-Ordovician Gargaf Formation. It consists of a quartzitic sandstone sequence. The Upper Cretaceous Bahi Formation might be present, but it is not differentiated from the Gargaf Formation. The Upper Cretaceous Sirte and Waha formations are absent in this well. The Gargaf Formation is overlain by the Upper Cretaceous Kalash Formation which starts with about 20 ft of conglomerate and then continues with argillaceous limestone. A shale unit is present near the top of this formation.

The Upper Palaeocene Hagfa Formation mainly consists of a shale sequence with stringers of calcareous shale and siltstone. The Khalifa Formation is believed to be

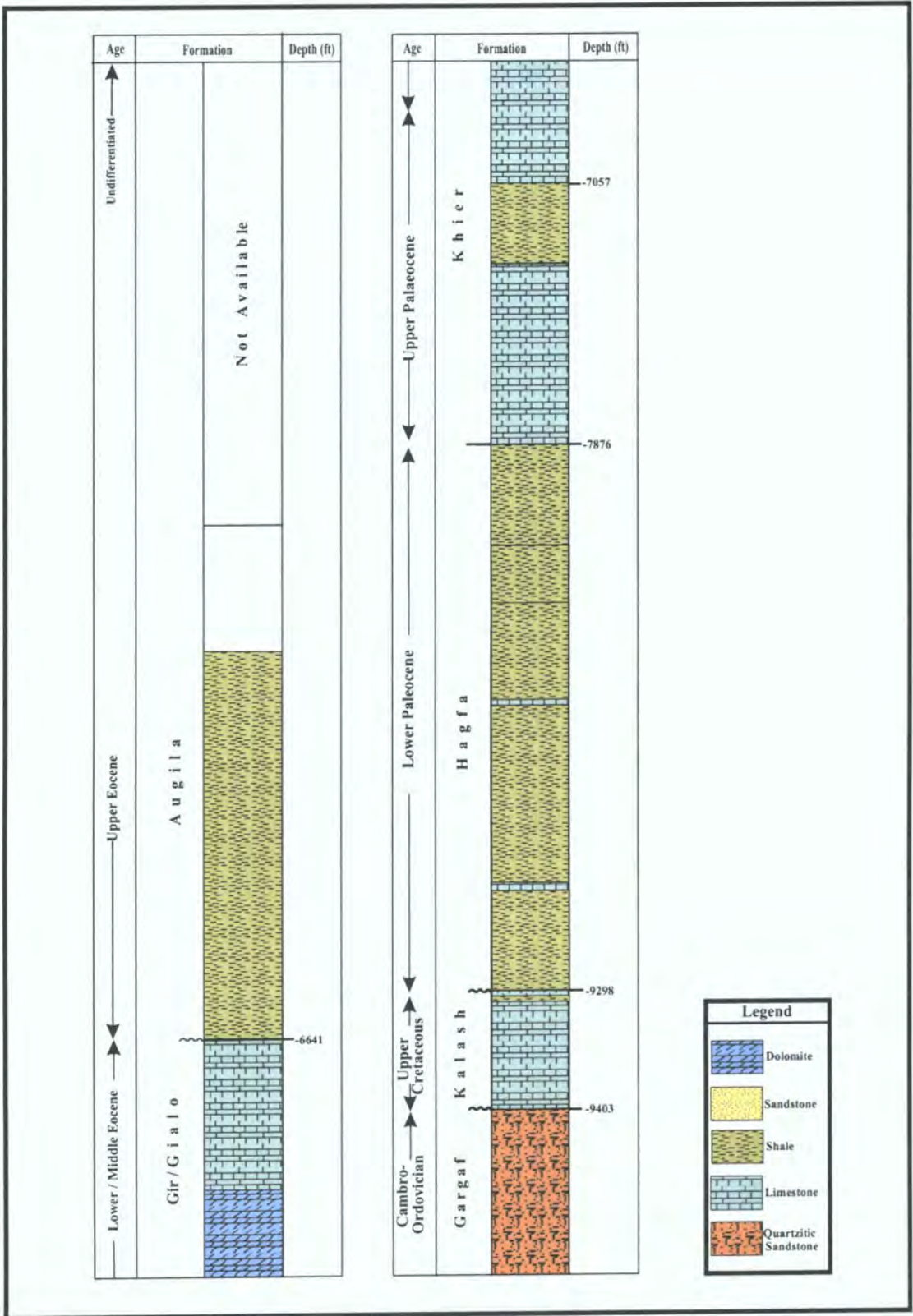


Figure 3.4. Lithologic log of Well S12-6. Depths were measured in feet from sea level. Not to scale.

present in this well, represented by its shale unit, but it is not differentiated from the underlying Hagfa Shale. The Lower Palaeocene Harash Formation is believed to overlie the Hagfa Formation, but is not differentiated from the Kheir Formation in this well. The Lower Palaeocene-Upper Eocene Kheir Formation consists of limestone overlain by a shale unit. The Middle Eocene Gialo Formation overlies the Kheir Formation, represented by thick limestone section. It is not differentiated from the Gir Formation which also consists of limestone.

The Augila Formation consists of a thick shale section. The Arida Formation and other Oligocene and Miocene strata are believed to be present in this well, but they are not differentiated.

3.4.4 H12-6 well description, Assumood Field

The sedimentary sequence in well H12-6 is illustrated in Fig. 3.5. The well was drilled to a total depth of 10857 ft sub-sea. The stratigraphic sequence of well H12-6 starts with the Cambro-Ordovician Gargaf Formation which consists of quartzitic sandstone. The Gargaf Formation is overlain by 38 ft of quartzitic sandstones of the Upper Cretaceous Bahi Formation. The Bahi Formation has a similar lithology to the Gargaf Formation which makes it difficult to differentiate between them. The Upper Cretaceous Sirte Formation overlies the Bahi Formation and is divided into two units, a lower dolomite unit and an upper shale unit. The Sirte Formation is overlain by a limestone section of the Upper Cretaceous Kalash Formation.

The thick shale section of the Lower Palaeocene Hagfa Formation contains interbeds of limestone. The Upper Palaeocene Khalifa Formation overlies the Hagfa Formation. It is divided into two members, a lower shale member and an upper limestone member. The shale member is thicker than the limestone member in this well. It is overlain by the Upper Palaeocene Harash Formation which is also divided into two units, lower limestone porous unit overlain by a tight unit. The Harash Formation is

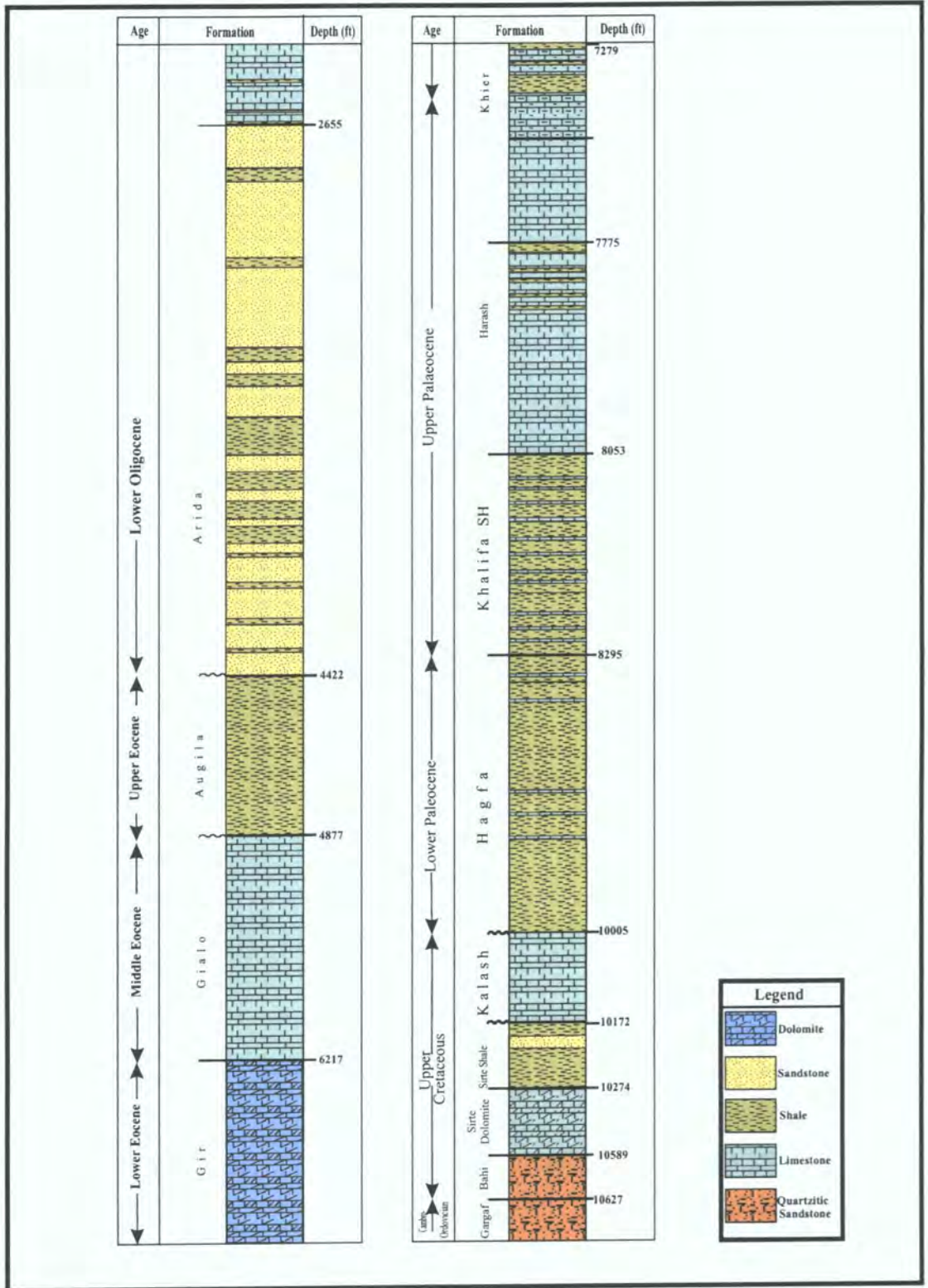


Figure 3.5. Lithologic log of well H12-6. Depths were measured in feet from sea level. Not to scale.

overlain by the Upper Palaeocene-Lower Eocene Kheir Formation which is divided into a limestone unit and a marl unit. The Kheir Formation is overlain by limestones of the Lower Eocene Gir Formation. The limestones of the Gialo Formation overlie the Gir Formation which makes it difficult to differentiate between them.

Oligocene rocks unconformably overlie the Gialo Formation. These rocks are represented by a shale section of the Augila Formation overlain by sand and shale units of the Arida Formation. Above the Arida Formation limestone, shale and sand of undifferentiated Oligocene and Miocene rocks are present.

DATA ACQUISITION AND PROCESSING

4.1 Introduction

Seismic work in the area of study began in 1967 and was followed by other programmes with the most recent data having been acquired in 1998. Successive programmes were acquired to increase the density of the seismic data gathered from the study area. Different seismic parameters were used in order to improve the data quality as the seismic techniques developed, especially with increases in the number of recording channels available and with the introduction of more powerful vibrators.

A total of 1196.3 km of 2-D seismic data have been acquired in the study area. These data are comprised of 48 seismic lines. These lines are divided into eight vintages of data starting from 1971 to 1998. The seismic lines are shown on the seismic base map in Fig.4.1 and are also listed in Table. 4.1.

Various orientations were chosen for the seismic lines crossing the study area (Fig. 4.1). The majority of the lines used are oriented SW-NE. This orientation was chosen in the light of the tectonic structure in the study area and in the Sirt Basin in general. The faulting regime in the Sirt Basin has a NW-SE trend, so it is desirable to orientate the majority of seismic lines perpendicular to that direction.

Several lines are oriented in directions lying between N-S and NW-SE to get good control from tying the seismic data in loops, and also to detect possible minor faulting perpendicular to the main structural trend. The 1998 lines were located for

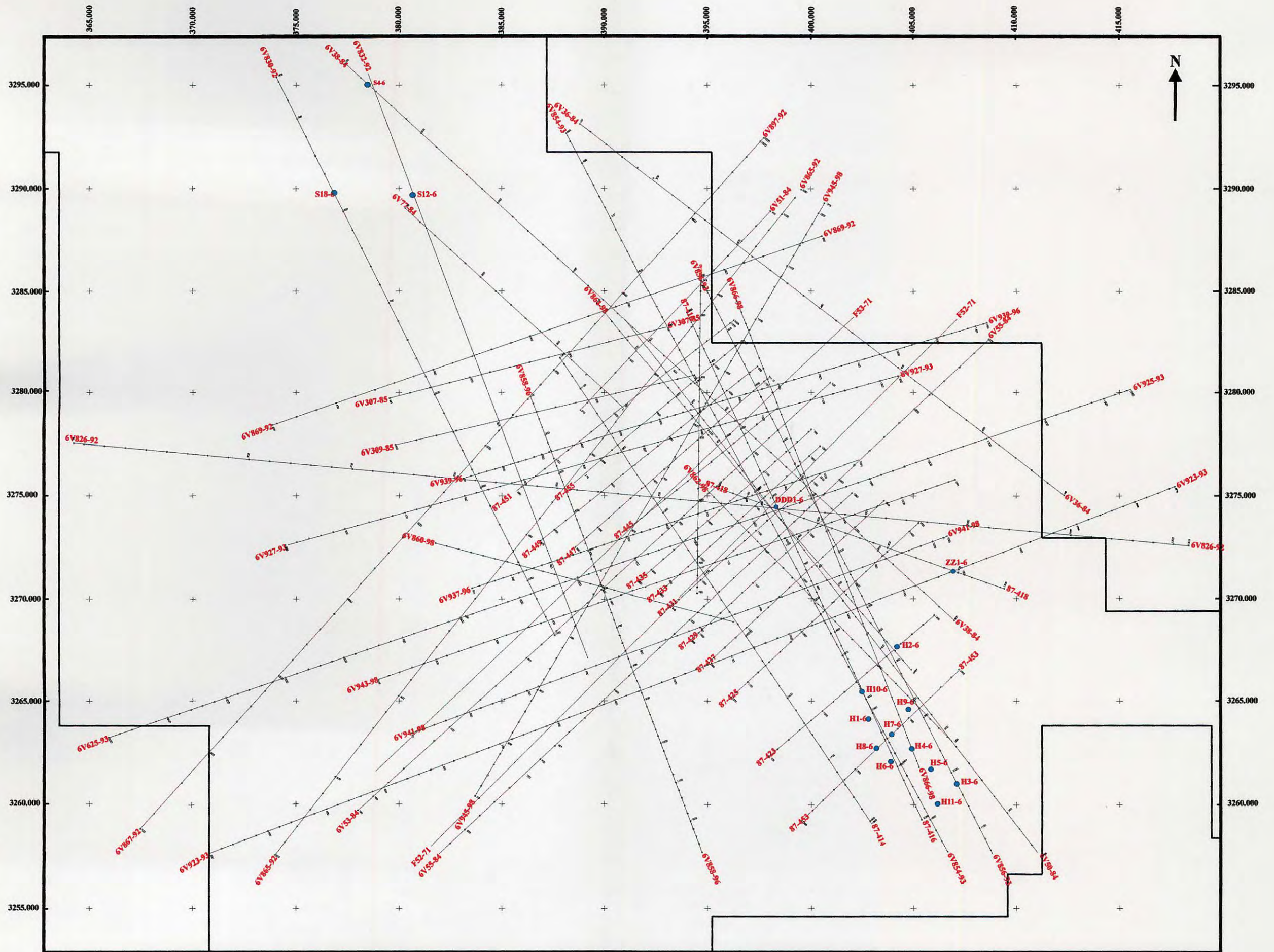


Fig. 4.1. Seismic base map.

Table 4.1: The North Assumood area line numbers, shot point numbers and line lengths in kilometres.

<u>1971 Data</u>	<u>Shot Points</u>	<u>Length (km)</u>
6VF52-71	1-370	37.00
6VF53-71	1-319	31.90
		<u>Total 68.90km</u>
<u>1984 Data</u>	<u>Shot Points</u>	<u>Length (km)</u>
6V36-84	107-700	29.65
6V38-84	100-900	40.00
6V45-84	276-570	14.70
6V50-84	95-755	33.00
6V51-84	100-370	13.50
6V53-84	100-720	31.00
6V55-84/85	100-850	37.50
6V77-84	100-390	14.50
		<u>Total 213.85 km</u>
<u>1985 Data</u>	<u>Shot Points</u>	<u>Length (km)</u>
6V307-85	101-381	14.00
6V309-85	101-401	15.00
		<u>Total 29 km</u>
<u>1987 Data</u>	<u>Shot Points</u>	<u>Length (km)</u>
87-414	1050-1752	25.27
87-416	376-1078	25.27
87-418	1111-1466	12.78
87-425	1121-1420	10.76
87-427	1030-1302	9.79
87-429	1036-1280	8.78
87-431	945-1161	7.78
87-433	976-1220	8.78
87-435	890-1134	8.78
87-445	881-1097	7.78
87-447	760-1059	10.76
87-449	726-1053	11.77
87-451	651-1006	12.78
87-453	1200-1444	8.78
87-455	770-1000	8.28
		<u>Total 178.11km</u>

<u>1992 Data</u>	<u>Shot Points</u>	<u>Length (km)</u>
6V826-92	131-1213	54.10
6V830-92	456-1058	30.10
6V865-92	125-1028	52.92
6V867-92	101-1003	45.10
6V869-92	336-898	28.10
		<u>Total 210.32 km</u>
<u>1993 Data</u>	<u>Shot Points</u>	<u>Length (km)</u>
6V923-93	203-1867	49.92
6V925-93	203-1941	52.10
6V927-93	203-1225	30.66
6V931-93	245-747	15.06
6V854-93	425-1885	43.80
6V856-93	103-1867	52.92
		<u>Total 244.46 km</u>
<u>1996 Data</u>	<u>Shot Points</u>	<u>Length (km)</u>
6V937-96	101-1091	19.80
6V939-96	101-1431	26.60
6V858-96	101-1766	33.30
		<u>Total 79.70 km</u>
<u>1998 Data</u>	<u>Shot Points</u>	<u>Length (km)</u>
6V860-98	101-599	14.94
6V862-98	101-696	17.85
6V964-98	101-887	23.58
6V866-98	170-991	24.63
6V941-98	101-1025	27.72
6V943-98	101-1091	29.70
6V945-98	101-1219	33.54
		<u>Total 171.96 km</u>

Cumulative total 1196.3 km

particular objectives specified by the interpreter, and are oriented in various directions. All data vintages were located to tie the wells previously drilled.

4.2 Seismic data acquisition

4.2.1 History and data quality

All seismic surveys that have been conducted in the area of study have been comprised of 2-D lines; to date no 3-D data have been acquired in this area. The seismic data have been acquired by several geophysical companies. Table 4.2 shows these companies with the respective data vintages.

COMPANY	SEISMIC DATA VINTAGE
CGG (Companie Generale de Geophysique)	1971
WGC (Western Geophysical Company)	1984
S.S.L (Seismograph Service Limited)	1985
BOCO (Bulgarian Company)	1987, 1992, and 1993
AGESCO (Arab Geophysical Exploration Services Company)	1996 and 1998

Table 4.2. The geophysical companies which acquired the data.

Only a few lines were acquired in 1967 and these data are not available for this study. The next seismic survey was in 1971 where more than ten lines were shot with a Dinoseis source, 48 recording channels, a station interval of 100m, and subsurface coverage of 2400%. Only two seismic lines of this programme are used in this study, comprising about 68 km of profile. The data were reprocessed in November 1987 and are of good quality (Fig. 4.2).

Some other seismic acquisition programmes were carried out in 1976, 1979 and 1981 in the same concession, but none of these programmes crossed the study area. The

SW

NE

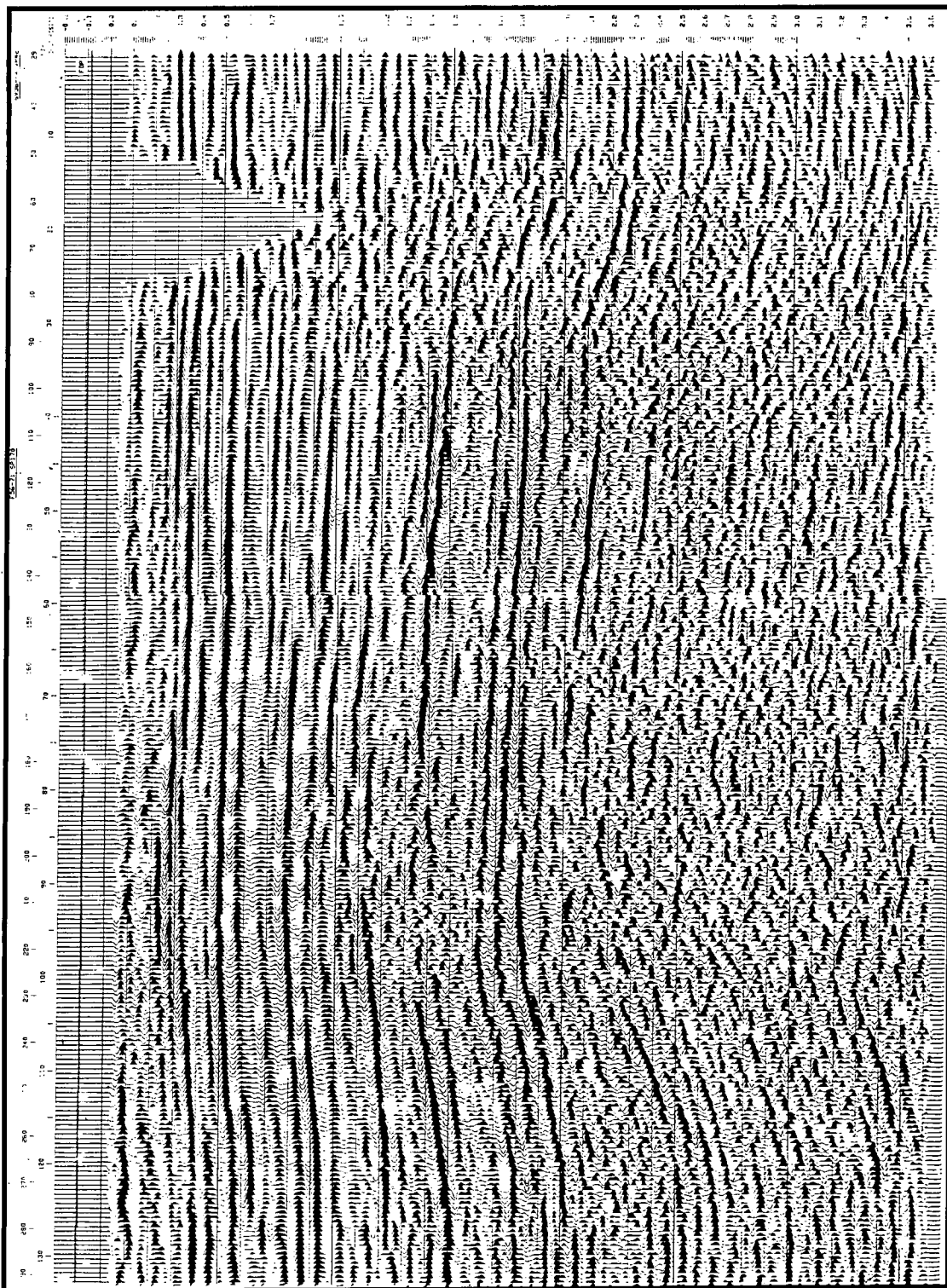


Fig. 4.2 Line F53-71

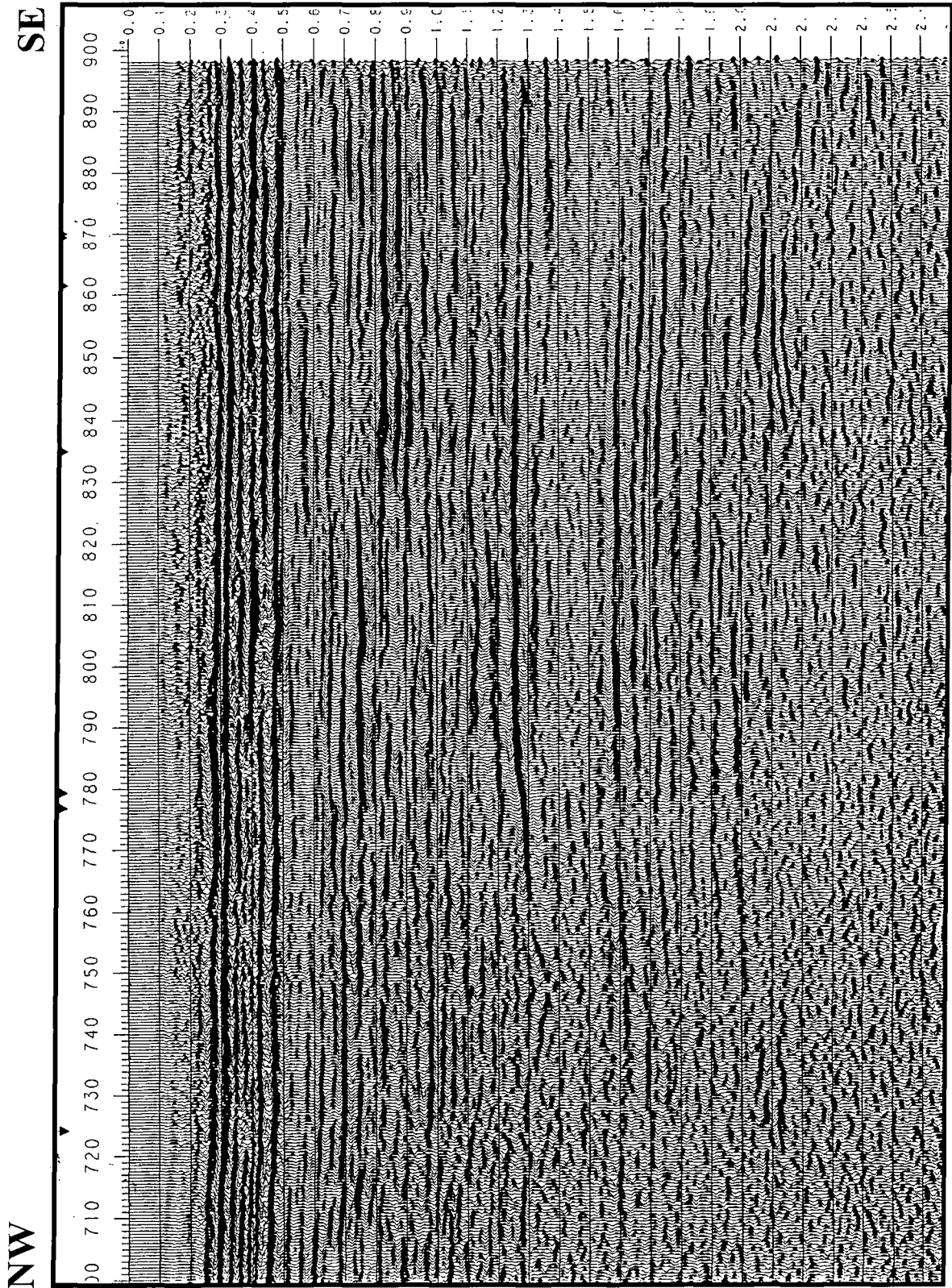


Fig. 4.3 Line 6V38-84

WSW

ENE

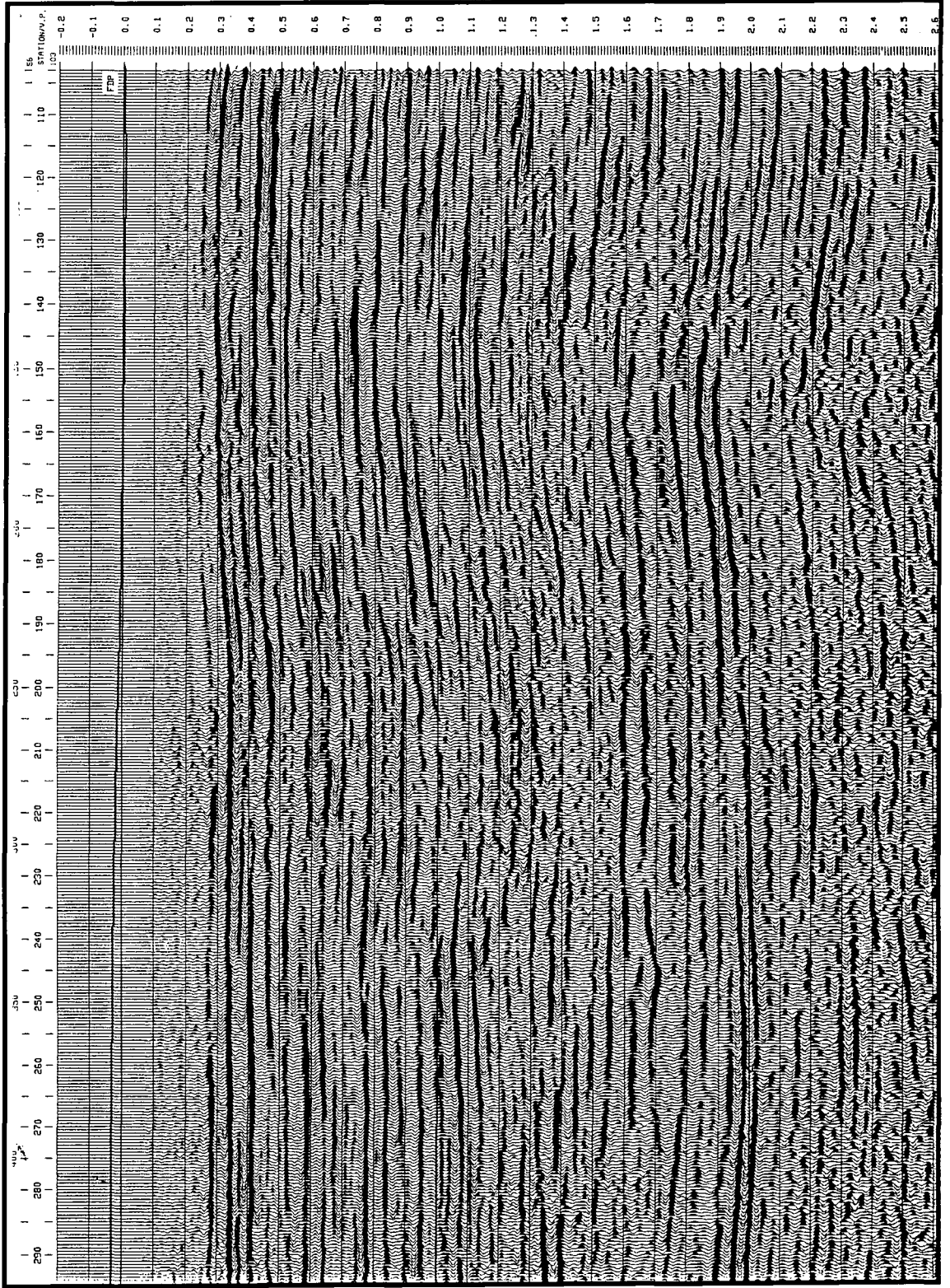
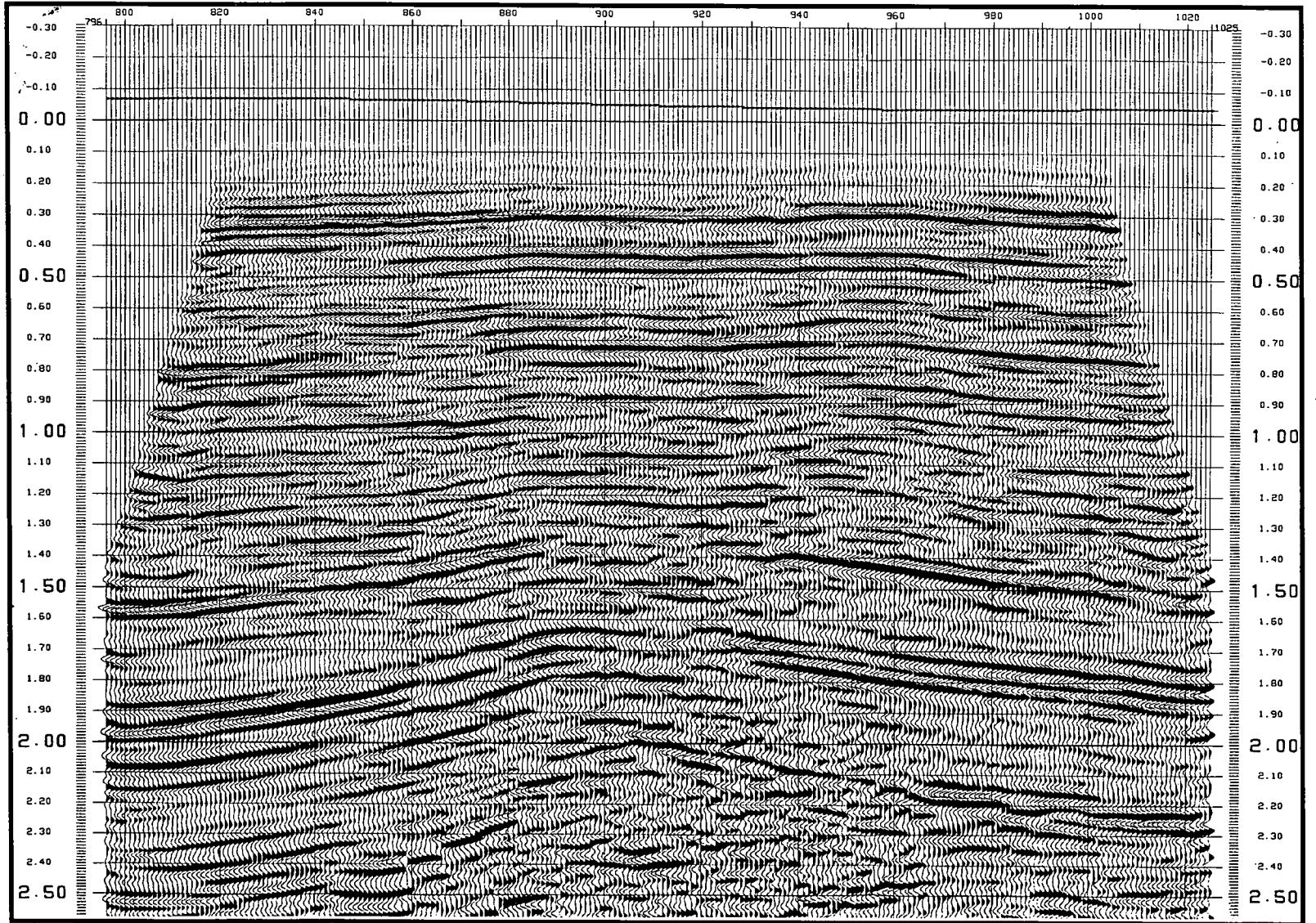


Fig. 4.4 Line 6V307-85

SW

NE



54

Fig. 4.5 Line 87-455

the area, where two lines tied the S12-6 and S18-6 Hateiba wells (Fig. 4.1). The energy source was Vibroseis, with 120 channels, a station interval of 50m, and subsurface coverage of 6000 %. These data were distinguished from the other data by using various sweep frequencies of 10-48Hz, 16-51Hz, 17-55Hz and 18-62Hz (Table 4.3). The data are of good quality (Fig. 4.6).

Another programme was acquired in 1993, including six lines used in this study, comprising about 245 km of profile. Line 6V923-93 ties the ZZ1-6 well (Fig. 4.1) The energy source was Vibroseis, with 240 channels, a station interval of 30 m, subsurface coverage of 6000%, and sweep frequencies from 10-56 Hz (Table 4.3). Line 6V931-93 was reprocessed in 1998. The data are of good quality: shallow and deep horizons can be picked with confidence (Fig. 4.7).

In 1996, about 80km of 2-D seismic profile were acquired in the area comprising three lines. Different acquisition parameters from the other vintages were used in this study (Table 4.3). The energy source was Vibroseis, with a much higher number of channels (480) than had previously been used in this area, a station interval of 20 m, subsurface coverage of 24000%, and sweep frequencies from 8-60 Hz (Table 4.3). Although the data were gathered with 480 channels, they are of poor quality (Fig. 4.8), especially in the deep horizons. Also the available lines are displayed in reverse polarity which makes it very difficult to match with the other data. As the normal polarity version of the 1996 data were not available for this study, the 1996 data were merely used as supplementary data in the interpretation to check the picks on the other lines.

The latest seismic programme acquired in the area was in 1998. Seven lines are used in this study, comprising about 172 km of profile. The energy source was Vibroseis, with 360 channels, a station interval of 30m, subsurface coverage of 12000%, and sweep frequencies from 10-60 Hz (Table 4.3). The data are of the best quality in the area (Fig. 4.9).

W

E

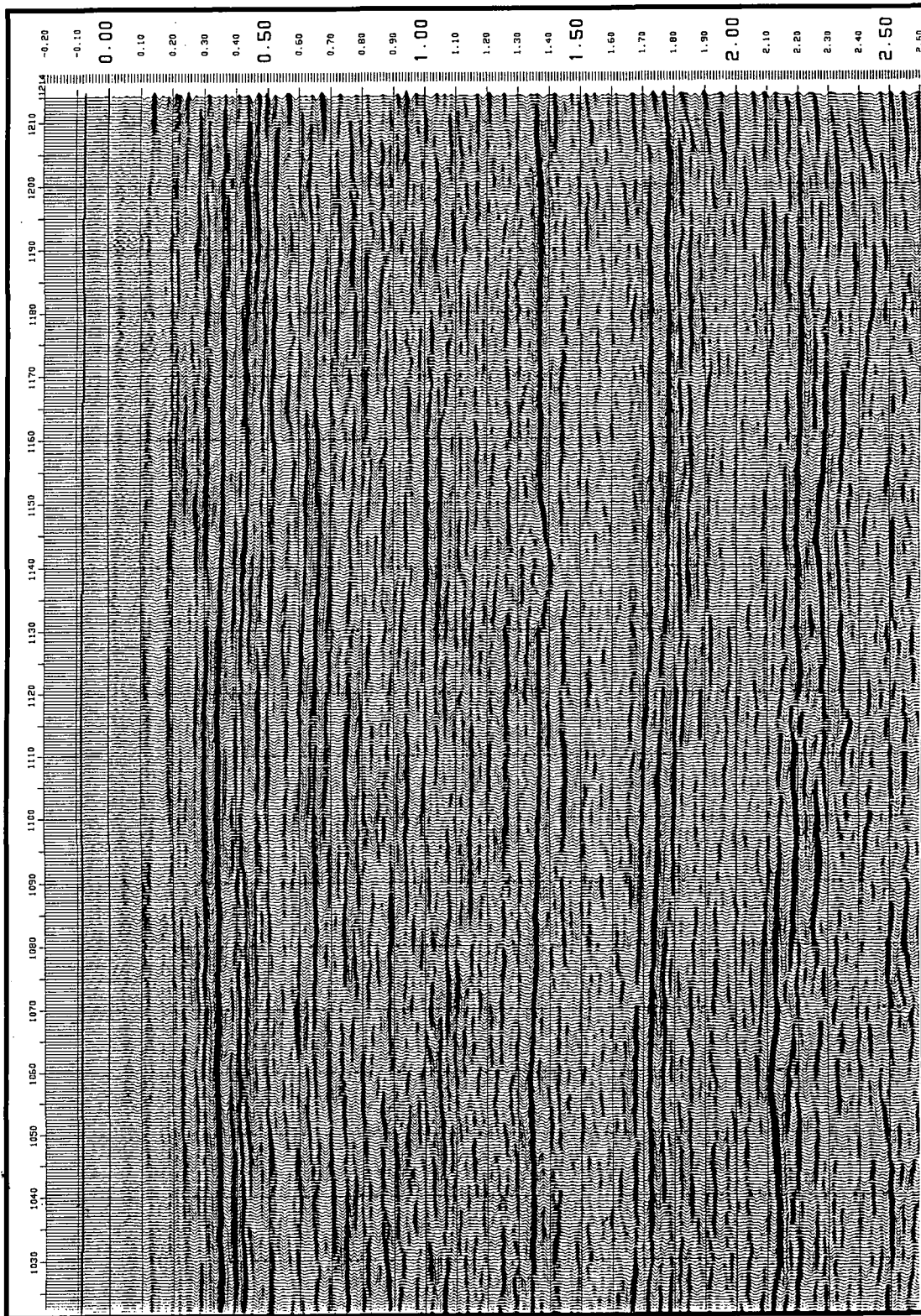


Fig. 4.6 Line 6V826-92.

NW

SE

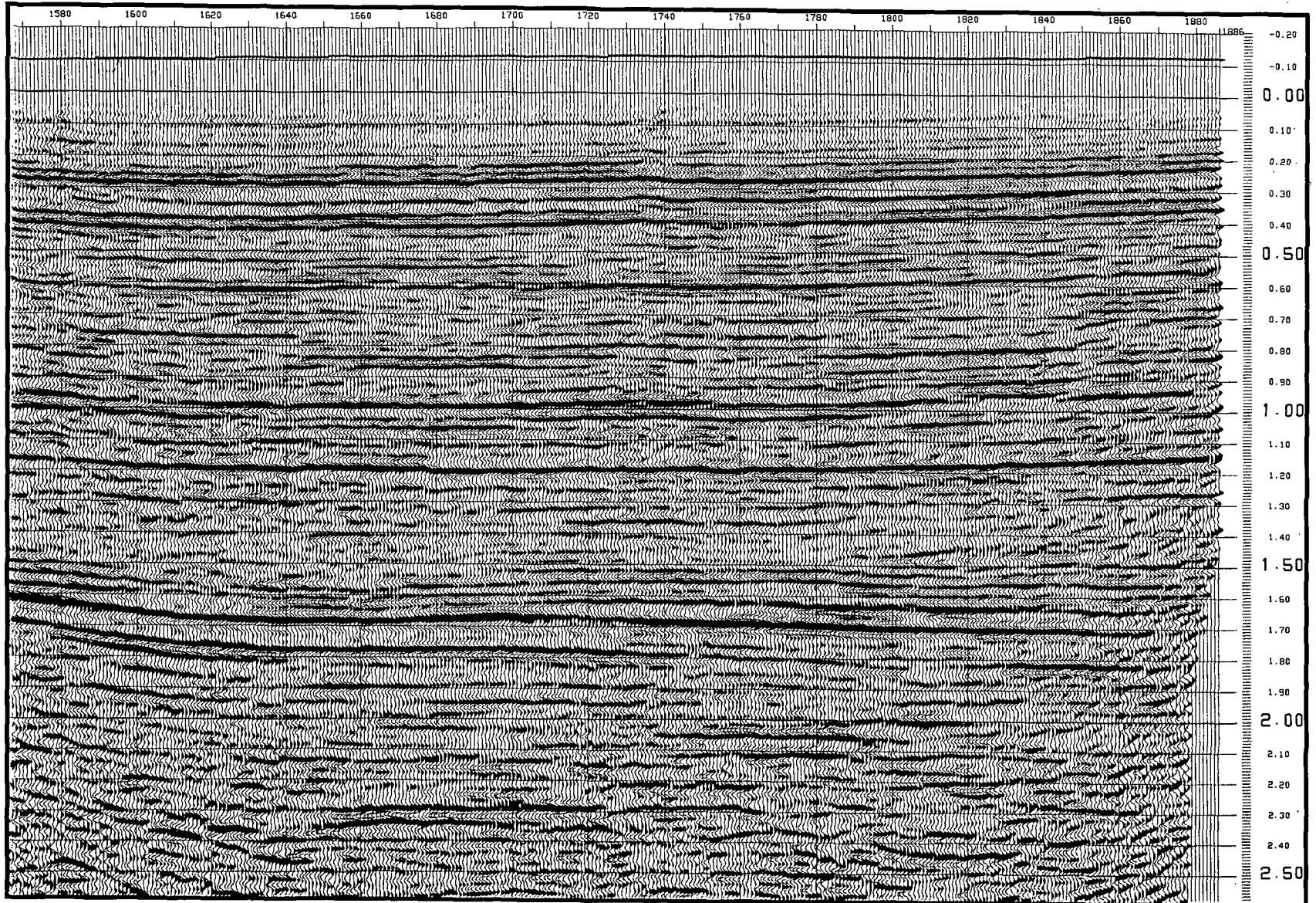


Fig. 4.7 Line 6V854-93

NW

SE

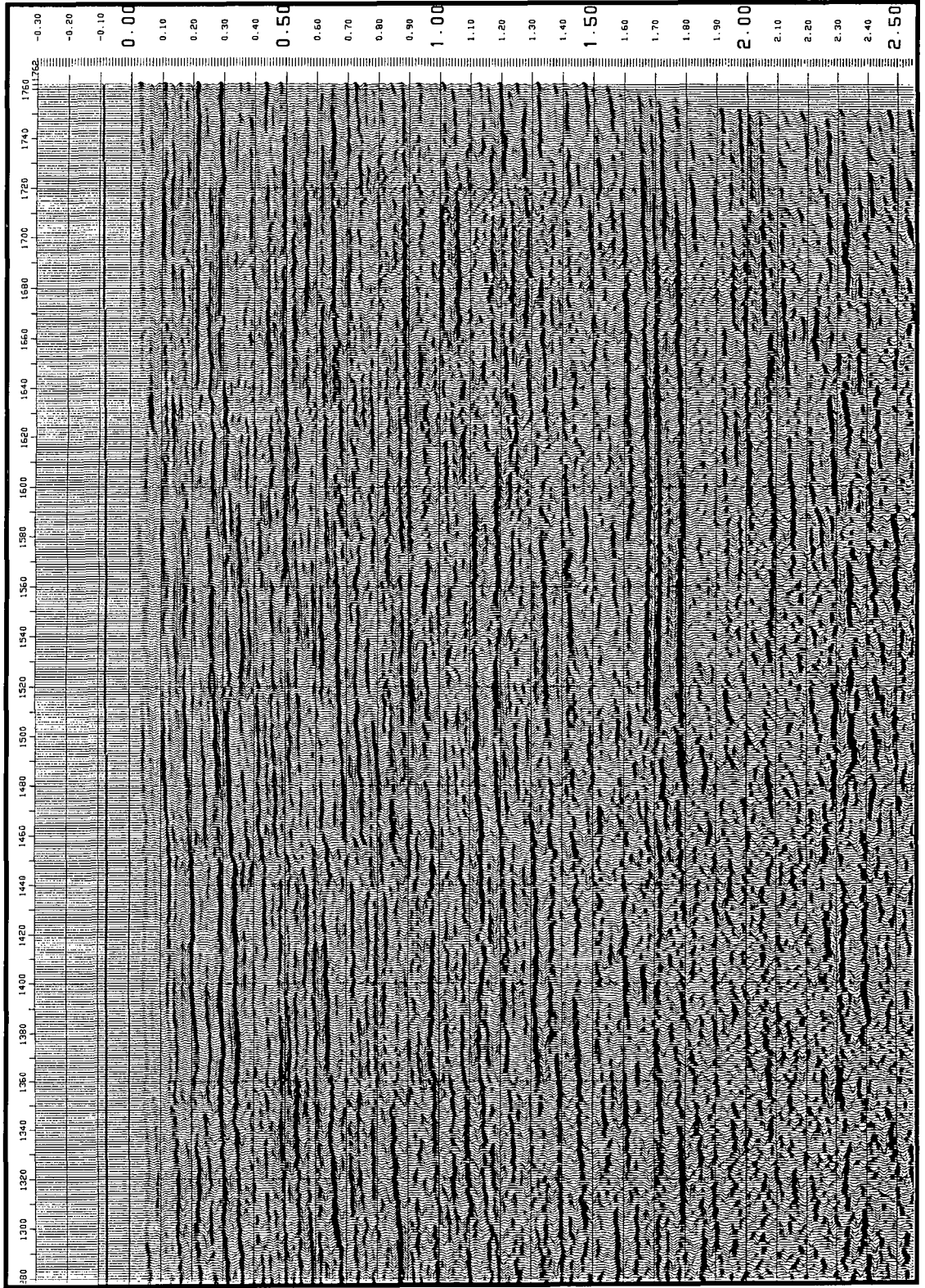


Fig. 4.8 1996 Line 6V858-96

SW

NE

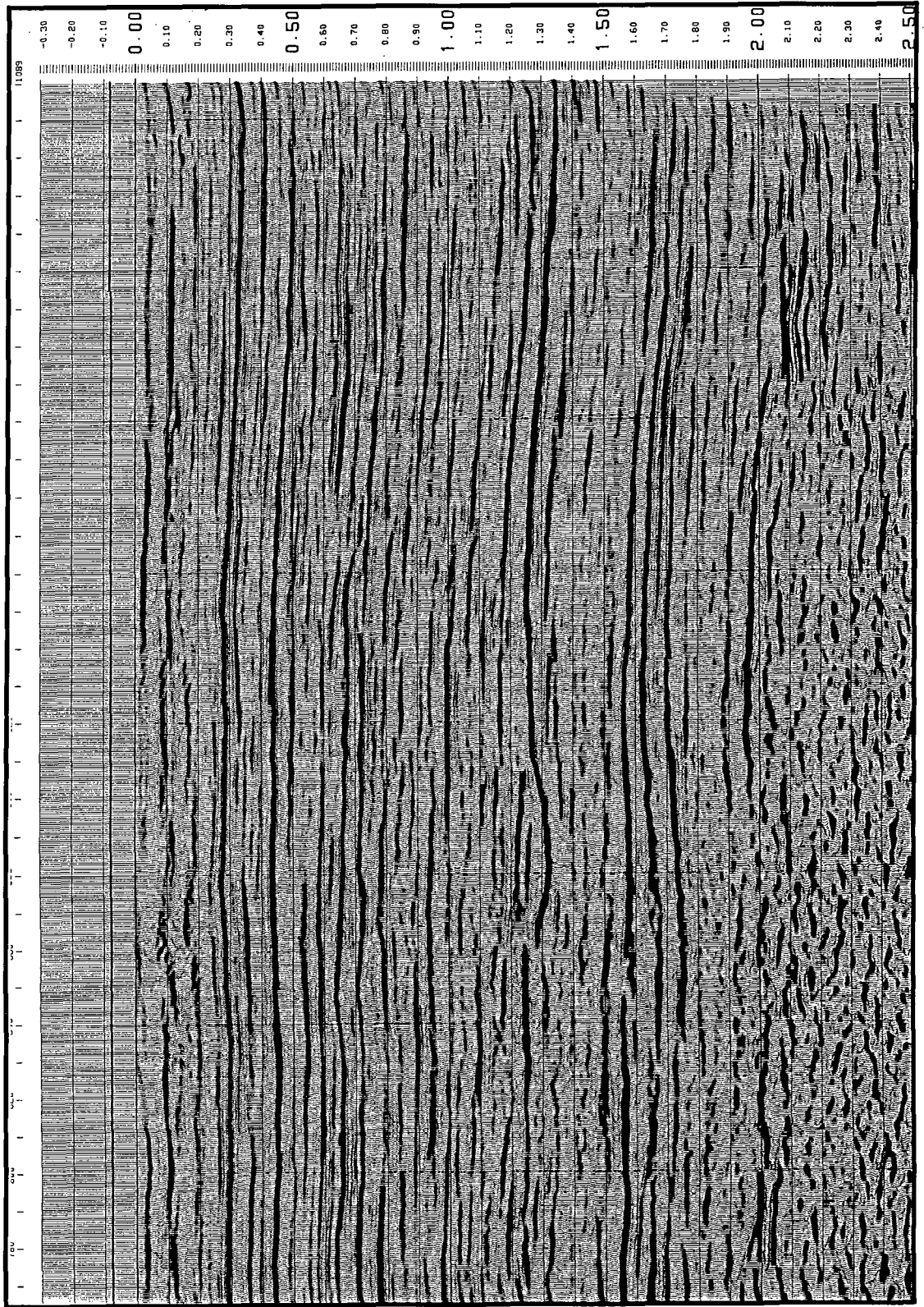


Fig. 4.9 Line 6V943-98

4.2.2 Receiver arrays

The receivers at each station are grouped in a certain configuration that is called the geophone array. Geophone arrays are designed to improve the signal-to-noise ratio following the analysis of noise tests, from which the characteristics of source-generated noise such as groundroll and airwaves may be determined.

The 1971 data were acquired using Dinoseis as the energy source, and the geophone array information is not available. The later seismic surveys in the area of study were acquired using Vibroseis with geophone arrays in the shape of parallelograms. As an example, the geophone array in 1998 is shown in Fig. 4.10.

The geophone configuration was adjusted for each survey (except between 1984 and 1985) in efforts to improve the data quality. Table 4.4 summarises the different geophone geometries for each data vintage.

	1984/1985	1987	1992	1993	1996	1998
Geophone per group	36	72	72	48	24	48
No. of strings	3	6	6	8	6	8
No. of geophones per string	12	12	12	6	4	6
Lateral spacing (m)	8	3.94	4.2	5	3.375	5
Stagger (m)	13.5	3	5	5.63	3.375	5
In-line spacing (m)	7	9	5	5	4.2	7.5
Array length (m)	115	63	71.2	64.375	27	60
Array width (m)	14	45	25	35	21	52.5
Array area (m ²)	1610	2835	1780	2254	567	3150

Table 4.4. Geophone array parameters used for each data vintage.

Table 4.4 shows that 72 geophones per group were used in 1987 and 1992, which is the largest number of geophones per group that has been used in the area of study. In 1996 only 24 geophones per group were used, which is the smallest number that has been used in the area. The 1996 data are of poor quality due to many factors.

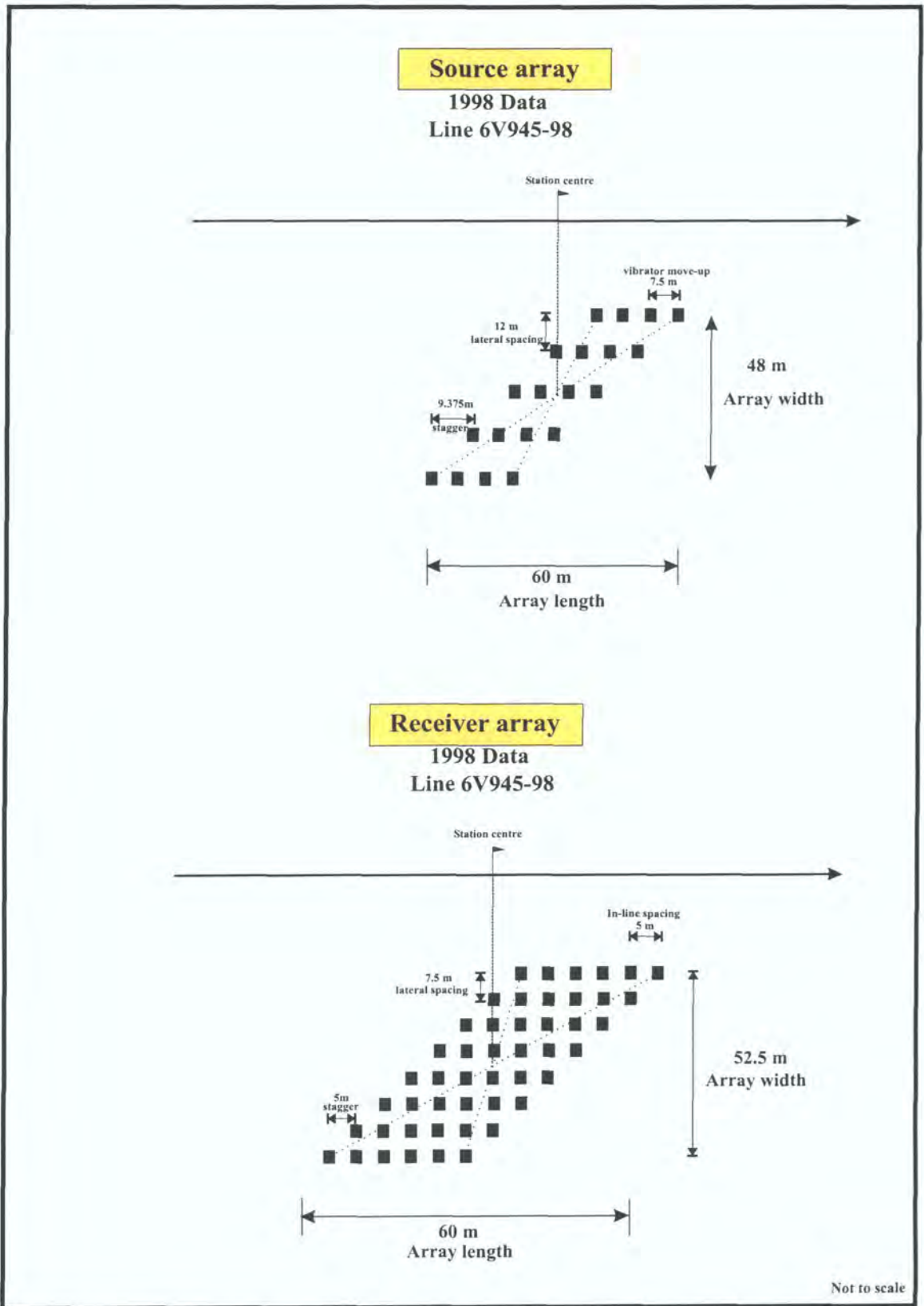


Fig. 4.10 The 1998 data source and receiver arrays

One of these factors is the geophone array which has the smallest area of all the geophone arrays that have been used in these surveys. The 1993 and 1998 data have quite similar geophone array geometries. These two data sets have very good quality. It seems that the geophone array geometry for the 1998 data was chosen to be similar to that used in 1993, presumably on the basis of quality comparisons with the previous data.

4.2.3 Source arrays

Another technique to improve the signal-to-noise ratio in seismic data acquisition is to optimise the source array design. Similar to the geophone arrays, parallelogram source arrays have been used for all the Vibroseis lines. As an example, the array used for one of the 1998 lines is shown in Fig. 4.10. Parameters of the source arrays used in each vintage are summarised in Table 4.5.

	1984/1985	1987	1992	1993	1996	1998
No. of vibrators	4	4	4	4	5	4
No. of move-ups/ station	8	8	8	8	2	4
No. of standing sweeps/move-up	1	1	1	4	1	1
Sweep length (s)	16	16	12	12	12	12
Group interval (m)	50	36	50	30	20	30
Vibrator move-up (m)	7.14	4.5	6.25	7.5	5	7.5
Stagger (m)	19.33	9	17.2	13.125	5	9.375 & 16.875
Lateral spacing (m)	8	20	10	5	7.5	12
Array length (m)	108	58.5	95.35	91.875	25	60&90
Array width (m)	24	60	30	15	30	48

Table 4.5. The vibrator array parameters used in each data vintage.

Table 4.5 shows that the vibrator array in 1996 has the shortest length of 25 m, and also the move-up and stagger were the same, which differs from the other source arrays. This could be another reason for the poor data. The vibrator array in 1993 has the shortest array width of 15m. The vibrator array used for the 1998 data has two array lengths, 60m and 90 m, which was due to a change in the stagger from 9.375m to

16.875m. The 60 m array length was used for lines 6V860-98 and 6V945-98, the 90 m array length was used for lines 6V862-98, 6V866-98, 6V941-98 and 6V943-98, and the array length was changed from 60 m to 90 m during the acquisition of line 6V864-98.

The vibrator array used for the 1996 data had the smallest number of sweeps per vibrator array, 10 sweeps with five vibrators generating two sweeps each. This may be one of the factors that had a negative effect on the 1996 data quality.

4.2.4 Static corrections

Static corrections are probably the most difficult thing to get right in processing land seismic reflection data. Poor static corrections can seriously affect the quality of stacked data; thus intensive care should be taken to analyse the causes of static shifts and to calculate the static corrections in any area. The quality of static corrections depends on the near-surface velocity information.

To calculate the near-surface velocities, upholes along each seismic line have to be drilled to different depths according to the depth of the weathered layers. These upholes are used to calculate the near-surface velocities by recording the seismic velocities between the surface and a geophone clamped at different levels in each borehole. From picking the first breaks, the near-surface velocities may be calculated. The velocity structure has to be interpolated between up-hole locations so that static corrections can be calculated for each source and receiver station. Surveyors measure the elevation of each source and receiver location, in addition to their lateral positions. By choosing a seismic datum, application of static corrections shift the data in time so that time zero corresponds to the seismic datum. Static corrections are negative time shifts of the data for source and receiver stations above the datum.

Static corrections in the area of study appear to contain errors since there are mis-ties at many intersections. Using different velocities in calculating the weathering

layer thickness from data vintage to another might be responsible for the observed mis-ties in the area.

4.3 Seismic data processing

All seismic data used in this study were processed by CGG except for the 1984 data which were processed by Western Geophysical company (WGC). Many lines were reprocessed in order to apply different seismic processing procedures to improve their quality. The 1971 data were reprocessed in 1987. All 1987 data were reprocessed in 1998 except for lines 87-418 and 87-414. Lines 6V931-93 and 6V50-84 were also reprocessed by CGG in 1998.

Seismic data used were all migrated sections except for the 1984 data. The data are all displayed in SEG normal polarity except for the 1996 data in which only the reverse polarity versions were available. The sections are plotted on a vertical scale of 10cm/s and horizontal scale of 1:25000. The data of different vintages were collected to different two-way times. The 1984, 1987, 1992 and 1993 were collected to 4 seconds TWT, 1996 were collected to 6 seconds and 1998 were collected to 5 seconds.

The 1987 data were slightly improved by reprocessing in 1998. The most significant differences applied in the reprocessing sequence were an F-K filter in common shot gathers and the use of an F-X filter in the common shot gathers instead of on the migrated section. The processing sequence for the 1998 data is given in Appendix 2. The F-X filter was applied to the data in order to suppress random noise. The other data vintages have similar processing sequences.

Comparison of the processing sequences of all data vintages does not reveal any significant change which could explain the differences in data quality. It seems likely that the differences in data quality between the various surveys were due to using different parameters in data acquisition.

The 1996 data have the poorest quality of all the data acquired in the area since 1984. In 1996, the group interval and source point spacing were only 10 m, yielding a CDP spacing of 5 m. Professor David Smythe of Glasgow University has pointed out that if the 1996 data were reduced nine-fold by summing seismograms from three adjacent source points and three adjacent receiver groups, then the reduced data would simulate the acquisition parameters used in 1998, which yielded excellent data. This is an interesting suggestion for re-processing the 1996 data and might improve the quality of the sections.

INTERPRETATION

5.1 Introduction

There are two techniques for seismic data interpretation: the first is to use seismic sections displayed on paper, and the second is to use seismic data interpretation software on a workstation. Workstation-based interpretation is the more common technique nowadays, especially for 3D data, as it is faster and offers a variety of facilities for changing the display parameters. The seismic data in this study have been interpreted on paper sections. For 2D data, paper sections have the advantage that the whole sections are visible to the interpreter at the same time, whereas the size of the screen is a limitation on a workstation.

Seismic interpretation starts by using well data in order to identify the stratigraphic formations on seismic sections. Synthetic seismograms from nine wells were available for this study. Four horizons were identified at well locations on the seismic sections and colour coded. These horizons are: the Upper Cretaceous Kalash Formation in dark blue, the Lower Palaeocene Hagfa Formation in light blue, the Upper Palaeocene-Lower Eocene Kheir Formation in green, and the Middle Eocene Gialo Formation in yellow. Using the intersections between seismic sections, these horizons were correlated over all the data. In some parts of the area, the top Kalash horizon was very difficult to correlate because of poor signal-to-noise ratio and heavy faulting. Also,

as there is no well data from the Wadayat Trough, it was difficult to trace the deeper seismic horizons from the Assumood Ridge down into the Wadayat Trough.

Three two-way time structure maps were generated using 1:25,000 base maps. These maps are: Top Upper Cretaceous Kalash Formation, Top Upper Palaeocene-Lower Eocene Kheir Formation and Top Middle Eocene Gialo Formation (Enclosures 1, 2 and 3). The base maps which were used to generate the time structure maps include seismic lines which were not available for this study. The seismic lines which were used are shown in Figure 4.1.

5.2 Synthetic seismograms

The sonic log is one of the most useful logs for seismic interpretation. It is an essential log to be included in any well logging programme, and especially in exploration wells. The sonic log measures the interval transit time (Δt) for a compressional sound wave travelling through the formation. It provides continuous velocity information with depth. This is measured in microseconds per foot. The sonic log responds to variations in lithology and to porosity. The importance of this log is for generating synthetic seismograms which enable the interpreter to recognize the formation tops and link them to their seismic response in the data. Also the sonic log is useful for calculating the seismic interval velocities that are used in depth conversion. The synthetic seismogram should be displayed on the same time-scale as the seismic data.

In this study, sonic logs for all available wells were digitized using a hand-held digitizer called Digi-Rat with its accompanying computer software. The digitized data were transferred to GMA software to generate the synthetic seismograms. The GMA software automatically calculates the reflection coefficients series from the sonic data by assuming a constant density. A suitable wavelet has to be input into the GMA software to be convolved with the reflection coefficient series to get the synthetic seismogram. The wavelet used to generate the synthetic seismograms was a zero-phase

Klauder wavelet obtained by autocorrelating a sweep with the following parameters: low frequency cut of 8 Hz, high frequency cut of 42 Hz, sweep length of 10 sec.

One of the necessary corrections to be applied to the digitized sonic data is check-shot information. The check-shot survey is used to calibrate the integrated travel times from the sonic log so that an adjusted synthetic seismogram can be generated. In particular, this calibration can be applied to adjust parts of the sonic log that have been affected by bad hole conditions, so that the synthetic seismogram should fit the seismic data better. The check-shot levels should include the following:

- Seismic reference datum (SRD), which is mean sea level in the area of study.
- The start of the sonic log run.
- Formation tops picked from well logs.
- Final total depth (FTD).

Other levels will be added to give a spacing of 300 feet to 500 feet between levels depending on the depth of the well and available time.

Check-shot data were available for all wells in the area. They were input to the GMA software, which then automatically adjusted the sonic data. Figures 5.1, 5.2, 5.3 and 5.4 display the synthetic seismograms with sonic logs for the wells DDD1-6, ZZ1-6, S12-6 and H12-6.

All synthetic seismograms gave a fair match to the seismic data. Figures 5.5 and 5.6 show the match of synthetic seismograms with seismic data at wells DDD1-6 and H12-6. Due to errors in the check-shot data and the sonic logs, the seismic events on the synthetic seismograms do not precisely correlate with the seismic data. Most of the synthetics had to be shifted up or down to fit the seismic data and commonly did not match all the seismic horizons with a constant time shift.

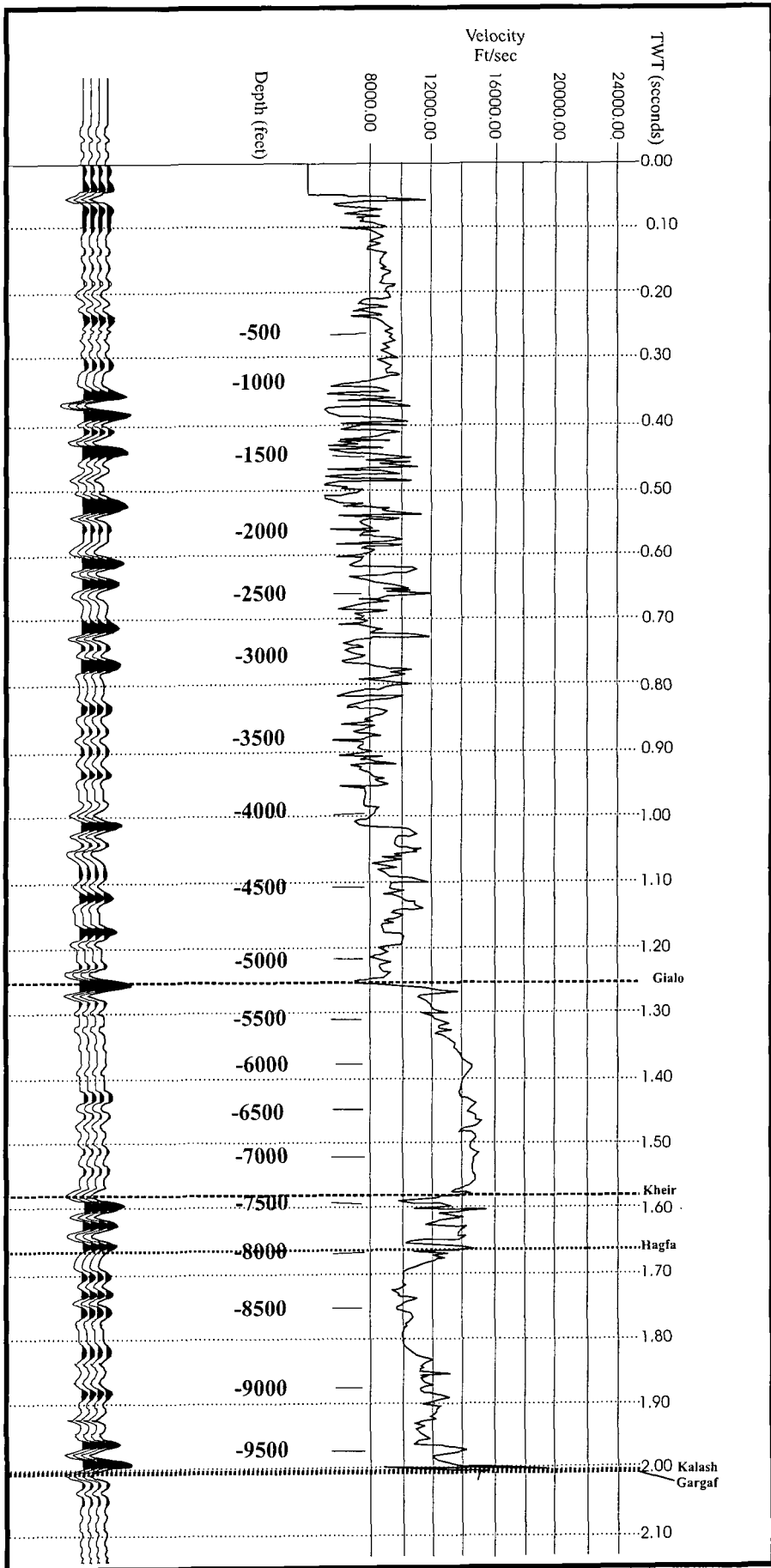


Fig. 5.1 DDD1-6 synthetic seismogram. The sonic log is plotted on the right with values of two-way time in seconds and depth in feet.

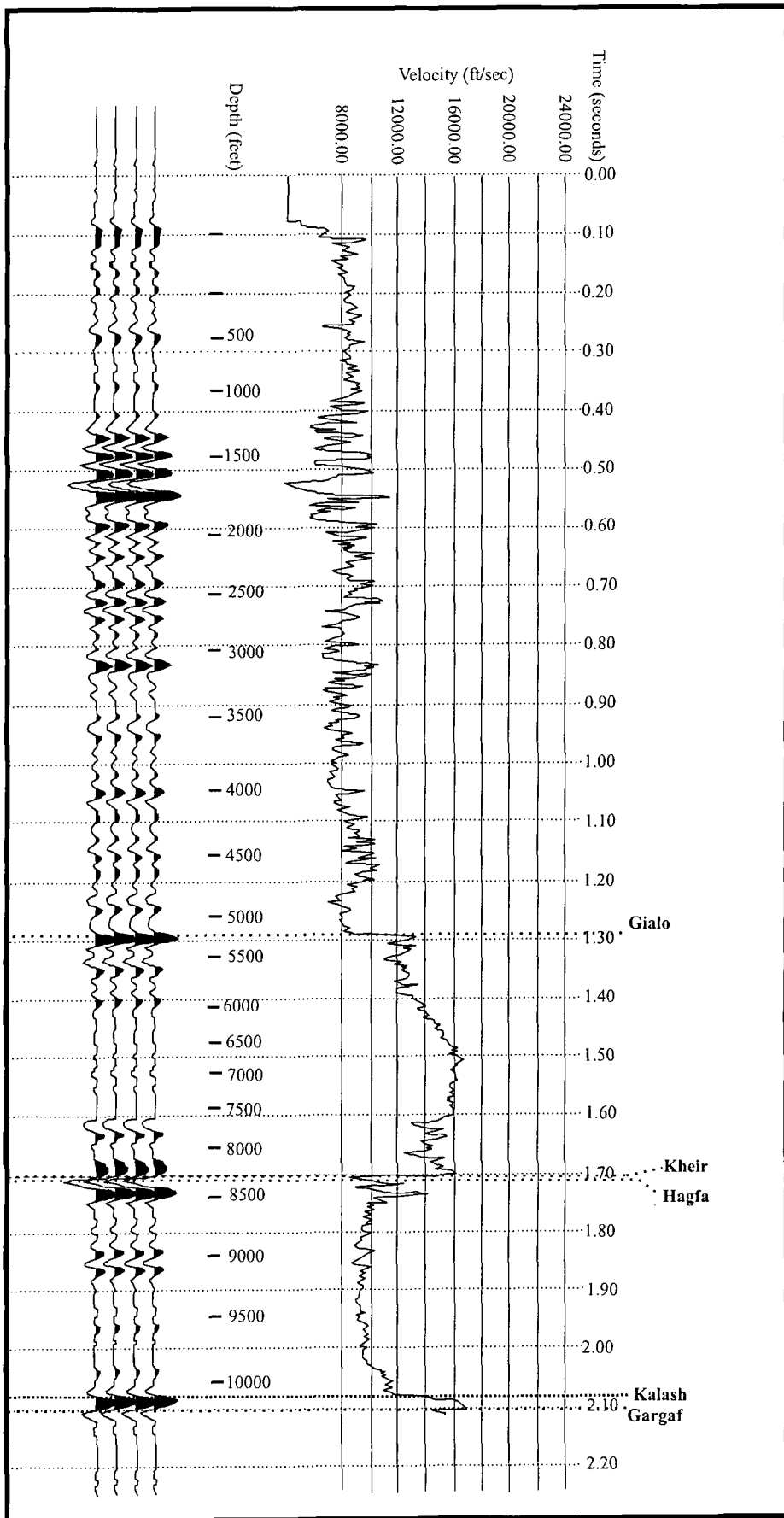


Fig. 5.2 ZZ1-6 synthetic seismogram. The sonic log is plotted on the right with values of two-way time in seconds and depth in feet.

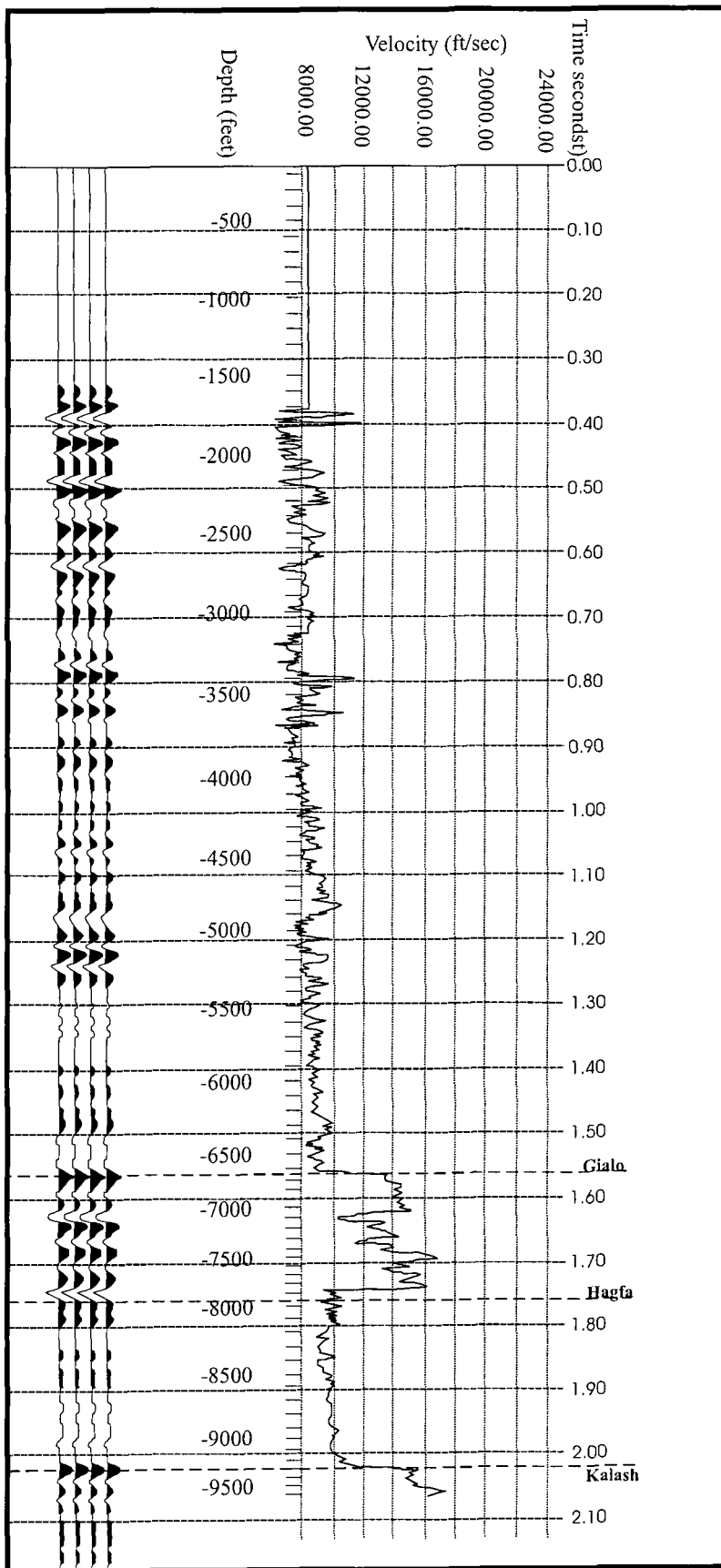


Fig. 5.3 S12-6 synthetic seismogram. The sonic log is plotted on the right with values of two-way time in seconds and depth in feet.

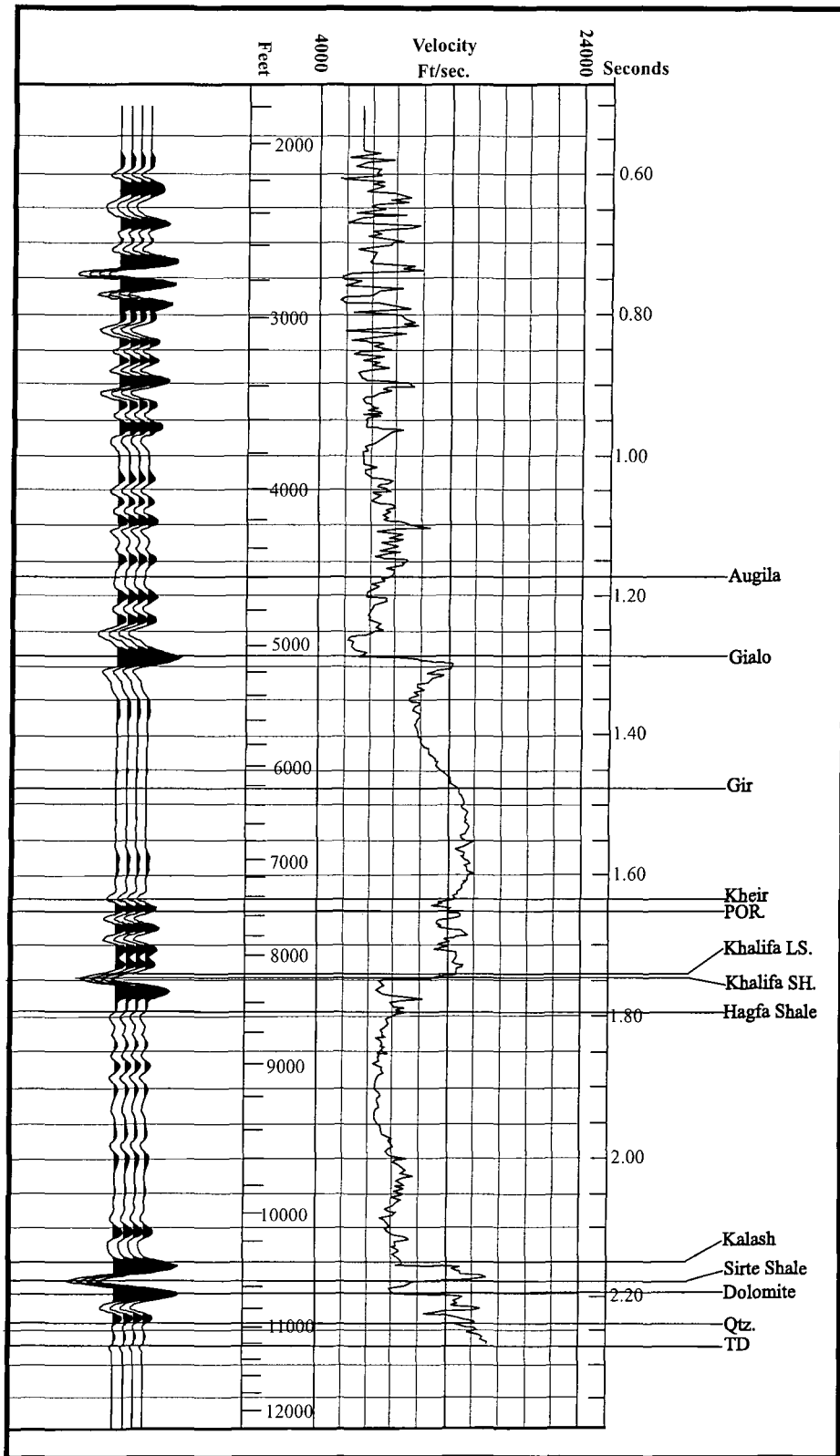


Fig. 5.4 H12-6 Synthetic seismogram. The sonic log is plotted on the right with values of two-way time in seconds and depth in feet.

NW



Line 6V864-98

SE

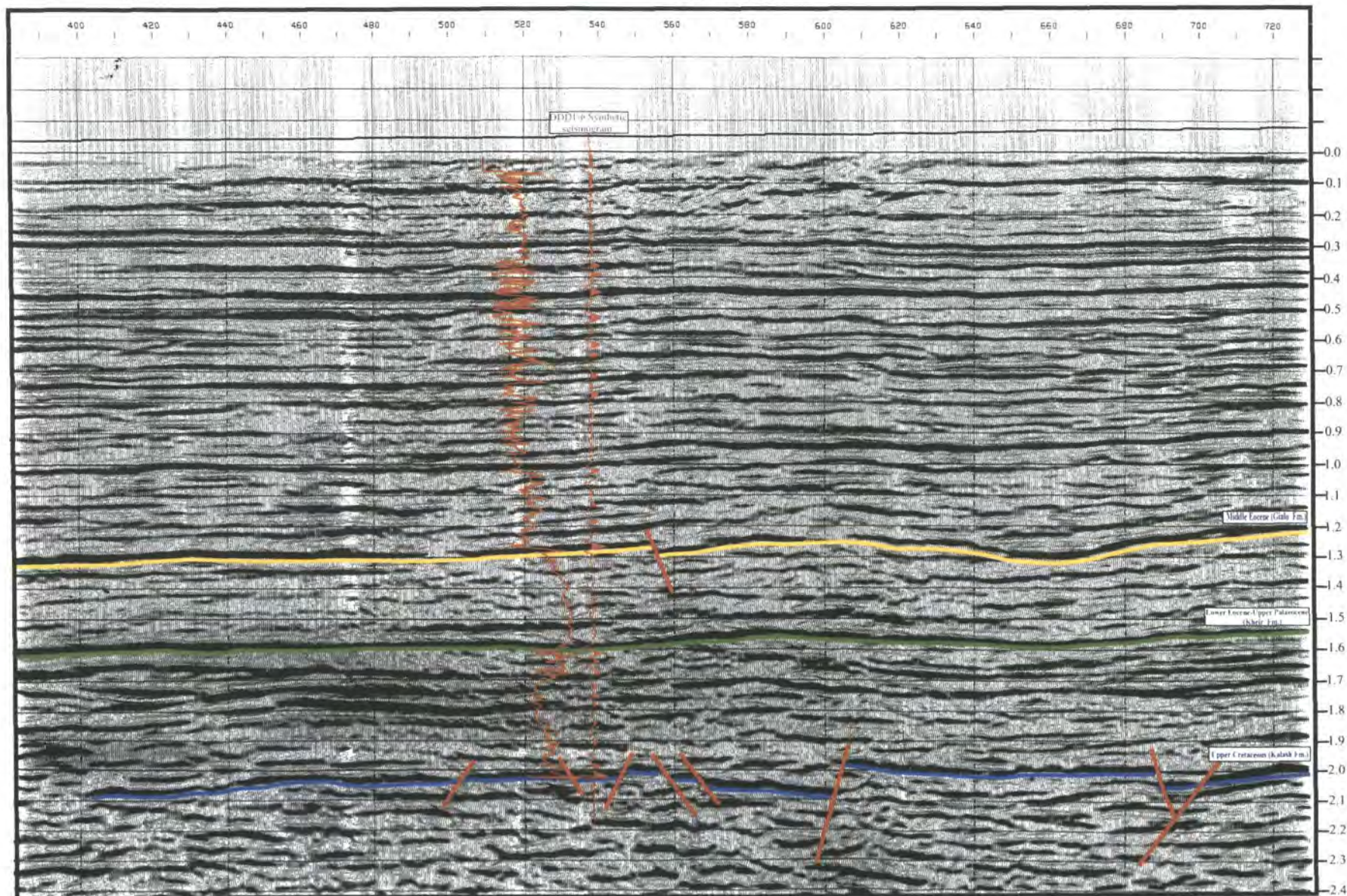


Figure 5.5. The correlation between DDD1-6 synthetic seismogram and seismic data

NW

Line 6V862-98

SE

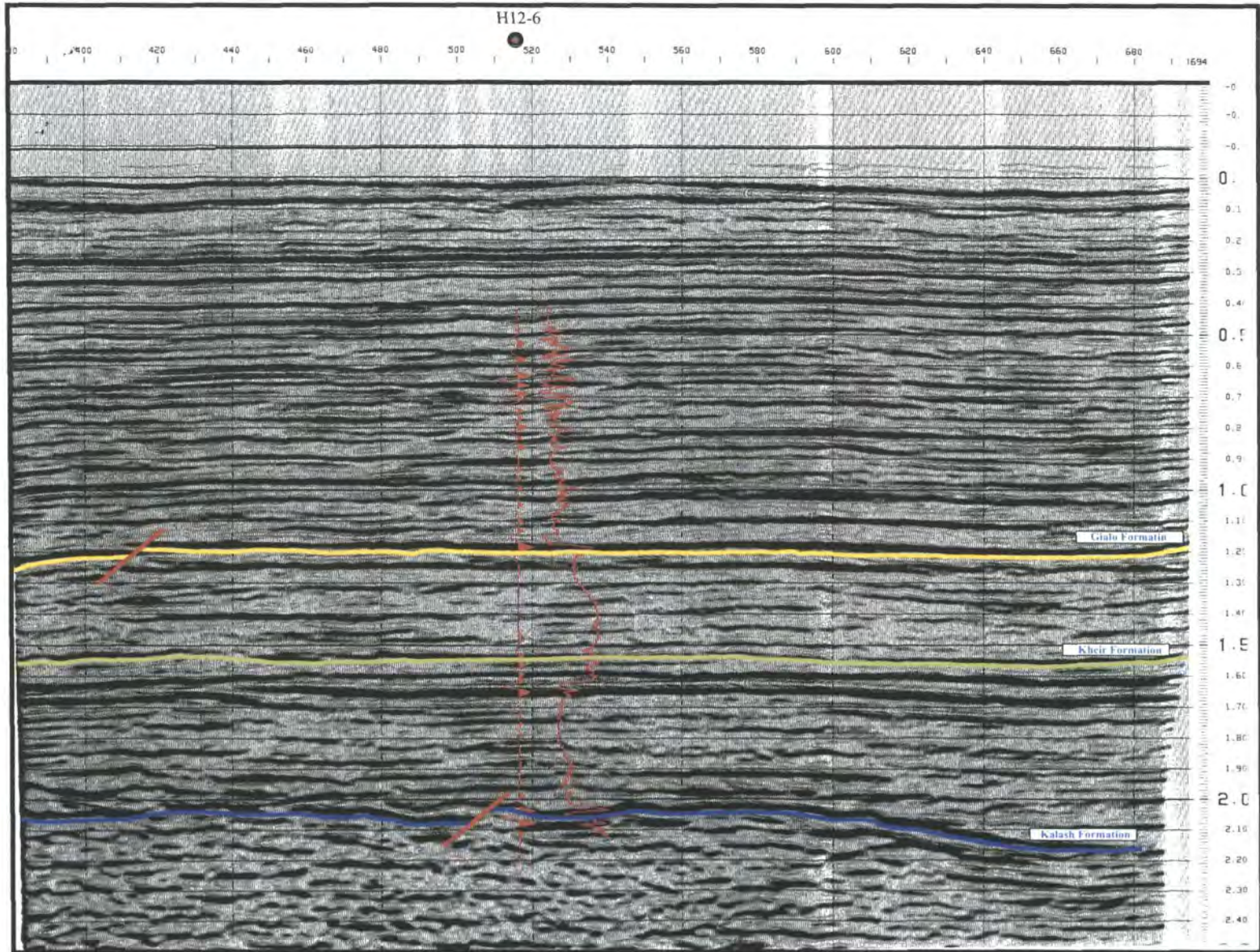


Fig. 5.6. The correlation between H12-6 synthetic seismogram and seismic data.

5.3 Mis-tie Corrections

A mis-tie is the difference in time to any horizon at the intersection point between any two seismic lines. Mis-ties can reduce the reliability of the interpretation, especially in detailed seismic stratigraphic studies or in areas of low relief structures where any small changes in dip can be critical (Indelicato and Moore, 1986).

Many efforts have been made to understand the mis-tie issue and how to correct the mis-ties. Brumbaugh (1992) suggested several factors that can cause mis-ties at intersection points, including near-surface weathering, geometrical effects, changes in recording parameters, diffractions, datum differences, survey errors, noise, reflection character differences, display polarity, improper picking, and digitising. Harper (1991) added that seismic data processing can cause some mis-ties because of a difference in the processing procedures, either between one line and another in the same survey or between different vintages of surveys. Indelicato and Moore (1986) suggested some methods to be applied to seismic data for correcting mis-ties. These include:

- 1- Honouring one line over another. This is done by forcing the lines that cross the chosen line to match it. Choosing this line may depend on many factors, including geologic well control, vintage of data, processing parameters, position of the line relative to the rest of the grid, and structural relationships.
- 2- Averaging the TWT values at each intersection by splitting the mis-tie between each line. The adjusted values are then linearly interpolated between intersections along each line.
- 3- Fitting all the mis-ties simultaneously by calculating optimum, constant time shifts to be applied to each line by least-squares regression.

Other techniques include the minmax-minisum strategy proposed by Indelicato and Moore (1986) and the mis-tie resolution technique (MRT) proposed by Indelicato (1986). Some of these techniques tend to change the dips seen on individual seismic lines.

The adjustments which apply to reduce the mis-ties between two crossing seismic lines can be classified into two types. “Translational” (Fig. 5.7) adjustment shifts the whole line up or down by a constant value. All other adjustments are called “rotational” (Fig. 5.7) because they change the dip or shape of the seismic line. The latter type of adjustment should be applied with a lot of care as it changes the shape of the surface being studied (Indelicato, 1986).

The data used in this study include seven different vintages of surveys, and many mis-ties were observed. Mis-ties were analysed at each of the three horizons. Datum shifts were observed according to data vintages. Some lines have been classified and were treated individually. These lines are F52-71, F53-71, 38-84 and 87-414. Mis-ties between lines in the 1971 data were not constant between lines and even reached 50 ms at some intersections. The 1971 data were, therefore, treated individually and were forced to fit the rest of the data.

It was found that line 38-84 could be divided into two parts, the first part having an average mis-tie of 40 ms and the second part having mis-ties ranging from 5 to 20 ms. Each part was treated separately. The first part was considered as a rogue line and the mis-ties were forced to match the rest of the intersecting lines. The second part of the line has quite reasonable mis-ties with values which are typical for the study area. They were treated as standard mis-ties and were split equally at the intersection points between this line and the others.

For line 6V87-414, the mis-tie values were all close to the average value of 20 ms, so a bulk shift of 20 ms along the line was applied. This shift generated residual mis-ties at the intersections which were subsequently treated as standard mis-ties and corrected by splitting the mis-tie values equally between the intersecting lines.

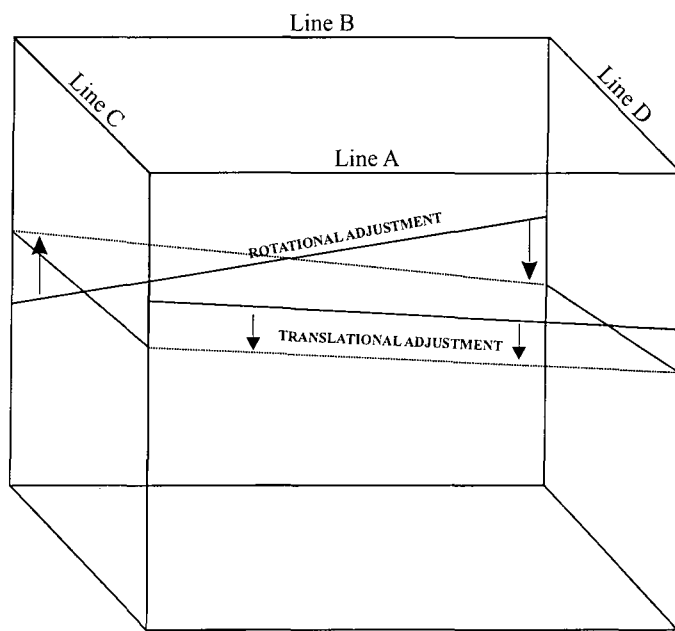


Fig. 5.7. Four-node example illustrating translational and rotational adjustments

After correcting for the constant contributions to the mis-ties for the four lines given above, the residual mis-ties were averaged at the intersections. Mis-ties which are less than the contour interval were ignored at some intersections.

5.4 Calculation of dip angles and expected mis-tie values

The unmigrated stacked sections tie at the intersections between the dip and strike lines, because the zero-offset raypaths are the same. The migrated stacked sections for dip and strike lines can mis-tie for a valid geometrical reason. The dip line will be migrated correctly, but the strike line will not be correctly migrated over dipping strata where the event will appear at a shorter TWT than on the migrated dip line. Figure 5.8 illustrates how the mis-tie between strike and dip lines occurs.

T_s : two way time on the migrated strike line at the intersection.

T_d : two way time on the migrated dip line at the intersection.

α : dip angle.

V : velocity (assumed to be constant).

Dip angle and expected mis-tie error can be calculated as follows:

$$PR = OP \tan \alpha$$

$$T_d = (2PR/V) = (2/V) OP \tan \alpha$$

$$PQ = PS \text{ (radius of circle)}$$

$$PS = OP \sin \alpha$$

$$T_s = 2PQ/V = 2 PS/V = (2/V) OP \sin \alpha = T_d \cos \alpha$$

$$\text{Mis-tie} = T_d - T_s$$

$$= T_d - T_d \cos \alpha$$

$$= (1 - \cos \alpha) T_d$$

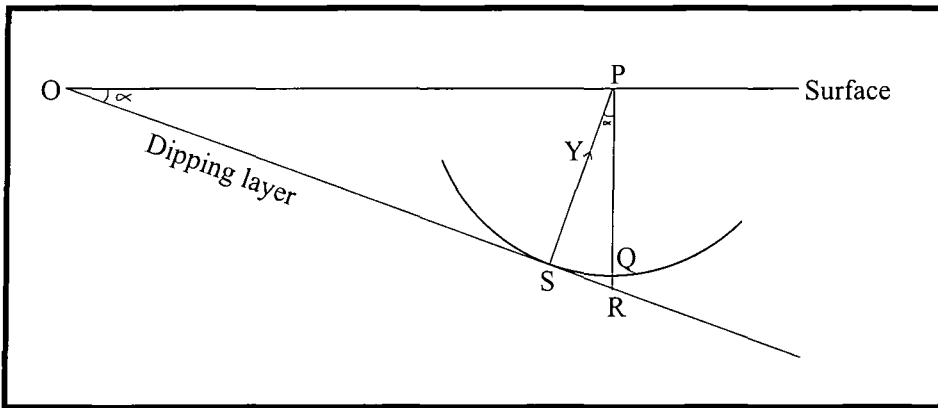


Fig. 5.8 Diagram to illustrate how the mis-tie between migrated strike and dip lines occurs.

Several intersections on migrated seismic lines displaying dipping horizons were chosen to calculate the dip angle and the expected mis-tie error value. These calculations were applied on three different horizons, shallow (Gialo horizon), medium (Kheir horizon) and deep (Kalash horizon). Table 5.1 shows all the tested lines and the results.

The dip angles range from 3.1 to 11.8 degrees, while the expected mis-tie values range from 2.4 to 30.0 ms. These results show that areas of steep dip have contributed to the observed mis-ties in the area. The table below shows that most of mis-tie values are similar to the general mis-ties in the area and close to the contour interval.

Table. 5.1 Dip angle and mis-ties expected error at the intersection between dip and strike lines.

line number	shot point	horizon	dip angle (deg)	mis-tie error (ms)
6V925-93	1240-1260	Kalash	7.5	20.0
6V854-93	780-800	Gialo	11.8	30.0
6V854-93	780-800	Kheir	3.7	3.5
6V927-93	820-840	Kheir	8.4	18.9
6V927-93	820-840	Gialo	6.3	8.2
6V931-93	400-420	Gialo	8.0	14.0
6V931-93	400-420	Kheir	7.7	15.9
6V931-93	560-580	Kheir	5.5	8.3
6V931-93	390-410	Kalash	7.7	19.9
6V931-93	600-620	Kalash	5.2	10.0
87-447	920-940	Gialo	3.3	2.4
87-447	920-940	Kheir	6.1	9.8
87-447	900-920	Kalash	4.8	8.8
87-455	960-980	Gialo	4.3	4.1
87-455	860-880	Gialo	6.7	9.7
87-455	860-880	Kheir	7.0	12.6
87-431	1060-1080	Kheir	5.9	8.7
87-431	1060-1080	Kalash	8.4	24.4
87-416	420-440	Gialo	4.7	4.8
87-416	420-440	Kheir	3.1	2.4
87-416	420-440	Kalash	6.8	15.0

5.5 Middle Eocene Gialo Formation

The Top Gialo horizon appears to have a strong response on the seismic sections in the whole area due to the good acoustic impedance contrast at the contact between the overlying Augila Shale Formation and the Gialo carbonates. This formation lies at a depth of 5248 ft in well DDD1-6 and 5361 ft in well ZZ1-6. It deepens towards the north, reaching a depth of 6641 ft sub-sea in the Hatieba Gas Field.

The most distinctive feature on this horizon is the channel, which was interpreted on many lines (Figures 5.9 and 5.10). The channel has north-south direction, width of about 1300m and depth of about 100m. No unconformity has been noted at this level, so the channel is probably a submarine erosional channel. It was stated in a Sirte Oil Company internal report that this channel may separate gas contained in the Gialo reservoir in the Assumood Gas Field area from possible gas accumulations in the same formation on the other side of the channel. This has provided encouragement for further study of the DDD1-6 area for structural closures. Re-evaluation of the DDD1-6 logs indicates that there is untested gas in the upper part of the Gialo Formation (Sirte Oil internal report).

The two-way time (TWT) values of the Top Gialo horizon were digitised by hand, then posted on the 1: 25,000 seismic base map (Enclosure 1). The seismic base map contains lines which are not available for this study. The actual lines used are plotted on the reduced scale seismic base map which was shown as Figure 4.1. The misties were calculated at every intersection point and were solved as explained previously; then the TWT values were hand-contoured with a contour interval of 10 ms.

The TWT values range from 1130 ms to 1800 ms, with the lowest value being located on the Assumood Field in the south and the highest value being located in the Wadayat Trough in the northwest of the study area. Two faults were interpreted and

SW

Seismic Line 6V927-93

NE

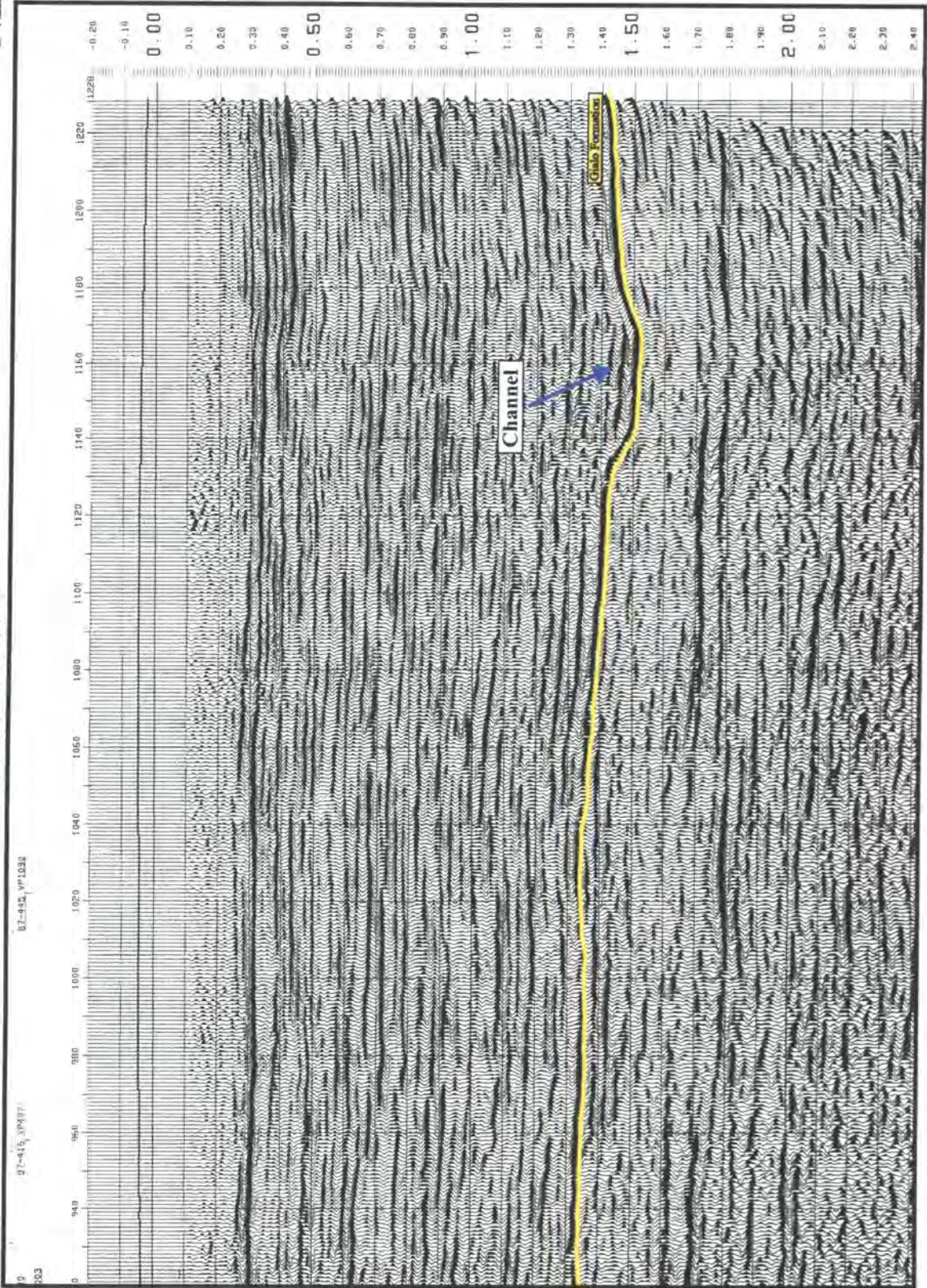


Fig. 5.9. The Middle Eocene channel on line 6V927-93.

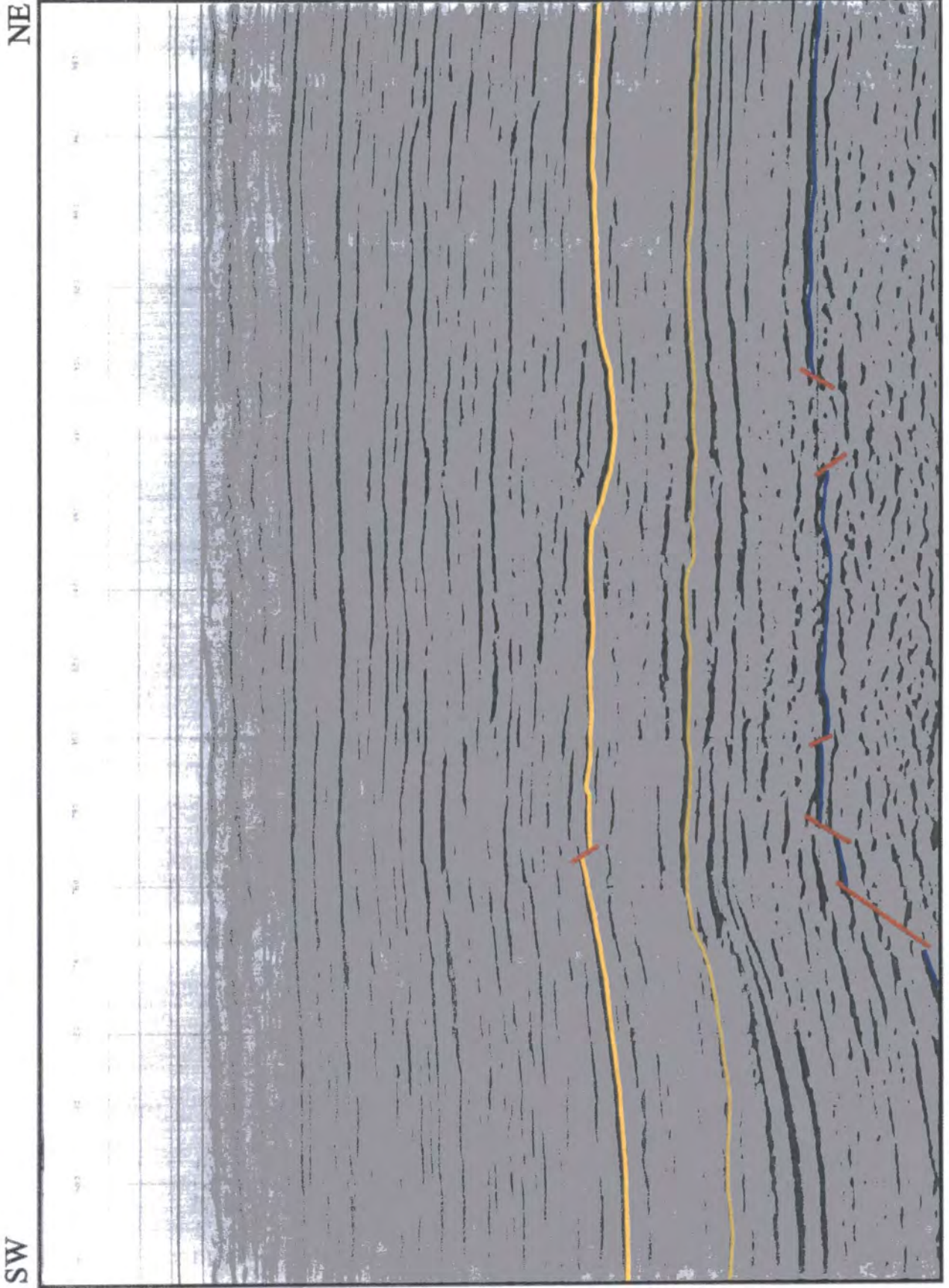


Fig. 5.10 The channel on Line 6V943-98.

plotted on the map. Both faults strike NW-SE which is the regional trend in the Sirt Basin. The faults have throws of about 30 ms (60m).

The DDD1-6 well was drilled in 1965. It was proposed as an exploration well based on gravity, magnetic and old seismic survey data. All these data were coordinated using old land survey equipment which are not as accurate as modern survey instruments, such as Global Positioning Systems (GPS) receivers. The DDD1-6 well was considered to be non-commercial and the area has consequently been discounted as a non-prospective area. By looking at the map in Figure 5.11, it can be seen that the DDD1-6 well missed the top of the structure in the Gialo Formation. The crest of the structure is represented by a closure (marked in red) and located 4 km south-southwest of the DDD1-6 well. The structure is bounded in the east by the channel and in the west by the Wadyat Trough.

The map shows that the contour density increases towards the north of the area, indicating steeper dips representing a carbonate bank in the Middle Eocene. The complete map (Enclosure 1) shows topographic lows located along the Wadayat Trough. The map also shows the high structure of the Assumood Field.

5.6 Upper Palaeocene-Lower Eocene Kheir Formation

The Kheir Formation, as mentioned in the previous chapter, consists of different lithologies including shale, marl and limestone. So it may be represented by all of them or, in the case of erosion or non-deposition, may be represented by only one lithology. The Kheir Formation was mapped in order to get information about the underlying Harash Formation, as its top is not seismically resolvable. The interpreted data show that the Top Kheir horizon has a variable seismic response, ranging from weak to quite strong, which indicates that lateral lithological changes are probable. Well data show that the Kheir Formation is represented by only two units in the wells where the drilling has reached this level, an upper marl unit underlain by a limestone unit. The horizon is at a depth of

7075 ft sub-sea in well H3-6 in the Assumood Field and at a depth of 7678 ft in well ZZ1-6. Its thickness ranges from 310 ft in well DDD1-6 to 665 ft in well H3-6 and is 425 ft thick in well ZZ1-6. The Kheir Formation was not reached by drilling at some of the Assumood Field wells. On the synthetic seismogram, this formation has a negative response (black loop).

Two-way time values of the Top Kheir horizon were posted on the 1:25,000 seismic base map (Enclosure 2). Mis-ties at every intersection were calculated, categorised and corrected; then the TWT values were hand-contoured using a 20 ms contour interval. The TWT values range from about 1500 ms to 2000 ms. There is a topographic high located on the Assumood Field in the south, while the deepest part of this horizon is located in the Wadayat Trough in the northeast. No faults were recognised at this horizon.

5.7 Upper Cretaceous Kalash Formation

Seismically, the Kalash Formation is represented by a strong seismic response. This character is attributed to the good acoustic impedance contrast generated at the contact between the carbonates of the Kalash Formation and the overlying thick shale sequence of the Hagfa Formation. The Kalash Formation was subjected to the active tectonic regime which affected the whole of the Sirt Basin in Early Cretaceous times. Consequently, the Kalash horizon is heavily faulted, which has made it quite difficult to recognise and laterally to correlate this horizon on the seismic sections. It was successfully traced over most of the area, except in a few localities where it was not possible to trace it.

The depth of the Kalash Formation ranges from 8448 ft in the Hateiba Field area to 11300 ft in the O1-6 well in the Sahl Field. It lies at a depth of 10364 ft in the H2-6 well in the Assumood Field, while it is at a depth of 9621 ft in well DDD1-6. Thickness

increases towards the west where it is about 500 ft in the Attahaddy Gas Field. The smallest reported thickness is 37 ft in the DDD1-6 well.

The digitized TWT values of the Kalash Formation were posted on the 1:25,000 seismic base map (Enclosure 3). As mentioned previously, the base map included other seismic lines which were not available for this study. The available lines are plotted on the reduced scale base map shown in Figure 4.1. Mis-tie values were calculated at each intersection. The mis-ties were categorised where some lines were treated separately and most mis-ties were corrected by splitting the mis-tie between the intersecting lines. Then the TWT values were hand-contoured using a 20 ms contour interval.

The TWT values range from about 1940 ms to 2500 ms. The smallest values corresponding to structural highs were found at two locations: the first forms a closure located south-west of the DDD1-6 well, while the second forms a closure north-west of the ZZ1-6 well. The largest TWT values are located in the Wadayat Trough. It was difficult to interpret all Kalash faults due to different data vintages, the lack of the well data and the seismic data quality for the deep formations. The faults which could be traced on more than one seismic line are plotted on Enclosure 3. The main fault (which is continuous) mapped at the Kalash level strikes NW-SE and forms the western border to the Wadayat Trough. Other faults, parallel to the main fault, are located in the Wadayat Trough. The rest of the faults strike in different directions, including N-S, NE-SW and E-W. These faults are located to the east of the main fault.

Two prospective locations for the Kalash Formation have been identified in this map. They are structural high closures (marked in red) (Fig. 5.12). The first closure (A) is located about 2.5 km south-west of the DDD1-6 well. It is bounded to the west by the main fault bordering the Wadayat Trough and separated by faults from the other sides (Enclosure 3). The second closure (B) is located between wells DDD1-6 and ZZ1-6. It is

a faulted closure and appears to be bigger than the (A) closure. These two closures are at similar locations to the closures seen at the Gialo level.

The Assumood Field area appears to have no structural high at the Kalash level, while the DDD1-6 area does have a structural high. This indicates that gas accumulations in the Kalash are more likely to exist in the study area than the Assumood Field area. Also the wells DDD1-6 and ZZ1-6 are not located on structural highs at this level. It might be that these two wells were drilled for other shallower formations.

5.8 General structure of the area

The Sirt Basin formed as a result of tensional tectonics. There are large areas of uplift and subsidence with associated normal faulting, while the absence of compressional folds is noticeable (Brady, et al., 1980). Most of the faults cutting the Mesozoic and Tertiary section are normal faults. Gumati and Kanes (1985) suggested that there is a possibility of having listric faults related to compaction system in the Sirt Basin.

This study included an interpretation of three different horizons: the shallowest is the Middle Eocene Gialo Formation, the middle horizon is the Upper Palaeocene-Early Eocene Kheir Formation, and the deepest horizon is the Upper Cretaceous Kalash Formation. Faults were recognised on two horizons, the shallowest and the deepest, whereas no faults could be clearly identified at the Kheir horizon.

All faults recognised in this study have been classified as small normal faults with limited continuity (Roberts and Yielding, 1994) except for one fault which forms the eastern boundary of the Wadayat Trough and is classified as a major fault. From the interpreted seismic sections, it can be seen that the Upper Cretaceous Kalash Formation is heavily faulted. This can be attributed to the main rift system that affected the whole Sirt Basin in the Early Cretaceous (see chapter 2). The Wadayat Trough was structured as a result of this block faulting.

Faults are commonly traceable either upwards or downwards, but in this case the faults which are interpreted at the Gialo horizon could not be linked to the Kalash horizon faults. Figure 5.10 shows one of the two faults interpreted on the Gialo horizon. The other fault does not cross this line. It has about 30 ms (57m) vertical displacement. An even larger displacement might be expected on the underlying horizons if the fault is linked to one of those interpreted at the Kalash level. The question arises why there is no connection between faults that displace the Upper Cretaceous and faults that displace the Middle Eocene.

Two possible reasons are suggested to explain why there is no evidence of the Gialo faults on the strata above and below. One is that these faults are isolated and of small scale, resulting from a local extensional regime. A second explanation is that they are not faults but the margins of another channel.

5.9 Velocity investigations

Interval velocities are needed for depth conversion of two-way time maps. Lateral variations in velocity have to be investigated before applying depth conversion. Velocities can be determined from either seismic data or well data.

In this study, velocity investigations have been made in order to see whether the structural features seen on the two-way time maps will change significantly after depth conversion. The first velocity calculation used the interval velocities obtained from stacking velocities listed in boxes on each seismic section. The second used well data to calculate the interval velocities. The last velocity calculation used average velocity calculated at three wells in different parts in the area. The average velocities have been calculated from the two-way times picked on the seismic sections at the well locations and the real depth.

To test the interval velocities calculated from stacking velocity analyses, the depths of the Gialo, Kheir and Kalash formations were calculated at most wells in the

area (Table 5.2). Depths were calculated by the layer-cake technique in which the interval velocities and two-way times were used to calculate the thickness of each interval down to each formation. Depth calculations were made from data of vintages 1984, 1987, 1992, 1993 and 1998. The results were compared with the real depths of the above-mentioned formations at each well and differences in depth were calculated at each well. Most differences were over 100 m for the Gialo Formation, with depths calculated from stacking velocities being shallower. But the difference ranged from 49 m to 227 m shallower at well DDD1-6 using velocities from the 1992 and 1993 data. Greater differences were obtained from the Hatieba and Attahaddy areas.

Table 5.2 Depth conversion calculations for the Gialo Formation.

data vintage	well number	calculated depth (m)	real depth (m)	difference (m)
1984	S12-6	2168	2025	+ 143
1987	H1-6	1284	1442	- 158
1987	H7-6	1280	1434	- 154
1987	H8-6	1284	1434	- 150
1987	H10-6	1301	1455	- 154
1987	DDD1-6	1462	1573	- 111
1992	ZZ1-6	1514	1588	- 74
1992	DDD1-6	1524	1573	- 49
1993	DDD1-6	1346	1573	- 227
1993	ZZ1-6	1439	1588	- 149
1993	H3-6	1333	1467	- 134
1993	FF6-6	1131	1264	- 133
1993	FF10-6	967	1239	- 272
1998	H2-6	1385	1543	- 158
1998	H12-6	1395	1487	- 92
1998	DDD1-6	1507	1573	- 66

In the Kheir Formation, the differences ranged from 6 m to 292 m with depths calculated from stacking velocities generally being shallower. There is only one exception: the depth calculated from stacking velocities was 203 m greater at well S12-6 in the Hateiba Field. The results are shown in Table 5.3.

In the Kalash Formation, most of the differences ranged from 0 to 100 m with depths calculated from stacking velocities being shallower. Greater depths of 22 m and 86 m were obtained at well S12-6 in the Hateiba Field and well DDD1-6, respectively. The results are shown in Table 5.4.

Table 5.3 Depth conversion calculations for the Kheir Formation.

data vintage	well number	calculated depth (m)	real depth (m)	difference (m)
1984	S12-6	2367	2164	+203
1984	DDD1-6	2265	2259	-6
1987	H7-6	1905	2186	-280
1992	DDD1-6	2182	2259	-77
1993	ZZ1-6	2175	2341	-166
1993	H1-6	1884	2176	-292
1998	H7-6	2030	2280	-250
1998	H12-6	2039	2219	-180
1998	H12-6	1990	2219	-229
1998	DDD1-6	2146	2259	-118

Table 5.4 Depth conversion calculations for the Kalash Formation.

data vintage	well number	calculated depth (m)	real depth (m)	difference (m)
1984	S12-6	2857	2835	+22
1984	DDD1-6	3019	2933	+86
1987	H7-6	2925	2958	-33
1992	DDD1-6	3019	2933	+86
1993	ZZ1-6	2998	3094	-99
1993	H1-6	2874	2937	-63
1998	DDD1-6	2933	2933	0
1998	H7-6	2875	3160	-285
1998	H12-6	2950	3050	-100
1998	H12-6	2952	3050	-98

The results show that interval velocities obtained from stacking velocities are not reliable for depth conversion. Also the velocity analysis panels on the seismic data show that the velocities were picked at different (random) time levels and were not picked on the same coherent seismic events. In order to improve the depth conversion

using interval velocities from seismic data, stacking velocities should be re-picked along the same coherent seismic horizons.

The second investigation used the DDD1-6 and H12-6 velocity logs in order to identify different velocity intervals and link them to their corresponding reflectors. The continuous velocity logs were divided into 18 and 22 velocity intervals for the wells DDD1-6 and H12-6, respectively. Then the thickness of each interval was calculated down to the Gialo and Kalash formations. It was not possible to recognize the Kheir Formation on both velocity logs. The upper 0.5s of each velocity log is missing at these wells. The average velocity of the next interval was taken to represent the missing parts. These depth estimates for the Top Gialo and Kalash horizons gave shallower depths than the true depths. The difference in depth for the Gialo Formation was 13 m at well DDD1-6 and 41 m at well H12-6. The difference in depth for the Kalash Formation was 7 m at well DDD1-6 and 74 m at well H12-6. As the upper 0.5s is missing from the velocity data, it is difficult to say how reliable this method is, even though the results are better than those resulting from stacking velocities.

The last investigation has been done by calculating the average velocities to the top Gialo, Kheir and Kalash horizons at three wells in different parts of the area. The average velocity is very commonly used in depth conversion in the case where reliable velocity information is not available. In this study, the average velocity was calculated for the DDD1-6, H12-6 and ZZ1-6 wells (Tables 5.3; 5.4; 5.5). Average velocity was obtained simply by dividing the real depth found in the well by the one-way travel time obtained from picking the horizon on the seismic section.

Table 5.5 The average velocity calculations for the Gialo Formation.

well	One-way time (sec)	depth (m)	velocity (m/sec)
DDD1-6	0.633	1573	2487
H12-6	0.585	1487	2542
ZZ1-6	0.630	1588	2521

Table 5.6 The average velocity calculations for the Kheir Formation.

well	One-way time (sec)	depth (m)	velocity (m/sec)
DDD1-6	0.795	2259	2842
H12-6	0.768	2219	2889
ZZ1-6	0.805	2341	2908

Table 5.7 The average velocity calculations for the Kalash Formation.

well	One-way time (sec)	depth (m)	velocity (m/sec)
DDD1-6	1.010	2933	2904
H12-6	1.020	3050	2991
ZZ1-6	1.030	3094	3004

It can be seen that the average velocity values at the chosen wells were similar, so it is interesting to consider whether the differences are significant compared to the errors. The depth values from the wells are believed to be accurate whereas the picked travel times are affected by many factors. Static corrections are probably the largest source of error in the time values. From the mis-tie calculations which were previously discussed, the average mis-tie value was about 15 ms which gives an estimated error of $\pm 2.5\%$ at the Gialo horizon (average two way travel time of 600 ms), an estimated error of $\pm 1.9\%$ at the Kalash horizon (average two way travel time of 790 ms) and an estimated error of $\pm 1.5\%$ at the Kalash horizon (average two way travel time of 1020 ms). Consequently, the average velocities have an estimated error of 2.5%, 1.9% and 1.5% for the horizons Gialo, Kheir and Kalash, respectively. The values in Tables 5.3 5.4 and 5.5 lie within this range, which suggests that a constant value for the average velocity would be consistent with the observations. It is concluded that subsurface features seen on the two-way time maps will not be significantly different on the depth maps.

5.10 Reserves

Conservative estimates of reserves have been calculated for the prospective closures which were identified at the Top Gialo and Top Kalash horizons. Reservoir volume was

calculated graphically from the 1:25,000 two-way time maps. The volume of each closure was calculated assuming the structure is filled to the spill point. The spill point for the Gialo Formation was taken at a contour of 1245 ms. The apparent spill point for closure A at the Top Kalash horizon is between contours of 1980 ms and 2000 ms located somewhere along the major fault zone to the east-southeast. It was taken to be 1980 ms to get a conservative estimate of reserves, bearing in mind that the structure on the two-way time map may be tilted due to lateral velocity variations. The same contour value of 1980 ms was taken as the spill point for closure B on the Top Kalash horizon. Thicknesses of the Gialo and Kalash reservoirs above the spill point were calculated using average velocities of 2500 m/s and 2950 m/s, respectively.

The volumetric reserves were simply calculated using the following formula:

$$\text{Gas in place (in BCF)} = 43.56 \times 10^{-6} \phi (1-S_w) (\text{F.V.F.}) (\text{Reservoir volume})$$

where the reservoir volume is in acre-feet. The Formation Volume Factor is

$$(\text{F.V.F.}) = (P_{\text{reservoir}} \times T_{\text{standard}}) / (P_{\text{standard}} \times T_{\text{reservoir}})$$

where standard pressure is 14.65 psia and standard temperature is 520 R. Reservoir temperature and pressure were taken from DDD1-6 data. Average porosity values were taken to be the same as those reported for the Assumood Field, as was the water saturation in the Gialo Formation. The water saturation for the Kalash Formation was taken from the DDD1-6 well. The parameters used to calculate the reserves for the Gialo and Kalash reservoirs are listed in the Table 5.6.

Reservoir parameters	Gialo closure	Kalash	
		closure A	closure B
Reservoir pressure (psia)	2390	4761	4761
Reservoir temperature (deg. Rankin)	611	739	739
Formation Volume Factor	138.8	228	228
Average porosity (%)	20.3	18	18
Average water saturation (%)	15	37	37
Reservoir volume(Acre-feet)	36,333.4	81,544.76	126,398.22

Table 5.8. Reservoir parameters used to calculate reserves.

The above listed parameters were used to calculate the reserves for the three prospective closures. The estimated reserves of gas in place at the Gialo Formation are 37 BCF; estimated reserves for the Kalash A closure are 91 BCF and for the Kalash B are 142 BCF.

5.11 Carbonate buildups in the Palaeocene

Carbonate buildups, including reefs and banks, form important and prolific hydrocarbon reservoirs in many operating areas of the world, particularly in the United States, Canada, North Africa, Mexico, Southeast Asia and the Middle East (Bubb and Hatlelid, 1977). Figure 5.13 shows the different types of carbonate buildups which are easily can be recognized from seismic interpretation. Bubb and Hatlelid (1977) explained the procedure of recognition of carbonate buildups. They proposed three general steps for the interpretation procedure, the first of which is to convert all available well data into a format compatible with seismic interpretation. The second step is to interpret the depositional sequences from the seismic data by finding their ages and boundaries. The third step is recognition of seismic facies units within sequences.

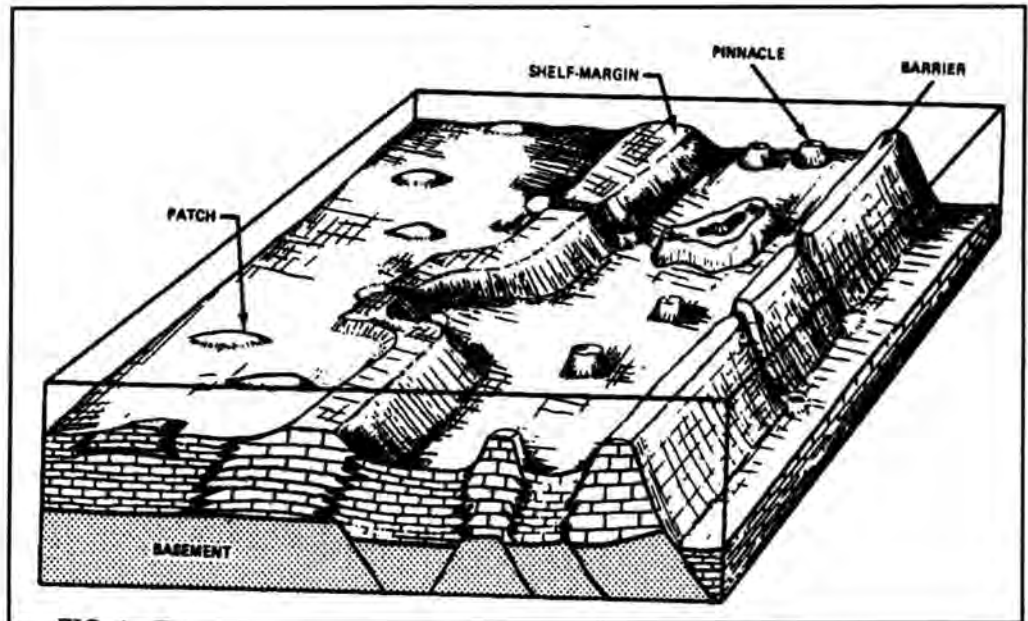
Bubb and Hatlelid (1977) also proposed two criteria for recognition of carbonate buildups from the seismic sections. These are direct and indirect criteria (Fig. 5.14). The direct criteria can be divided into two types. The first is recognition from the boundary outline, in which the reflection events define the boundary of the buildup. The second type of direct criterion is seismic facies change manifested as changes in amplitude, frequency, or continuity of reflections within the buildup, or between the buildup and laterally adjacent time-synchronous reflections. The indirect criteria are divided into four types. The first is drape, which occurs when a strong contrast exists in the lithology of buildup and off-buildup sediments. The second type is velocity anomalies, where a velocity contrast exists between the buildup and adjacent strata. A high velocity carbonate buildup will cause 'velocity pull-up' of underlying reflectors. The third type is spurious events, in which the edges of the buildup are marked by termination of

surrounding beds or changes in internal bedding geometry. The last type of indirect criterion is basin architecture, in which the basin architecture such as fault-block edges, position of hinge line or contemporaneous structural highs can indicate carbonate buildups along the seismic section.

Palaeocene carbonates are major reservoirs in the Sirt Basin. The Palaeocene was a time of major reefal growth when carbonate banks were developed. Many oil fields in the Sirt Basin produce from the Palaeocene carbonate reservoirs, including the Intisar, Nasser, Bahi, Wadi, Zaqqut and Az-Zahraa–Al-Hufrah fields (Fig 1.3) (Bezan, 1996).

During this study the seismic sections were examined for evidence of Palaeocene mounds and buildups, especially for the carbonate mound type that may form in the shale sequences. The data seem to have no such features.

Fig. 5.13 Types of carbonate buildups most easily recognized from seismic interpretation (after Bubb and Hatlelid, 1977).



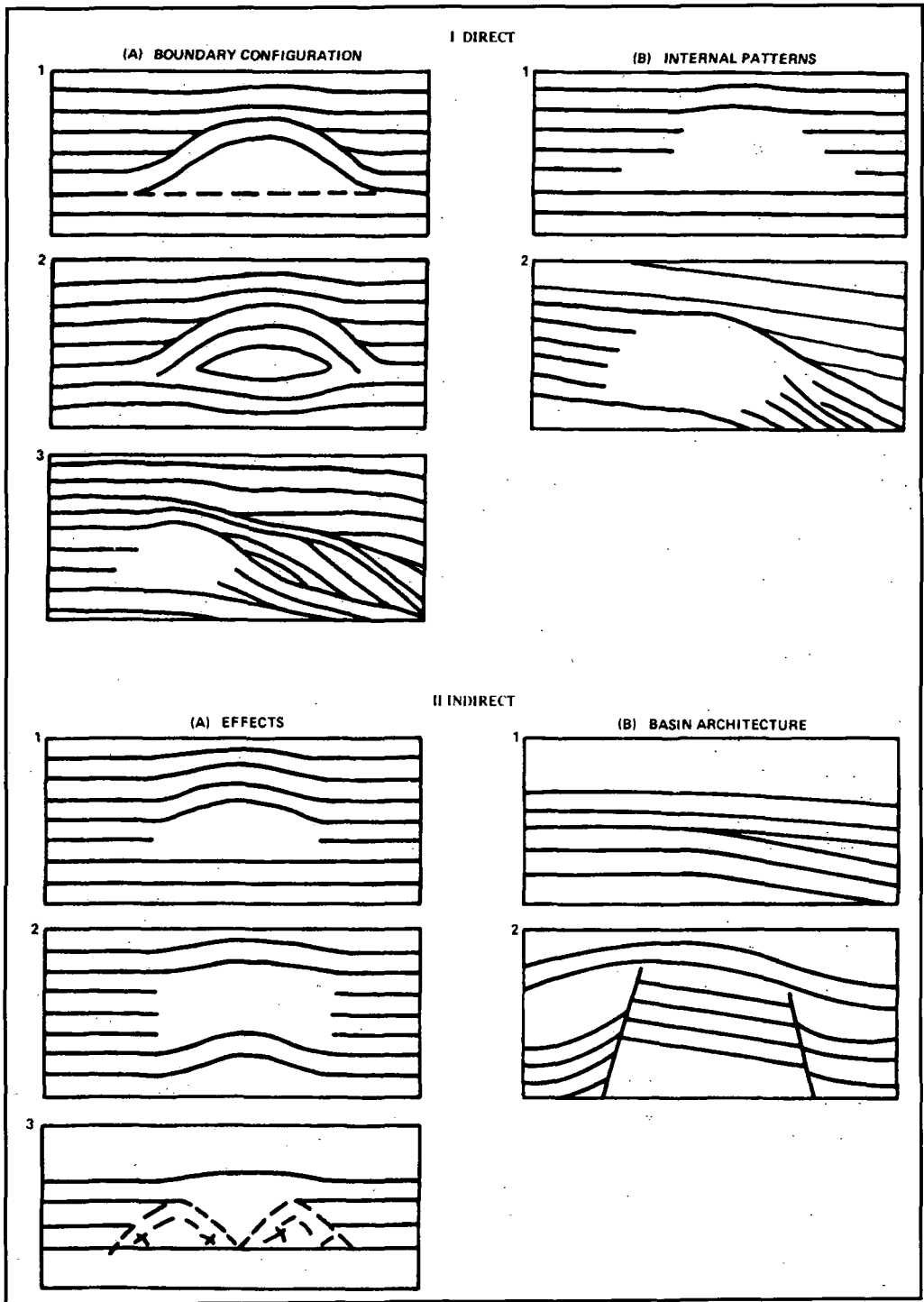


Fig. 5.14 Direct and indirect criteria for recognizing carbonate buildups (after Bubb and Hatlelid, 1977).

CONCLUSIONS & RECOMMENDATIONS

6.1 Conclusions

- 1- Two prospective locations for the Kalash Formation were identified. The first is located south of well DDD1-6 and the second is located south-west of well ZZ1-6. The location south of well DDD1-6 is the shallowest position of the Top Kalash horizon in the study area, which makes it the most prospective location for the Kalash level.
- 2- No prospective location was found on the Top Kheir horizon. Lateral changes in the lithology of the Kheir Formation may have limited the accuracy of mapping this formation.
- 3- One prospective location for the Gialo Formation was identified. It is located close to the structural closure on the Top Kalash horizon south of the DDD1-6 well. This prospect may have accumulated hydrocarbons at the Gialo level due to the barrier formed by the channel oriented northeast-southwest. Comparing the two high structures that have been interpreted on the Gialo and Kalash horizons with the Assumood Field structure, the new prospective locations are about 225 m shallower assuming an average velocity of 2500 m/sec.

- 4- The study proved that the DDD1-6 and ZZ1-6 wells were not drilled on structural highs. The new prospective locations are close to the drilled locations, especially in the DDD1-6 case. These two wells were drilled according to gravity and magnetic data, so it is not surprising that they missed the crests of the structures.
- 5- No Palaeocene carbonate buildups could be identified in the area.

6.2 Recommendations

The new prospective location of south DDD1-6 is recommended as the best for exploration drilling, especially for the Kalash and Gialo formations. This location is a structural high at both the Top Gialo and Top Kalash horizons. This recommendation is supported by the re-evaluation of previous well data, which has suggested the presence of untested gas intervals at the Kalash and Gialo formations in the DDD1-6 well.

The other new prospective location southwest of well ZZ1-6 is also recommended for drilling with the Kalash Formation as the primary target. However, since the seismic coverage is sparse around this target it may be advisable to shoot an additional set of seismic lines to improve resolution of the structure.

References

Abushagur, S.A., 1991. Cyclic transgressive and regressive sequences and their association with hydrocarbons, Ghani Field, Sirt Basin, Libya. In: Salem, M. J. and Belaid, M. N. (eds), The Geology of Libya, volume V. Elsevier, Amsterdam, 1827-1840.

Barbieri, R., 1996. Micropalaeontology of the Rakb (Cenomanian to Early Maastrichtian) in the Hameimat Basin, Northern Libya. In: Salem, M.J., Mouzughi, A.J. and Hammuda, O.S. (eds), The Geology of the Sirt Basin, volume I. Elsevier, Amsterdam, 185-194.

Barr F.T. and Berggren, W.A., 1980. Lower Tertiary biostratigraphy and tectonics of northeastern Libya. In Salem, M.J. and Busrewil, M.T. (eds), The Geology of Libya, volume I. Academic Press, London, 163-192.

Barr, F.T. and Weegar, A.A., 1972. Stratigraphic Nomenclature of the Sirt Basin, Libya. Published by the Petroleum Exploration Society of Libya, Tripoli, Libya.

Bender, A., Coelho, F. and Bedregal, R., 1996. A basin modelling study in the southeastern part of Sirt Basin, Libya. In: Salem, M.J., Mouzughi, A.J. and Hammuda, O.S. (eds), The Geology of the Sirt Basin, volume I. Elsevier, Amsterdam, 139-155.

Bezan, A., 1996. The Palaeocene sequence in the Sirt Basin. In: Salem, M.J., Mouzughi, A.J. and Hammuda, O.S. (eds), The Geology of the Sirt Basin, volume I. Elsevier, Amsterdam, 97-117.



Bezan, A. and Malak, E., 1996. Oligocene sediments of Sirt Basin and their hydrocarbon potential. In: Salem, M.J., Mouzughi, A.J. and Hammuda, O.S. (eds), *The Geology of the Sirt Basin*, volume I. Elsevier, Amsterdam, 119-127.

Brady, T.J., Campbell, N.D.J. and Maher, C.E., 1980. Intisar 'D' Oil Field, Libya. In: Halbouty, M. T., (ed.), *Giant Oil and Gas Fields of the Decade 1968-1978*. American Association of Petroleum Geologists Mem. 30, 543-564.

Broughton, P. and Buthfer, M., 2000. Southern Jahama Platform deep gas exploration: SSSS1-6 prospect description, Concession 6. Geological note 204, Sirte Oil Company, pp 29, unpublished report.

Brumbaugh, D.L., 1992. SMAP revisited and revised. *Geophysics*, 57, 258-262.

Bu-Argoub, F.M., 1996. Palynological and palynofacies studies of the Upper Cretaceous sequence in well C275-65, Sirt Basin, NE Libya. In: Salem, M.J., Mouzughi, A.J. and Hammuda, O.S., (eds), *The Geology of the Sirt Basin*, volume I. Elsevier, Amsterdam, 418-453.

Bubb, J.N. and Hatlelid, W.G., 1977. Seismic recognition of carbonate buildups. In: Payton, C. E. (ed.), *Seismic Stratigraphy – Applications to Hydrocarbon Exploration*, American Association of Petroleum Geologists Mem. 26, 185-204.

Burke, K. and Dewey, J., 1974. Two plates in Africa during the Cretaceous. *Nature*, 249, 313-316.

Conant, L.C. and Goudarzi, G.H., 1967. Stratigraphic and tectonic framework of Libya. *American Association of Petroleum Geologists Bulletin*, 51, 719-730.

El-Alami, M.A., 1996. Habitat of oil in Abu Attiffel area, Sirt Basin, Libya, In: Salem, M.J., El-Hawat, A.S. and Sbeta, A.M., (eds), 1996. The Geology of the Sirt Basin, volume II. Elsevier, Amsterdam, 337-348.

El-Ghoul, A., 1996. An approach to locate subtle Waha structural traps on the Zelten Platform: geology and geophysics. In: Salem, M.J., Busrewil, M.T., Misallati, A.A. and Sola, M. (eds), The Geology of the Sirt Basin, volume III. Elsevier, Amsterdam, 137-154.

El-Makhrouf, A.A., 1996. The Tibisti-Sirt orogenic belt, Libya. In: Salem, M.J., Busrewil, M.T., Misallati, A.A. and Sola, M. (eds), 1996. The Geology of the Sirt Basin, volume III. Elsevier, Amsterdam, 107-121.

Fairhead, J.D. and Green, C.M., 1989. Controls on rifting in Africa and regional tectonic model for the Nigeria and east Niger rift basins. *Journal of Africa Earth Sciences*, 8, 231-249.

Fouad, K.M., 1991. Tectonic framework of Libya. In: M.J. Salem, A.M. Sbeta and M.R. Bakbak (eds), The Geology of Libya VI. Elsevier, Amsterdam, 2451-2460.

Futyan, A. and Jawzi, A.H., 1996. Petrography and reservoir quality of the Lower Cretaceous sandstone in the deep Mar Trough, Sirt Basin. In: Salem, M.J., El-Hawat, A.S. and Sbeta, A.M. (eds), The Geology of the Sirt Basin, volume II. Elsevier, Amsterdam, 287-308.

Gras, R. and Thusu, B., 1998. Trap architecture of the Early Cretaceous Sarir Sandstone. In: Macgregor, D.S., Moody, R.T.J. and Clark-Lowes, D.D. (eds), *Petroleum Geology of North Africa*. Geological Society, London, Special Publication No. 132, 317-334.

Gumati, Y.D. and Kanes, W.H., 1985. Early Tertiary subsidence and sedimentary facies - northern Sirt Basin, Libya. *American Association of Petroleum Geologists Bulletin*, 69, 39-52.

Gumati, Y.D., Kanes, W.H. and Schamel, S., 1996. An evaluation of the hydrocarbon potential of the sedimentary basins of Libya. *Journal of Petroleum Geologists*, 19, 95-112.

Gumati, Y.D. and Nairn, A.E.M., 1991. Tectonic subsidence of the Sirt Basin, Libya. *Journal of Petroleum Geology*, 14, 93-102.

Gumati, Y. D. and Schamel, S., 1988. Thermal maturation history of the Sirt Basin, Libya, *Journal of Petroleum Geology*, 11, 205-218.

Hallett, D. and El Ghoul, A., 1996. Oil and gas potential of the deep trough areas in the Sirt Basin, Libya. In: Salem, M.J., El-Hawat, A.S. and Sbeta, A.M., (eds), 1996. *The Geology of the Sirt Basin*, volume II. Elsevier, Amsterdam, 455-483.

Harding, T., 1984. Graben hydrocarbon occurrences and structural style. *American Association of Petroleum Geologists Bulletin*, 68, 333-362.

Harper, M.D., 1991. Seismic mis-tie resolution technique. *Geophysics*, 56, 1825-1830.

Ibrahim, M.W., 1991. Petroleum geology of the Sirte Group Sandstone, eastern Sirt Basin. In: Salem, M.J. and Busrewil, M.T., (eds), *The Geology of Libya*, Al-Fateh University, Tripoli, VII, 2757-2779.

Indelicato, G.J. and Moore, G. C., 1986. Seismic mis-tie adjustment procedure (SMAP) using a minimax-minisum strategy. *Geophysics*, 51, 673-678.

Klitzsch, E., 1968. Die Gothlandium-Transgression in der zentral-Sahara. *Deutsch Geol. Gesellschaft, Zeitschrift.*, 117, 492-501.

Macgregor, D.S. and Moody, R.T.J., 1998. Mesozoic and Cenozoic petroleum systems of North Africa. In: Macgregor, D.S., Moody, R.T.J. and Clark-Lowes, D.D., (eds), *Petroleum Geology of North Africa*. Geological Society, London, Special Publication No. 132, 201-216.

Perrella, G., 1990. Evaluation of the minor reservoirs of the Assumood Field. Geological note 178. (Sirte Oil Company internal report).

Roberts, A. and Yielding, G., 1994. Continental extensional tectonics. In: Hancock, P. L. (ed.), *Continental deformation*, Pergamon Press, 223-250.

Roohi, M., 1996. Geological view of source-reservoir relationships in the western Sirt Basin. In: Salem, M.J., El-Hawat, A.S. and Sbeta, A.M., (eds), *The Geology of the Sirt Basin*, volume II. Elsevier, Amsterdam, 323-336.

Sinha R. and Mriheel I., 1996. Evolution of subsurface Palaeocene sequence and shoal carbonates south-central Sirt Basin. In: Salem, M.J., El-Hawat, A.S. and Sbeta, A.M., (eds), 1996, *The Geology of the Sirt Basin*, volume II. Elsevier, Amsterdam, 153-195.

Selley, R.C., 1997. The Sirt Basin of Libya. In: Selley, R.C., (ed.), *African Basins, Sedimentary Basins of the World*, 3, Elsevier, Amsterdam, 27-37.

Sghair, A.M.A., 1996. Petrography, diagenesis and provenance of the Bahi Formation in the western part of the Sirt Basin, Libya. In: Salem, M.J., El-Hawat, A.S. and Sbeta, A.M., (eds), *The Geology of the Sirt Basin*, volume II. Elsevier, Amsterdam, 65-81.

Skuce, A.G., 1996. Forward modelling of compaction above normal faults: an example from the Sirt Basin, Libya. In: Buchanan, P.G. and Nieuwland, D.A., (eds), *Modern Developments in Structural Interpretation, Validation and Modelling*, Geological Society Special Publication no. 99, 135-146.

Van Der Meer, F.D. and Cloetingh, S.A. P. L., 1993. Late Cretaceous and Tertiary subsidence history of the Sirt Basin, Libya: an example of the use of backstripping analysis. *ITC Journal*, volume 1, 68-76.

Van Houten, B.F., 1983. Sirt Basin, north-central Libya, Cretaceous rifting above a fixed mantle hotspot? *Geology*, 11, 115-118.

Walston, V.A., 1970. Associated or non-associated gas? Northern Concession 6, Libya. Geological note no. 39, Esso Standard Libya Inc. internal report.

Weimer, R. 1998. Annual technical meeting. Internal Sirte Oil Company report.

Wennekers, J.H.N., Wallace, F.K. and Abugares, Y.I., 1996. The geology and hydrocarbons of the Sirt Basin: a synopsis. In: Salem, M.J., Mouzoughi, A.J. and Hammuda, O.S., (eds), *The Geology of the Sirt Basin*, volume I. Elsevier, Amsterdam, 3-56.

Williams, J.J. 1968, The sedimentary and igneous reservoirs of the Augila oil field. In: *geology and Archaeology of northern Cyrenaica, Libya*. (ed. F. T. Barr). Petroleum Exploration Society Libya, Tripoli, 10th Annual field conference, 197-205.

Wilson, J.T., 1963. A possible origin of the Hawaiian Islands. *Canadian Journal of Physics*, 41, 863-880.

APPENDIX

1

WELL DATA AVAILABLE

Assumood Field

WELL	H1-6	H2-6	H3-6
KB	152'	151'	180'
TD	10,291'	10,985'	10,300'
ARIDA	2765'(-2613')	3010'(-2859')	2822'(-2642')
AUGILA	4430'(-4278')	4756'(-4605')	4551'(-4371')
GIALO	4882'(-4730')	5212'(-5061')	4992'(-4812')
GIR	6480'(-6328')	6600'(-6449')	6525'(-6345')
KHEIR MARL	7288'(-7136')	7631'(-7480')	7255'(-7075')
KHEIR LS	7410'(-7258')	7780'(-7629')	7455'(-7275')
HARASH	7774'(-7622')	8165'(-8014')	7920'(-7740')
HARASH POROSITY	7955'(-7803')	8333'(-8182')	8095'(-7915')
KHALIFA	8068'(-7916')	8445'(-8294')	8185'(-8005')
HAGFA	9786'(-9634')	8737'(-8586')	8550'(-8370')
KALASH	8310'(-8158')	10,515'(-10,364')	NDE
WAHA	NP	NDE	NDE
SIRTE SHALE	NP	10,692'(-10,541')	NDE
SIRTE DOLOMITE	NP	10,865'(-10,714')	NDE
SIRTE SAND	9985'(-9833')	10,915'(-10,764')	NDE
SIRTE SHALE	NP	NP	NDE
BAHI	NP	NDE	NDE
QUARTZITE	10,150'(-9998')	NDE	NDE

WELL	H4-6	H5-6	H6-6
KB	164'	195'	194'
TD	5,265'	5,250'	5,270'
ARIDA	2770'(-2606')	2775'(-2580')	NL
AUGILA	4480'(-4316')	4490'(-4295')	4425'(-4231')
GIALO	4900'(-4736')	4915'(-4720')	4879'(-4685')
GIR	NDE	NDE	NDE
KHEIR MARL	NDE	NDE	NDE
KHEIR LS	NDE	NDE	NDE
HARASH	NDE	NDE	NDE
HARASH POROSITY	NDE	NDE	NDE
KHALIFA	NDE	NDE	NDE
HAGFA	NDE	NDE	NDE
KALASH	NDE	NDE	NDE
WAHA	NDE	NDE	NDE
U. SIRTE SHALE	NDE	NDE	NDE
SIRTE SAND	NDE	NDE	NDE
SIRTE SHALE	NDE	NDE	NDE
BAHI	NDE	NDE	NDE
QUARTZITE	NDE	NDE	NDE

WELL	H7-6	H8-6	H9-6
KB	197'	180'	160'
TD	10,272'	10,281'	5,275'
ARIDA	2783'(-2586')	2750'(-2570')	2805'(-2645')
AUGILA	4457'(-4260')	4445'(-4265')	4560'(-4400')
GIALO	4900'(-4703')	4884'(-4704')	5000'(-4840')
GIR	6580'(-6383')	6550'(-6370')	NDE
KHEIR MARL	7366'(-7169')	7306'(-7126')	NDE
KHEIR LS	7548'(-7351')	7440'(-7260')	NDE
HARASH	7915'(-7718')	7890'(-7710')	NDE
HARASH POROSITY	NP	8078'(-7898')	NDE
KHALIFA	8210'(-8013')	8208'(-8028')	NDE
HAGFA	8490'(-8293')	8644'(-8464')	NDE
KALASH	9900'(-9703')	9798'(-9618')	NDE
WAHA	NP	NP	
SIRTE SHALE	NDE	NDE	NDE
SIRTE SAND	NDE	NDE	NDE
SIRTE SHALE	NDE	NDE	NDE
BAHI	NP	9913'(-9733')	NDE
QUARTZITE	10,038'(-9841')	9953'(-9773')	NDE

WELL	H10-6	H11-6	H12-6
KB	156'	203'	183'
TD	5,260'	5,285'	11,040'
ARIDA	2790'(-2634')	2845'(-2642')	2838'(-2655')
AUGILA	4489'(-4333')	4540'(-4337')	4605'(-4422')
GIALO	4930'(-4774')	4955'(-4752')	5060'(-4877')
GIR	NDE	NDE	6400'(-6217')
KHEIR MARL	NDE	NDE	7462'(-7279')
KHEIR LS	NDE	NDE	7572'(-7389')
HARASH	NDE	NDE	7958'(-7775')
HARASH POROSITY	NDE	NDE	8095'(-7912')
KHALIFA	NDE	NDE	8236'(-8053')
HAGFA	NDE	NDE	8478'(-8295')
KALASH	NDE	NDE	10,188'(-10,005')
WAHA	NDE	NDE	NP
SIRTE SHALE	NDE	NDE	10,355'(-10,172')
SIRTE DOLOMITE	NDE	NDE	10,457'(-10,274')
SIRTE SAND	NDE	NDE	NP
SIRTE SHALE	NDE	NDE	NP
BAHI	NDE	NDE	10,772'(-10,589')
QUARTZITE	NDE	NDE	10,810'(-10,627')

Hateiba Field

WELL	S4-6	S12-6	S18-6
KB	135'	134'	122'
TD	8883'	9493'	9304'
ARIDA	ND	ND	ND
AUGILA	ND	ND	ND
GIALO	6792'(-6927')	6507'(-6641')	6154'(-6276')
GIR	ND	ND	ND
KHEIR	7080'(-7215')	6923'(-7057')	6502'(-6624')
HARASH	ND	ND	ND
KHALIFA	ND	ND	ND
HAGFA	7865'(-8000')	7742'(-7876')	7288'(-7410')
KALASH	ND	9164'(-9298')	8326'(8448')
WAHA	8602'(-8738')	ND	ND
BAHI	ND	ND	8526'(-8648')
QUARTZITE	8675'(-8810')	9275'(-9403')	8606'(-8728')

Attahaddy Field

WELL	FF6-6	FF9-6	FF10-6
KB	328'	283'	376'
TD	12,065'	12,000'	12,630'
ARIDA	2252'(-1942')	2237'(-1954')	2175'(-1799')
AUGILA	3970'(-3642')	3948'(-3665')	3966'(-3590')
GIALO	4475'(-4147')	4485'(-4202')	4440'(-4064')
GIR	6322'(-5994')	6396'(-6113')	6256'(-5880')
KHEIR	7500'(-7172')	7430'(-7147')	7451'(-7075')
HARASH	ND OR NP	ND OR NP	ND OR NP
KHALIFA	ND OR NP	ND OR NP	ND OR NP
HAGFA	7819'(-7491')	7696'(-7413')	7780'(-7404')
KALASH	10,360'(-10,022')	9998'(-9715')	10,593'(-10,217)
SIRTE SHALE	ND OR NP	10,444'(-10,161')	11,030'(-10,654')
WAHA	ND OR NP	ND OR NP	ND OR NP
BAHI	11,312'(-10,984')	ND OR NP	ND OR NP
QUARTZITE	11,595'(-11,267')	10,792'(-10,509')	12,345'(-11,969')

SEMI-REGIONAL WELLS

WELL	DDD1-6:	ZZ1-6
KB	89'	152'
TD	9805'	10,515'
ARIDA	3065'(-2976')	3218'(-3066')
AUGILA	4805'(-4716')	5055'(-4903')
GIALO	5248'(-5159')	5361'(-5209')
GIR	6420'(-6331')	6800'(-6648')
U. KHEIR MARL	7500'(-7411')	7830'(-7678')
KHEIR LS	7630'(-7541')	7922'(-7770')
KHEIR MARL	-	NP
HARASH	7810'(-7721')	8255'(-8103')
HARASH POROSITY	7920'(-7831')	8345'(-8193')
KHALIFA	8054'(-7965')	8477'(-8325')
HAGFA	8230'(-8141')	8710'(-8558')
KALASH	9710'(-9621')	10,301'(-10,149')
U. SIRTE SHALE	NP	NP
SIRTE SAND	NP	NP
SIRTE SHALE	NP	NP
WAHA	NP	NP
BAHI	NP	NP
QUARTZITE	9747'(-9658')	10,471'(-10,319')

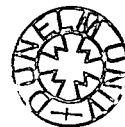
LEGEND:

NL: NOT LOGGED
 NP: NOT PRESENT
 ND: NOT DIFFERENTIATED
 NDE: NOT DEEP ENOUGH

THE 1998 PROCESSING SEQUENCE

Record length	5s.
Sample interval	4ms.
Polarity	SEG normal polarity unchanged during processing.
Demultiplex	Demultiplex field data and transcribe to CGG format.
Geometry labelling	Label geometry and VP display.
Amplitude recovery	Gain ramp applied.
Mute	First break suppression.
F-K filter	In shot domain. Velocity in the range 2000 m/s suppressed.
F-X filter	Predictive filter in the F-X domain.
CMP gather	Sort into CMP domain.
Spiking decon.	120 ms operator, window 100-1600 ms 5% white noise. 120 ms operator, window 1300-4000 ms 5% white noise.
Static correction	Field statics correction to floating datum plane.
Normal move-out	Velocity analyses at selected locations, approximately 1.5 kms apart.
Static correction	Short wavelength residual statics. Filter 10-35 Hz, max shift +/- 28 ms, window 600-2900 ms.
Muting	Offset 150 270 1870 3705 metres. Time 0 250 1500 1920 ms.
Internal mute	Offset: 75 600 650 metres. Time: 1500 2100 5000 ms.
Dip move-out	Application of DMO.
Normal move-out	Revised velocities picked on DMO data.

Equalisation	Operator	1000 ms	0-5000 ms.
Stack	Normal	120 fold	CDP interval 15.0 m.
Filter	Time	0.0-5.0s	8-50 Hz.
Equalisation	Operator	1000 ms.	
Static correction	To datum at mean sea level.		
Migration	45 deg. finite difference wave equation migration in F-X domain using 95% stacking velocities.		
Trace mix	3 trace, weighted (1:2:1), running mix.		
Time-varying filter	Time	0.0-1.0s	10-50 Hz.
		1.2-2.0s	10-45 Hz.
		2.0-5.0s	8-35 Hz.
Equalisation	Operator	200 ms	000-400 ms.
	Operator	600 ms	400-5000 ms.
Display	Gain 3db, bias 5%.		



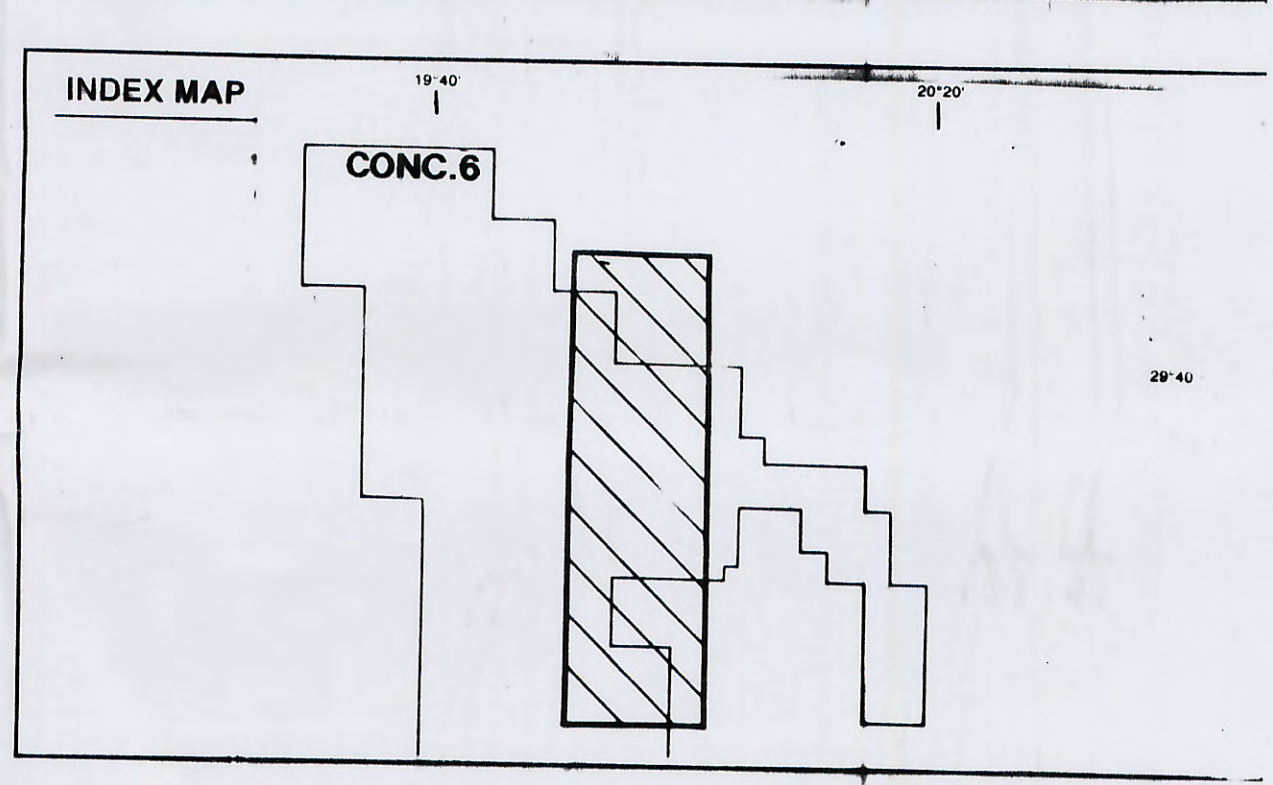


CONCESSION 6 (NORTH)

UPPER PALAEOCENE-LOWER EOCENE
KHEIR FORMATION
TIME STRUCTURE MAP

SCALE: 1:25,000

DATUM: M.S.L. AUTHOR: A BEN SALEM
C.I.: 20 msec. DATE: OCTOBER, 1999
REVISED: DRPT:



CONC. 6

